RADIATION LAB REPORT

PRELIMINARY RESULTS FOR STUDY OF THEORETICAL AND EXPERIMENTAL CHARACTERIZATION OF DISCONTINUITIES IN SHIELDED MICROSTRIP

L.P. Dunleavy and P.B. Katehi

Electrical Engineering and
Computer Science Department
University of Michigan
Ann Arbor, Michigan

August 1987

RL-846 = RL-846

TABLE OF CONTENTS

LIST OF FIGURES

Figure

LIST OF APPENDICES

Appendix

CHAPTER I

INTRODUCTION:

Millimeter-wave integrated circuits are becoming increasingly important in a variety of scientific and military applications, and a wide range of solid state circuitry has been demonstrated in both hybrid and monolithic form. However, the inability to accurately predict the electrical characteristics of various circuit components is a serious barrier to the widespread and cost effective application of these technologies.

Accurate microstrip discontinuity modeling is key to improving the cost effectiveness of microwave and millimeter-wave circuit designs. Typical millimeter-wave IC's contain various active and passive elements interconnected by microstrip transmission lines as illustrated in Figure 1.1. In the vicinity of transmission line junctions and other discontinuities, evanescent fields are excited which cause unwanted parasitic effects, and generate space and surface waves that can significantly affect circuit operation. These discontinuity effects can be modeled by the use of lumped equivalent circuits; however, there are a number of different approaches that can be used to approximate the values of the equivalent circuit elements.

The majority of existing approaches are based on either quasi-static solutions or use a planar waveguide model. Despite their inherent accuracy limitations, equivalent circuits derived from such solutions are adequate for many applications since an approximate design, at the least, provides a starting point after which the circuit may be tuned to achieve

the desired performance. This is generally true of hybrid integrated circuits operating in the lower microwave range (at or below X-band).

Quasi-static techniques are well established and described in standard texts [1]-[3]. With these techniques, equivalent circuits are derived in terms of static (i.e. frequency independent) capacitances and low frequency inductances. Convenient analytical formulas for discontinuity parasitics are possible, yet their accuracy is questionable for frequencies above a few GHz.

Planar waveguide models provide a frequency dependent solution. In this approach, an equivalent planar waveguide geometry is proposed for the microstrip problem. This transformed problem is then solved using an appropriate analytical technique such as mode matching [1]-[4]. Models derived from this technique are generally considered accurate to higher frequencies than quasi-static models. However, although they can include dispersion effects in the solution, planar waveguide models cannot take surface wave effects into account. Even if the model were strictly valid, the accuracy is limited by the method used to approximate the effective width, and dielectric constant of the equivalent planar waveguide. Further, this approach does not provide a means to account for radiation effects when present.

In many cases, the limitations of the above two techniques cannot be tolerated. Often, circuit tuning is difficult or impossible; as a result, inaccurate circuit models lead to long design cycles with many costly circuit iterations. One example where this is true is in Monolithic Microwave Integrated Circuit(MMIC) design, where the small size and the fragility of MMICs make tuning virtually impossible.

Also, for both hybrid and monolithic circuits, the need for greater modeling accuracy increases with frequency. Parasitics have a greater effect on circuit behavior, and it becomes ever more important to accurately model surface wave effects, mutual interactions between circuit elements and radiation losses (if present). Hence for MMICs and for

both hybrid and monolithic millimeter-wave IC's, a more rigorous solution for microstrip discontinuities is necessary.

A technique that meets this requirement was recently developed by Katehi and Alexopoulos to treat discontinuites in open microstrip geometries [5]. In this technique, the currents on the microstrip conductors are first computed by a Galerkin's implementation of the method of moments. Based on this current, a transmission line model is used to evaluate frequency dependent equivalent circuits and scattering parameters [6].

This technique has so far been applied to solve for various discontinuities in open microstrip. Here, the top of the substrate is left open to the air as shown in Figure 1.2a. One application where open microstrip is used is in a monolithic antenna array where radiating elements are integrated along with passive and active components on the same or adjacent substrates. In open microstrip, radiation from circuit elements is unavoidable and requires accurate modeling at high frequencies.

Radiation is often avoided in practical circuit designs by enclosing parts of the circuitry in shielding boxes (or housings); hence, it is important to also establish an accurate method of solution for microwave and millimeter-wave circuits operating in a shielded microstrip environment. To this end, the new analytical methodology presented here is an extension of the approach of Katehi and Alexopoulos to shielded microstrip configurations of the type shown in Figure 1.2b. This report presents theoretical methodology and preliminary results for this new method that promises to provide more accurate circuit models for discontinuities in shielded microstrip.

While rigorous solutions to shielded discontinuities have been advanced by others, their accuracy is unclear and there are several structures which have not been adequately analyzed. One approach has been developed by Jansen et. al., who use what is referred to as a spectral domain iterative technique [7]-[10]. Although reasonable results have been demonstrated for several microstrip structures, the accuracy of their methods is

unclear since there has been little or no accompanying experimental verification, and only limited comparisons to other rigorous numerical solutions. Furthermore, there are important discontinuity structures that have not been addressed by these authors, leaving considerable room for contribution.

Another solution has been presented more recently by Rautio and Harrington [11], [11] who use a method of moments technique. However, the only results from this work we are aware of is for the input impedance and current distribution for an open circuited stub. Their solution is, in some respects, more general since they assume a two directional current distribution, while the present work uses one directional currents. Our approach also differs in the choice of basis functions and the method of circuit excitation employed.

The new analytical methods developed here have been applied to obtain results for open end and series gap discontinuities in shielded microstrip. Work is currently in progress to obtain results for coupled line filter structures.

To test these analytical methods, an experimental study is being conducted in cooperation with the Microwave Products Division of Hughes Aircraft Company. This work includes a study of "de-embedding" techniques, from which it has been concluded that the technique most suitable for this work is the thru-short-delay (TSD) method. With this method, the major factor influencing accuracy is microstrip connection repeatability. To explore this, a connection repeatability study was conducted [13], and the results were extended to evaluate the associated uncertainty in de-embedding accuracy. S-parameter measurements were then obtained for selected discontinuity structures. The numerical and experimental results are compared wherever possible, and demonstrate the accuracy and usefulness of the new theoretical methods.

The combination of theoretical and experimental work presented here represents an important contribution in the area of millimeter-wave IC design by lending more insight into the high frequency behavior of microstrip discontinuities than previously possible.

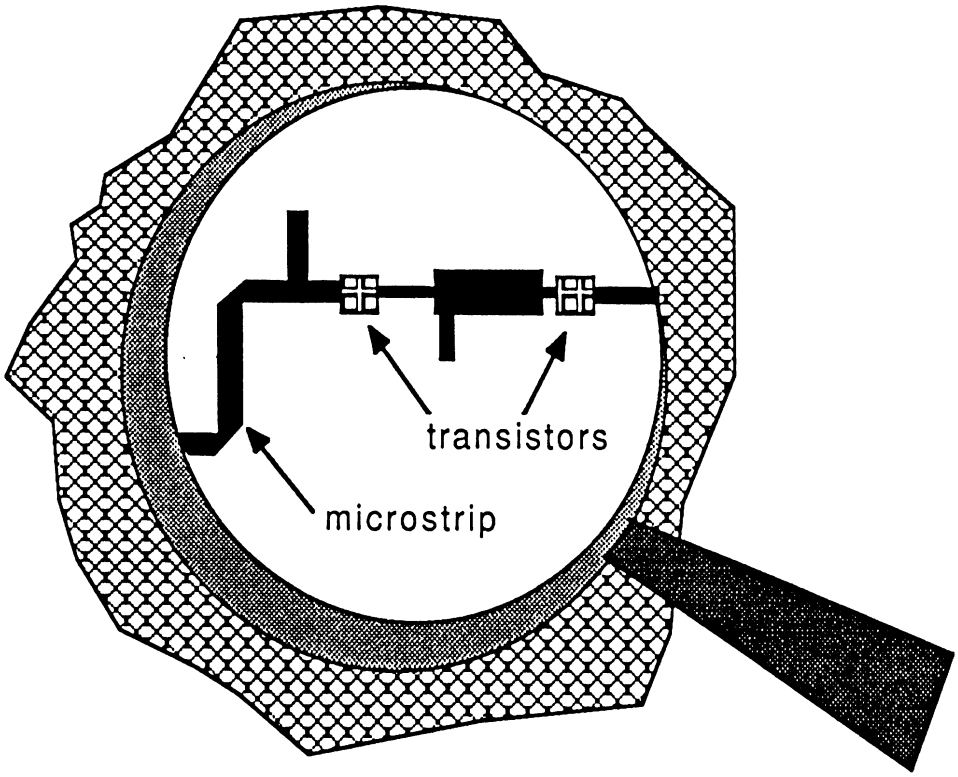

Figure 1.1: Typical millimeter-wave integrated circuit structure. Accurate modeling of discontinuities is key to cost effective designs.

a) Open microstrip

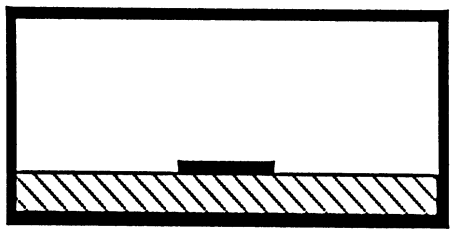

b) Shielded microstrip

Figure 1.2: Two basic classes of microstrip.

CHAPTER II

THEORETICAL METHODOLOGY

2.1 SUMMARY OF THEORETICAL APPROACH

2.1.1 Problem geometry

As a first step in the development of the theoretical technique for analyzing shielded microstrip discontinuities, consider the shielded microstrip geometry shown in Figure II. The shielding box forms a waveguide cavity, which –for most practical uses– is cut-off for the highest frequency of operation. That is, the cavity dimensions are usually such that non-evanescent modes are suppressed. However, the solution presented here, as far as the computation of the current distribution is concerned, is applicable whether the cavity is cut-off or not .

as far as the computation of the current distribution is concerned

2.1.2 Theoretical assumptions

In this solution, a few simplifying assumptions are made to reduce unnecessary complexity, and excessive computer time. Throughout the analysis, it is assumed that the width of the conducting strips is small compared to the effective (or guided) wavelength. In

this case, unidirectional currents may be assumed with negligible loss in accuracy. Also, while substrate losses are accounted for, it is assumed that the strip conductors, and the walls of the shielding box are lossless. These assumptions are valid for the high frequency analysis of the discontinuity structures of Figure 2.2, provided good conductors are used in the metalized areas.

2.1.3 Description of theoretical approach

The theoretical technique is based on a Galerkin's method formulation of the method of moments. The required integral equation is derived by first representing the coaxial feed by an equivalent magnetic current source. Reciprocity theorem is then applied to relate this magnetic current source and the electric current on the conducting strips to the electromagnetic fields inside the cavity.

By expanding the electric current into a series of sinusoidal subsectional basis functions, the integral equation is transformed into a matrix equation. The matrix equation is then solved to compute the current distribution. Finally, based on the current, either an equivalent circuit, or scattering parameters, or both are derived to characterize the discontinuity being considered. A flow chart illustrating this approach is shown in Figure 2.3.

2.2 FORMULATION FOR METHOD OF MOMENTS SOLUTION

The method of moments is a well established numerical technique for solving electromagnetic problems [14],[15]. A review of the basic approach is given in Appendix A. This section makes use of the method of moments to set up a matrix equation that provides for a computer solution to shielded microstrip discontinuity problems.

2.2.1 Formulation of integral equation using reciprocity theorem

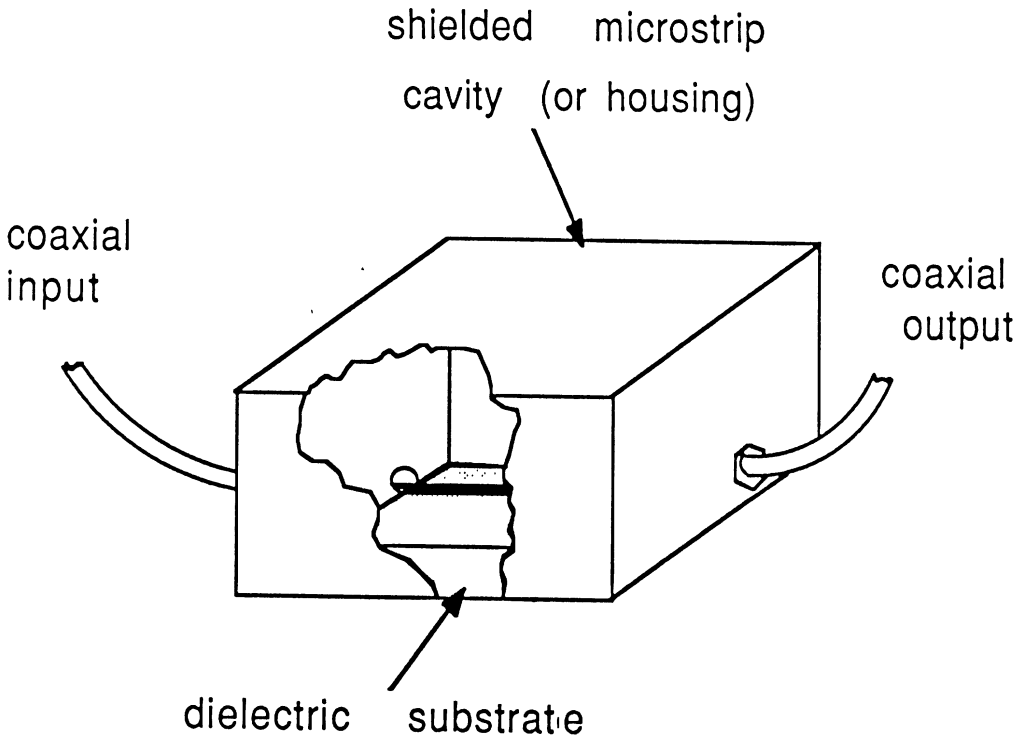

Figure 2.1: Basic geometry for the shielded microstrip cavity problem.

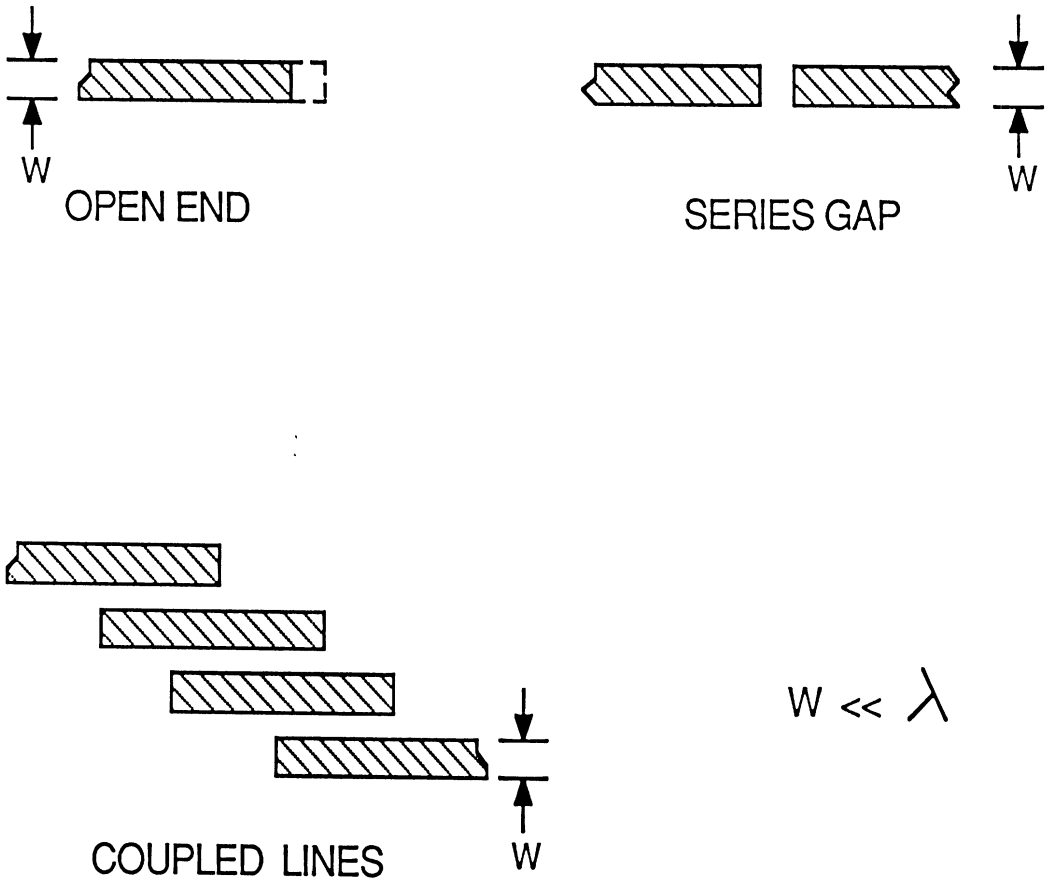

Figure 2.2: Discontinuities for which thin-strip approximation is valid

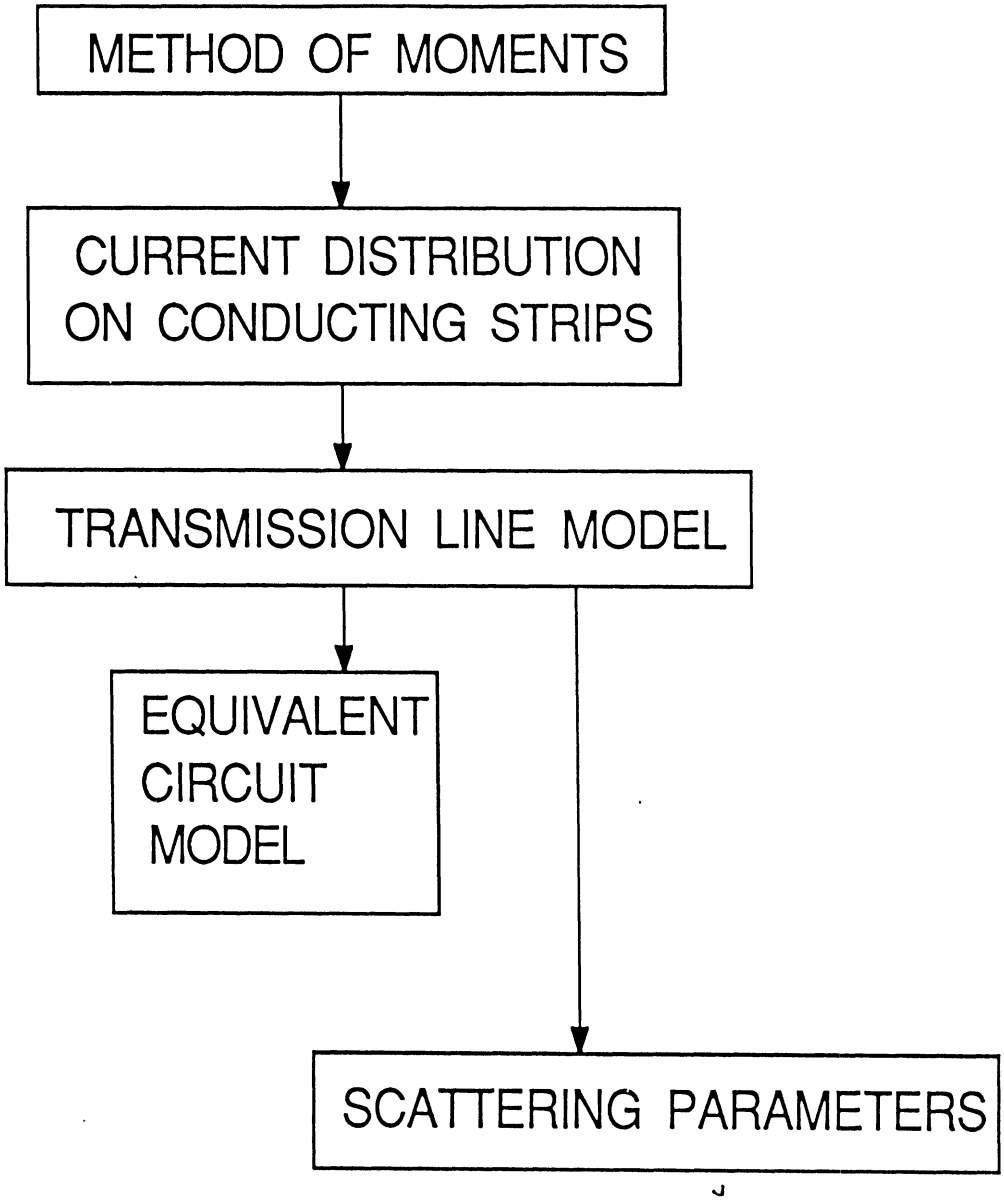

Figure 2.3: Flow chart illustrating theoretical approach for characterizing microstrip discontinuities

Consider the problem geometry of Figure 2.1. In most practical applications, the coaxial feed (or launcher) is designed to allow only transverse electromagnetic (TEM) propagation, and the feed's center conductor is small compared to a wavelength (i.e. $kr_a \ll 1$). In these cases, the radial electric field will be dominant on the aperture and we can replace the feed by an equivalent magnetic surface current whose only component is in the $\hat{\phi}$ direction (i.e.$\bar{M}_s = M_\phi \hat{\phi}$) where $\hat{\phi}$ refers to the cylindrical coordinate referenced to the center of the feeding aperture (see Figure 2.4). This method of modeling the feed with a magnetic current source will be discussed further in Section 2.5.

The magnetic current source is coupled with the current distribution $\bar{J}_s$ on the conducting strip to produce the total electric field $\bar{E}^{tot}$ and the total magnetic field $\bar{H}^{tot}$ inside the cavity as indicated in Figure 2.5.

We now propose an independent test current source $\bar{J}_q$ existing only on a small subsection of the conducting strip as shown in Figure 2.6. Using reciprocity theorem, the two sets of current sources are related according to

$$\int\int\int_V (\bar{J}_s \cdot \bar{E}_q - \bar{H}_q \cdot \bar{M}_s)\, dv = \int\int\int_V \bar{J}_q \cdot \bar{E}^{tot} dv \tag{2.1}$$

where the volume V is the interior of the cavity.

Since $\bar{J}_q$ is zero everywhere except over one subsection of the conducting strip, and x-directed (the thin strip approximation), the right hand side of (2.1) reduces to

$$\int\int\int_V \bar{J}_q \cdot \bar{E}^{tot} dv = \int\int_{S_q} |\bar{J}_q|\, E_x^{tot}(z = h) ds = 0 \tag{2.2}$$

where S_q is the surface of an arbitrary subsection and $E_x^{tot}(z = h)$ is the x-component of the total electric field which must vanish on the surface of the conductors ($z = h$) since they are assumed to be perfectly conducting.

Reducing the remaining volume integrals in (2.1) to surface integrals results in

$$\int\int_{S_{strip}} \bar{E}_q(z=h)\cdot\bar{J}_s ds = \int\int_{S_{feed}} \bar{H}_q(x=0)\cdot\bar{M}_s ds\,. \tag{2.3}$$

Note that this equation is not explicitly in the form of the operator equation of (A.1). This is because in using the reciprocity theorem formulation we have inherently placed it in the inner product form of (A.3).

2.2.2 Expansion of current with sinusoidal subsectional basis functions

In order to solve the integral equation (2.3), the current distribution $\bar{J}_s$ is expanded into a series of orthogonal functions as follows. Consider the strip geometry shown in Figure 2.7, let

$$\bar{J}_s = \psi(y)\sum_{p=1}^{NSECT} I_p\alpha_p(x)\,\hat{x} \tag{2.4}$$

where I_p are unknown current coefficients. The function $\psi(y)$ describes the variation of the current in the transverse direction and is given by

$$\psi(y) = \begin{cases} \dfrac{\frac{2}{\pi W}}{\sqrt{1-\left[\frac{2(y-Y_0)}{W}\right]^2}} & Y_0 - W/2 \le y \le Y_0 + W/2 \\ 0 & else \end{cases} \tag{2.5}$$

This variation was chosen to agree with that derived by Maxwell for the charge density distribution on an isolated conducting strip [16], and it has been used successfully by others to describe the transverse variation of microstrip currents [5], [17],[18]. As we will see later, with this choice, the y part of the surface integral on the left hand side of (2.3) can be solved in closed form.

The basis functions $\alpha_p(x)$ comprise an orthonormal set and are given by

$$\alpha_p(x) = \begin{cases} \frac{\sin[K(x_{p+1}-x)]}{\sin(Kl_x)} & x_p \le x \le x_{p+1} \\ \frac{\sin[K(x-x_{p-1})]}{\sin(Kl_x)} & x_{p-1} \le x \le x_p \\ 0 & else \end{cases} \tag{2.6}$$

for $p \neq 1$, and

$$\alpha_1(x) = \begin{cases} \frac{\sin[K(l_x - x)]}{\sin(Kl_x)} & 0 \leq x \leq l_x \\ 0 & else \end{cases} \tag{2.7}$$

for $p = 1$, where

$K = \omega\sqrt{\mu_o \epsilon_r \epsilon_0}$ is the real part of the wave number in the dielectric region

W is the width of the microstrip line

Y_0 is the y-coordinate of the center of the strip with respect to the origin of Figure 2.1

x_p is the x-coordinate of the pth subsection $(= (p-1)l_x)$

l_x is the subsection length $(l_x = x_{p+1} - x_p)$.

The x part of (2.3 can also be solved in closed form due to our choice of sinusoidal subsectional basis functions $\alpha_p(x)$.

2.2.3 Transformation of integral equation into a matrix equation

The integral equation (2.3) can now be transformed into a matrix equation by substituting the expansion given by (2.4) for the current $\bar{J}_s$. This results in the following:

$$\sum_{p=1}^{NSECT} \left[\int\int_{S_p} \bar{E}_q(x = h) \cdot \psi(y)\, \alpha_p(x)\, \hat{x} ds \right] I_p = \int\int_{S_{feed}} \bar{H}_q \cdot \bar{M}_s ds \tag{2.8}$$

which can be expressed as

$$[Z_{qp}][I_p] = [V_q] \tag{2.9}$$

where

S_p is the surface area of the p^{th} subsection

$[Z_{qp}]$ is the impedance matrix, which has the dimensions of NSECT x NSECT

$[I_p]$ is the unknown current vector, which has the dimensions of NSECT x 1

$[V_q]$ is the excitation vector, which has the dimensions of NSECT x 1

The individual elements of the impedance matrix are given by

$$Z_{qp} = \int\int_{S_p} \bar{E}_q(z=h) \cdot \psi(y)\, \alpha_p(x)\, \hat{x} ds \,. \tag{2.10}$$

The elements of the excitation vector are given by

$$V_q = \int\int_{S_{feed}} \bar{H}_q \cdot \bar{M}_s ds \,. \tag{2.11}$$

We can now solve for the current vector by matrix inversion and multiplication according to

$$[I_p] = [Z_{qp}]^{-1} [V_q] \,. \tag{2.12}$$

2.3 DERIVATION OF THE GREEN'S FUNCTION

To compute the elements of the impedance matrix, we must derive the Green's function associated with the electric and magnetic fields $\bar{E}_q$, $\bar{H}_q$. We will first define the problem geometry and outline the electromagnetic theory to be used; then, the boundary value problem will be solved for the Green's function.

2.3.1 Geometry and electromagnetic theory

The geometry used in the Green's function derivation is shown in Figure 2.8. The cavity is divided into two regions. Region 1 consists of the volume contained within the substrate ($z < h$), while region 2 is the volume above the substrate surface ($z > h$).

The Green's function will be defined as the electric field due to an infinitesimal current source located on the substrate surface of Figure 2.8. After deriving the Green's function, the fields associated with the test source $\bar{J}_q$ will be evaluated by integrating over the surface of the q^th subsection.

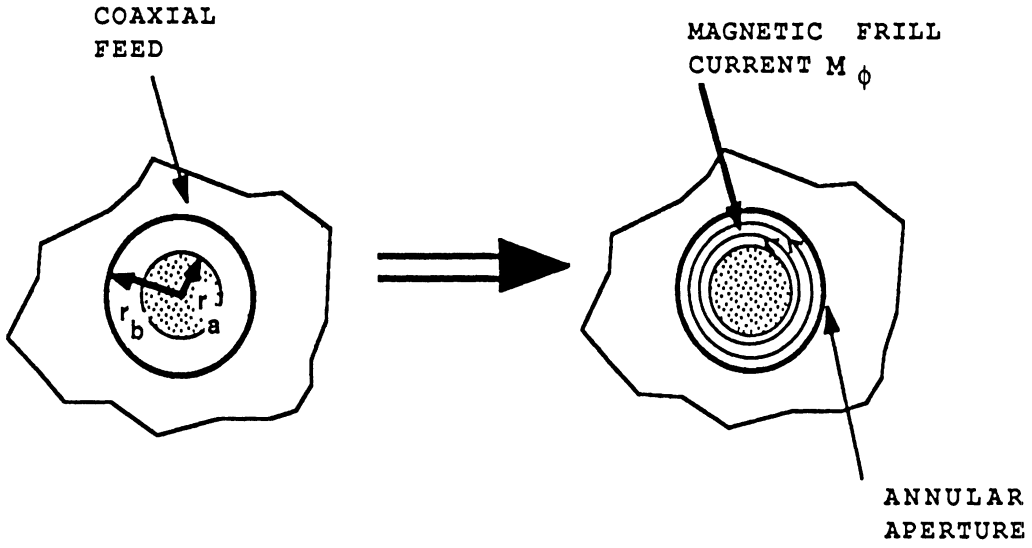

Figure 2.4: Representation of coaxial feed by a circular aperture with magnetic frill current M_ϕ.

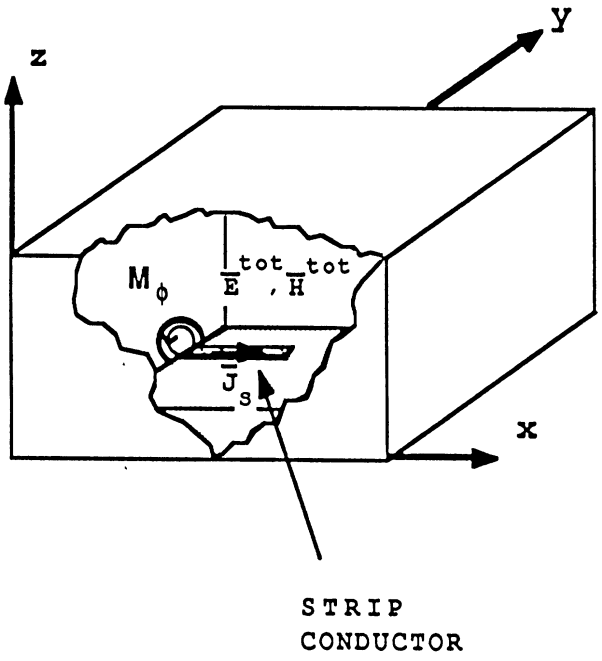

Figure 2.5: Total fields $\bar{E}_q$, $\bar{H}_q$ inside cavity produced by magnetic current source M_ϕ at aperture and electric current distribution $\bar{J}_s$ on the conducting strip

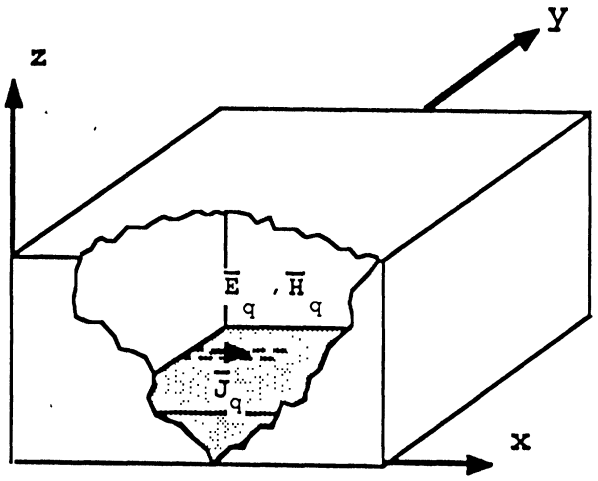

Figure 2.6: Test current field $\bar{J}_q$ on conducting strip and associated fields $\bar{E}_q$, $\bar{H}_q$.

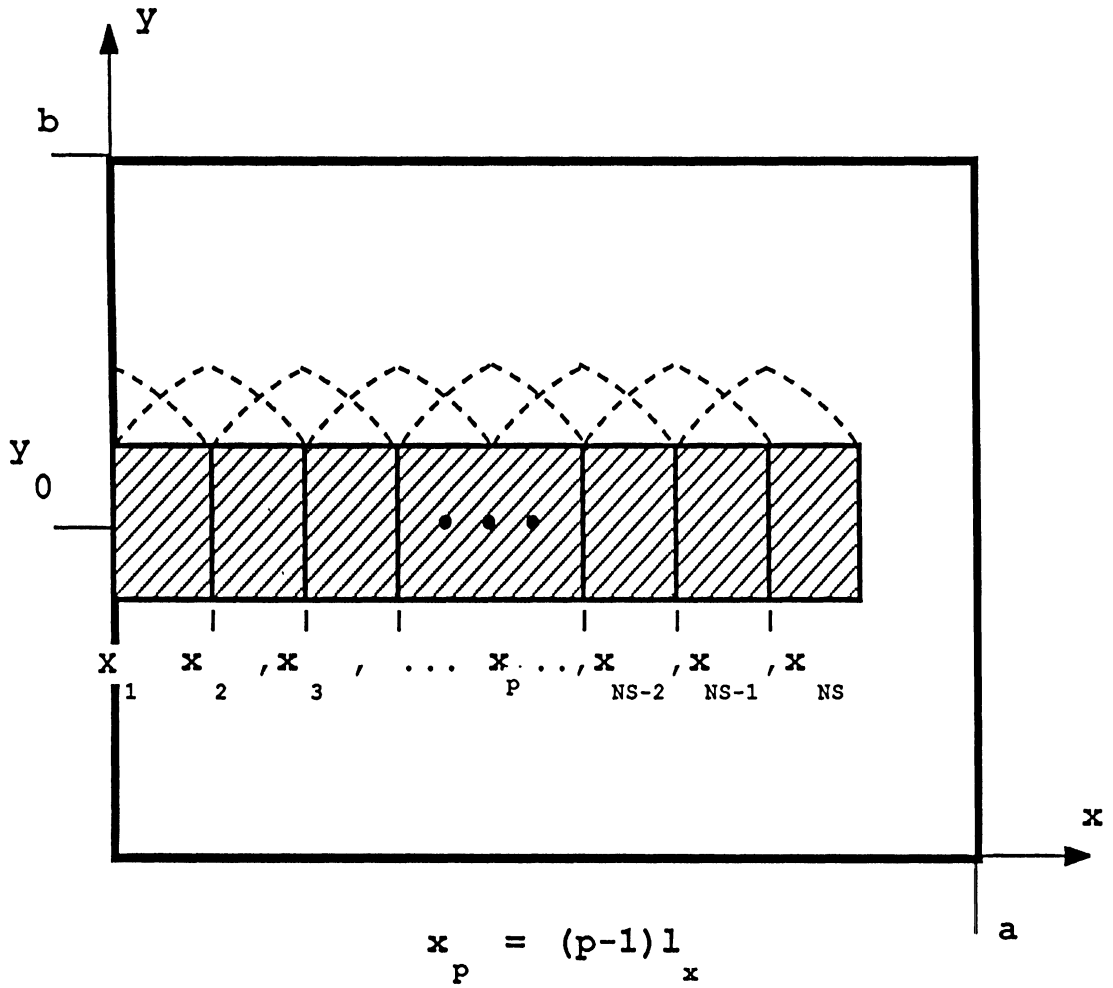

Figure 2.7: Strip geometry for use in basis function expansion of current.

The test source $\bar{J}_q$ and the associated fields within the cavity ($\bar{E}_q$,$\bar{H}_q$) are related through Maxwell's equations, which may be put in the following form:

$$\bar{\nabla} \times \bar{E}^i = -j\omega\mu_i\bar{H}^i \tag{2.13}$$

$$\bar{\nabla} \times \bar{H}^i = j\omega\epsilon_i\bar{E}^i + \bar{J} \tag{2.14}$$

$$\bar{\nabla} \cdot \bar{J} = -j\omega\rho \tag{2.15}$$

$$\bar{\nabla} \cdot \left(\epsilon_i\bar{E}^i\right) = \rho \tag{2.16}$$

$$\bar{\nabla} \cdot \left(\mu_i\bar{H}^i\right) = 0 \tag{2.17}$$

where μ_i is the permeability of medium i, ϵ_i is the complex permittivity of medium i, and ρ is the charge density associated with $\bar{J}$.

It is assumed that both regions are non-magnetic and that region 2 is air, hence

$$\mu_1 = \mu_2 = \mu_0 = 4\pi \times 10^{-7}\text{H/m} \tag{2.18}$$

$$\epsilon_i = \begin{cases} \epsilon_r^*\epsilon_0 & for\ i = 1 \\ \epsilon_0 & for\ i = 2 \end{cases} \tag{2.19}$$

where

$$\epsilon_r^* = \epsilon_r - j\frac{\sigma}{\omega\epsilon_0}\ . \tag{2.20}$$

In (2.20) σ denotes the conductivity of the substrate material, and the quantity $\frac{\sigma}{\omega\epsilon_0}$ is referred to as the loss tangent. In (2.13) - (2.17), $i = 1,2$ indicates that these equations hold in each of the regions respectively. In addition, and the assumed time dependence is $e^{j\omega t}$, and it is suppressed throughout the dissertation. To simplify the notation of this subsection, the subscript q is suppressed with the understanding that all the field quantities discussed here are associated with the test source $\bar{J}_q$ (i.e. $\bar{E}^i = \bar{E}^i_q$ etc.).

2.3.2 Solution to boundary value problem for Green's function

We now introduce the vector potentials $\bar{A}^i$ such that

$$\bar{H}^i = \frac{1}{\mu_o}\bar{\nabla} \times \bar{A}^i \,. \tag{2.21}$$

In view of (2.21), the electric field may be written as (Appendix B,(B.13))

$$\bar{E}^i = -j\omega \left(1 + \frac{1}{k_i^2}\bar{\nabla}\bar{\nabla}\cdot\right) \bar{A}^i \tag{2.22}$$

where $\bar{A}^i$ satisfies the inhomogeneous wave equation

$$\nabla^2 \bar{A}^i + k_i^2 \bar{A}^i = -\mu_0 \bar{J} \,. \tag{2.23}$$

The integral form of the electric field is given by (B.18) or in integral form (B.18)

$$\bar{E}^i = -j\omega\mu_0 \int\int\int_V \left[\left(1 + \frac{1}{k_i^2}\bar{\nabla}\bar{\nabla}\cdot\right)(\bar{\bar{G}}^i)^T\right] \cdot \bar{J} dv' \tag{2.24}$$

where $k_i^2 = \omega^2\mu_0\epsilon_i$ and $\bar{\bar{G}}^i$ is a dyadic Green's function [ref. Tai] satisfying the following equation

$$\nabla^2 \bar{\bar{G}}^i + k_i^2 \bar{\bar{G}}^i = -\bar{\bar{I}}\delta(\bar{r} - \bar{r}) \,. \tag{2.25}$$

In (2.24) and (2.25), the superscript T denotes the dyadic transpose operation, and $\bar{\bar{I}}$ is the unit dyadic given by $\hat{x}\hat{x} + \hat{y}\hat{y} + \hat{z}\hat{z}$.

Because of the existence of an air dielectric interface, a two component vector potential is necessary to satisfy the boundary conditions [19]. Accordingly, let

$$\bar{A}^i = A_x^i \hat{x} + A_z^i \hat{z} \,. \tag{2.26}$$

From (B.17) $\bar{A}^i$ is related to $\bar{\bar{G}}^i$ by the following volume integral:

$$\bar{A}^i = \mu \int\int\int_V \bar{J} \cdot \bar{\bar{G}}^i dv' \,. \tag{2.27}$$

$\bar{\bar{G}}^i$ may be expressed in most general form as follows:

$$\bar{\bar{G}}^i = \begin{bmatrix} G_{xx}^i \hat{x}\hat{x} & + & G_{xy}^i \hat{x}\hat{y} & + & G_{xz}^i \hat{x}\hat{z} \\ + G_{yx}^i \hat{y}\hat{x} & + & G_{yy}^i \hat{y}\hat{y} & + & G_{yz}^i \hat{y}\hat{z} \\ + G_{zx}^i \hat{z}\hat{x} & + & G_{zy}^i \hat{z}\hat{y} & + & G_{zz}^i \hat{z}\hat{z} \end{bmatrix} \,. \tag{2.28}$$

Assuming an infinitesimal x-directed current source given by

$$\bar{J} = \delta\left(\bar{r} - \bar{r}'\right)\hat{x} \tag{2.29}$$

in (2.27) allows for reducing $\bar{\bar{G}}^i$ to

$$\bar{\bar{G}}^i = G^i_{xx}\hat{x}\hat{x} + G^i_{xz}\hat{x}\hat{z} \tag{2.30}$$

The functional forms for the dyadic components of (2.30) are found by applying appropriate boundary conditions at the walls: $x = 0$, and a ; $y = 0$, and b ; and $z = 0$, and c. As detailed in Appendix C, these components may be expressed as

$$G^{(1)}_{xx} = \sum_{m=1}^{\infty}\sum_{n=0}^{\infty} A^{(1)}_{mn}\cos k_x x \sin k_y y \sin k^{(1)}_z z \tag{2.31}$$

$$G^{(1)}_{xz} = \sum_{m=1}^{\infty}\sum_{n=0}^{\infty} B^{(1)}_{mn}\sin k_x x \sin k_y y \cos k^{(1)}_z z \tag{2.32}$$

$$G^{(2)}_{xx} = \sum_{m=1}^{\infty}\sum_{n=0}^{\infty} A^{(2)}_{mn}\cos k_x x \sin k_y y \sin k^{(2)}_z (z-c) \tag{2.33}$$

$$G^{(2)}_{xz} = \sum_{m=1}^{\infty}\sum_{n=0}^{\infty} B^{(2)}_{mn}\sin k_x x \sin k_y y \cos k^{(2)}_z (z-c) \tag{2.34}$$

where

$$k_x = n\pi/a \tag{2.35}$$

$$k_y = m\pi/b \tag{2.36}$$

$$k^{(1)}_z = \sqrt{k_1^2 - k_x^2 - k_y^2} \tag{2.37}$$

$$k^{(2)}_z = \sqrt{k_0^2 - k_x^2 - k_y^2} \tag{2.38}$$

$$k = \omega\sqrt{\mu_0\epsilon_1} \tag{2.39}$$

$$k_0 = \omega\sqrt{\mu_0\epsilon_0}\,. \tag{2.40}$$

The coefficients $A^{(1)}_{mn}$, $A^{(2)}_{mn}$, $B^{(1)}_{mn}$, and $B^{(2)}_{mn}$ are found by applying boundary conditions at the substrate/air interface ($z = h$). The details of this analysis can be found in Appendix D. The results are:

$$A^{(1)}_{mn} = \frac{-\varphi_n \cos k_x x' \sin k_y y' \tan k^{(2)}_z (h-c)}{abd_{1mn}\cos k^{(1)}_z h} \tag{2.41}$$

$$A_{mn}^{(2)} = \frac{-\varphi_n \cos k_x x' \sin k_y y' \tan k_z^{(1)} h}{abd_{1mn} \cos k_z^{(2)}(h-c)} \tag{2.42}$$

$$B_{mn}^{(1)} = \frac{-\varphi_n (1-\epsilon_r^*) k_x \cos k_x x' \sin k_y y' \tan k_z^{(1)} h \tan k_z^{(2)}(h-c)}{abd_{1mn} d_{2mn} \cos k_z^{(1)} h} \tag{2.43}$$

$$B_{mn}^{(2)} = \frac{-\varphi_n (1-\epsilon_r^*) k_x \cos k_x x' \sin k_y y' \tan k_z^{(1)} h \tan k_z^{(2)}(h-c)}{abd_{1mn} d_{2mn} \cos k_z^{(2)}(h-c)} \tag{2.44}$$

where

$$\varphi_n = \begin{cases} 2 & for\ n = 0 \\ 4 & n \neq 0 \end{cases} \tag{2.45}$$

$$d_{1mn} = k_z^{(2)} \tan k_z^{(1)} h - k_z^{(1)} \tan k_z^{(2)}(h-c) \tag{2.46}$$

$$d_{2mn} = k_z^{(2)} \epsilon_r^* \tan k_z^{(2)}(h-c) - k_z^{(1)} \tan k_z^{(1)} h \tag{2.47}$$

Having derived the Green's function, we are now ready to proceed to the formulation for the elements of the impedance matrix and excitation vector.

2.4 IMPEDANCE MATRIX FORMULATION

The elements of the impedance matrix are given by (2.10)

$$Z_{qp} = \int\int_{S_p} \bar{E}_q(z=h) \cdot \psi(y')\, \alpha_p(x')\, \hat{x} ds' \tag{2.48}$$

which reduces to

$$Z_{qp} = \int\int_{S_p} E_{qx}(z=h) \psi(y')\, \alpha_p(x')\, ds' \tag{2.49}$$

after performing the inner product in (2.48). Hence, to evaluate the impedance matrix elements we need $E_{qx}(z=h)$; that is, the x-component of of the electric field due to the test currents $\bar{J}_q$ at the substrate/air interface ($z=h$).

Once $E_{qx}(z=h)$ has been found the above surface integration will be carried out —which, as we will see, can be completed in closed form.

2.4.1 Evaluation of the electric field due to the test currents

Since $\bar{J}_q$ is a surface current distribution, the volume integral in (2.24) is reduced to a

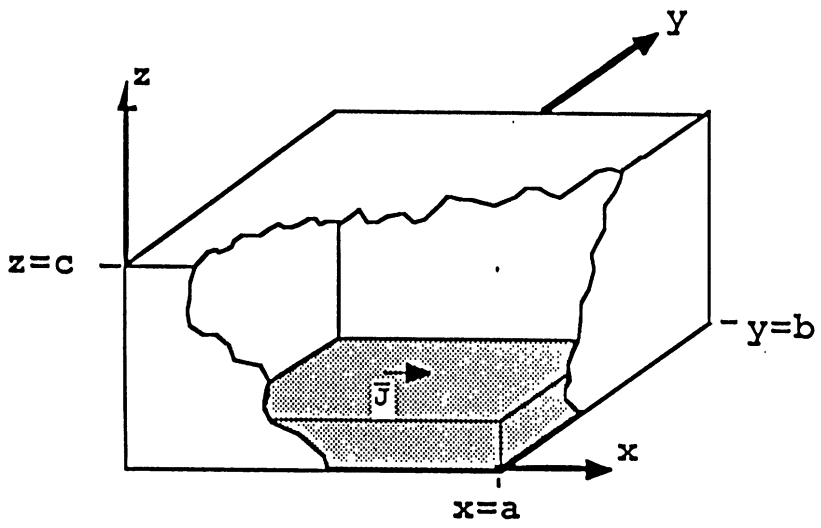

a) Cutaway view

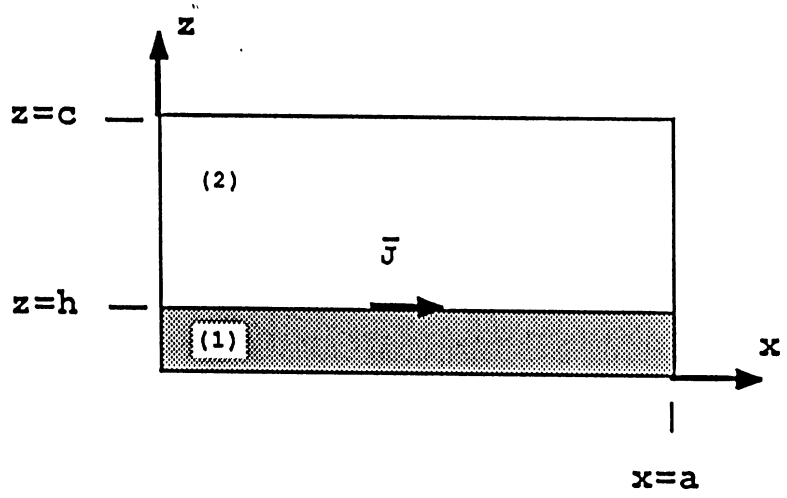

b) Cross section in x-z plane

Figure 2.8: Geometry used in derivation of the Green's function

surface integral as follows:

$$\bar{E}^i = -j\omega\mu_0 \int\int_{S_q} \left[\left(1 + \frac{1}{k_i^2} \bar{\nabla}\bar{\nabla}\cdot \right) (\bar{\bar{G}}^i)^T \right] \cdot \bar{J}_q dx' dy' \tag{2.50}$$

where S_q is the surface of the q^th subsection.

For better accuracy, the test currents $\bar{J}_q$ are expressed in terms of functions which are identical to the basis functions (Galerkin's method)

$$\bar{J}_q = \psi(y')\alpha_q(x')\hat{x} \tag{2.51}$$

where $\psi(y')$ is given by (2.5) with y' replacing y, and $\alpha_q(x')$ is given by (2.6) and (2.7) with p replaced by q and x replaced by x'.

We now substitute (2.51) for $\bar{J}_q$ in (2.50) to yield

$$\bar{E}^i = -j\omega\mu_0 \int\int_{S_q} \left[\left(1 + \frac{1}{k_i^2} \bar{\nabla}\bar{\nabla}\cdot \right) (\bar{\bar{G}}^i)^T \right] \cdot \psi(y')\alpha_q(x')\hat{x} dx' dy' \tag{2.52}$$

Let us define a modified dyadic Green's function $\bar{\bar{\Gamma}}^i$ by

$$\bar{\bar{\Gamma}}^i = -j\omega\mu_0 \left[\left(1 + \frac{1}{k_i^2} \bar{\nabla}\bar{\nabla}\cdot \right) (\bar{\bar{G}}^i)^T \right] . \tag{2.53}$$

Then, $\bar{E}_q^i$ can be expressed as

$$\bar{E}_q^i = \int\int_{S_q} \bar{\bar{\Gamma}}^i \cdot \psi(y')\alpha_q(x')\hat{x} dx' dy' . \tag{2.54}$$

The dyadic transpose of (2.30) yields

$$(\bar{\bar{G}}^i)^T = G_{xx}^i \hat{x}\hat{x} + G_{xz}^i \hat{z}\hat{x} . \tag{2.55}$$

When this expression is substituted in (2.53) and the divergence and gradient operations are performed we can express $\bar{\bar{\Gamma}}^i$ as (see Appendix E, (E.4))

$$\bar{\bar{\Gamma}}^i = \Gamma_{xx}^i \hat{x}\hat{x} + \Gamma_{yx}^i \hat{y}\hat{x} + \Gamma_{zx}^i \hat{z}\hat{x} \tag{2.56}$$

where

$$\Gamma_{xx}^i = G_{xx}^i + \frac{1}{k_i^2} \frac{\partial}{\partial x} \left(\frac{\partial G_{xx}^i}{\partial x} + \frac{\partial G_{xz}^i}{\partial z} \right) \tag{2.57}$$

$$\Gamma^i_{yx} = \frac{1}{k_i^2}\frac{\partial}{\partial y}\left(\frac{\partial G^i_{xx}}{\partial x} + \frac{\partial G^i_{xz}}{\partial z}\right) \tag{2.58}$$

$$\Gamma^i_{zx} = G^i_{xz} + \frac{1}{k_i^2}\frac{\partial}{\partial z}\left(\frac{\partial G^i_{xx}}{\partial x} + \frac{\partial G^i_{xz}}{\partial z}\right) . \tag{2.59}$$

Substituting this expression into (2.54) gives

$$\begin{aligned}\bar{E}^i_q = &\int\int_{S_q} \Gamma^i_{xx}\psi(y')\alpha_q(x')dx'dy'\hat{x} \\ &+ \int\int_{S_q} \Gamma^i_{yx}\psi(y')\alpha_q(x')dx'dy'\hat{y} \\ &+ \int\int_{S_q} \Gamma^i_{zx}\psi(y')\alpha_q(x')dx'dy'\hat{z} .\end{aligned} \tag{2.60}$$

Recall that we only need the x-component of this field which is given by

$$E^i_{qx} = \int\int_{S_q} \Gamma^i_{xx}\psi(y')\alpha_q(x')dx'dy' . \tag{2.61}$$

Furthermore, at $z = h$, boundary conditions require that $E^{(1)}_{qx}(z = h)$ and $E^{(2)}_{qx}(z = h)$ be identical. From the above equation it is obvious that this implies

$$\Gamma^{(1)}_{xx}(z = h) = \Gamma^{(2)}_{xx}(z = h) = \Gamma_{xx}(z = h). \tag{2.62}$$

This equality is verified in Appendix E, and the result of (E.18) may be put in the equivalent form

$$\begin{aligned}&\Gamma_{xx}(z = h) = \\ &\quad j\omega\mu_0 \sum_{m=1}^{\infty}\sum_{n=0}^{\infty} \frac{f_{mn}}{abd_{1mn}d_{2mn}} [\cos k_x x \sin k_y y \cos k_x x' \sin k_y y']\end{aligned} \tag{2.63}$$

where

$$\begin{aligned}f_{mn} = &\varphi_n \tan k_z^{(1)} h \tan k_z^{(2)}(h - c)\left[k_z^{(2)}\epsilon_r^*\left(1 - \frac{k_x^2}{k_1^2}\right)\tan k_z^{(2)}(h - c)\right. \\ &\left. -k_z^{(1)}\left(1 - \frac{k_x^2}{k_0^2}\right)\tan k_z^{(1)} h\right] .\end{aligned} \tag{2.64}$$

If we place (2.63) into (2.61) we obtain

$$\begin{aligned}E^{(1)}_{qx}(z = h) &= E^{(2)}_{qx}(z = h) = \\ E_{qx}(z = h) &= \int\int_{S_q} \Gamma^i_{xx}\psi(y')\alpha_q(x')dx'dy' \\ &= j\omega\mu_0 \sum_{m=1}^{\infty}\sum_{n=0}^{\infty} \frac{f_{mn}}{abd_{1mn}d_{2mn}} \cos k_x x \sin k_y y \mathcal{I}_{qmn} .\end{aligned} \tag{2.65}$$

where

$$\mathcal{I}_{qmn} = \int\int_{S_q} \cos k_x x' \sin k_y y' \psi(y') \alpha_q(x') dx' dy' \ . \tag{2.66}$$

This surface integration is evaluated in closed form in Appendix F; the result is

$$\mathcal{I}_{qmn} = \frac{\zeta_q K \cos k_x x_q \sin R_{1n} \sin R_{2n}}{d_{3n} \sin K l_x} \sin(k_y Y_0) J_0\left(\frac{k_y W}{2}\right) \tag{2.67}$$

where

$$\zeta_q = \begin{cases} 2 & for\ q = 1 \\ 4 & else \end{cases} \tag{2.68}$$

$$K = \omega\sqrt{\mu_0 \epsilon_0 \epsilon_r} \tag{2.69}$$

$$d_{3n} = K^2 - k_x^2 \tag{2.70}$$

$$R_{1n} = \frac{1}{2}(k + k_x) l_x \tag{2.71}$$

$$R_{2n} = \frac{1}{2}(k - k_x) l_x \tag{2.72}$$

$$x_q = (q-1) l_x \ . \tag{2.73}$$

Hence, the formulation for the x-component of the electric field $\bar{E}_q^i$ evaluated at the substrate surface is given by (2.65) where $\mathcal{I}_{qmn}$ is specified in (2.67), f_{mn} is given by (2.64), and d_{1mn} and d_{2mn} are defined by (2.46) and (2.47) respectively.

We are now ready to evaluate the impedance elements.

2.4.2 Evaluation of the impedance matrix elements

From (2.65) and (2.49) we have

$$Z_{qp} = j\omega\mu_0 \sum_{m=1}^{\infty} \sum_{n=0}^{\infty} \frac{f_{mn} \mathcal{I}_{qmn}}{abd_{1mn} d_{2mn}} \mathcal{I}_{pmn} \tag{2.74}$$

where

$$\mathcal{I}_{pmn} = \int\int_{S_p} \cos k_x x \sin k_y y \psi(y) \alpha_p(x) dx dy \ . \tag{2.75}$$

Since (2.75) is the same integral as (2.66), we again use the results of Appendix F (by

substituting p for q) to produce

$$\mathcal{I}_{pmn} = \frac{\zeta_p K \cos k_x x_p \sin R_{1n} \sin R_{2n}}{d_{3n} \sin K l_x} \sin(k_y Y_0) J_0\left(\frac{k_y W}{2}\right) . \tag{2.76}$$

where

$$\zeta_p = \begin{cases} 2 & for\ p = 1 \\ 4 & else \end{cases} \tag{2.77}$$

and

$$x_p = (p-1) l_x . \tag{2.78}$$

Finally, from (2.74), we can write out the entire expression for Z_{qp} by replacing the abbreviated notation for d_{1mn}, d_{2mn}, f_{nm}, $\mathcal{I}_{qmn}$, and $\mathcal{I}_{pmn}$ with their defined expressions to yield:

$$\begin{aligned} Z_{qp} = & \\ & j\omega\mu_0 \sum_{m=1}^{\infty} \sum_{n=0}^{\infty} \frac{\varphi_n \tan k_z^{(1)} h \tan k_z^{(2)}(h-c)}{\left[k_z^{(2)} \tan k_z^{(1)} h - k_z^{(1)} \tan k_z^{(2)}(h-c)\right]} \cdot \\ & \frac{\left[k_z^{(2)} \epsilon_r^* \left(1 - \frac{k_x^2}{k_1^2}\right) \tan k_z^{(2)}(h-c) - k_z^{(1)} \left(1 - \frac{k_x^2}{k_0^2}\right) \tan k_z^{(1)} h\right]}{\left[k_z^{(2)} \epsilon_r^* \tan k_z^{(2)}(h-c) - k_z^{(1)} \tan k_z^{(1)} h\right]} \cdot \\ & \frac{\zeta_q \zeta_p \cos k_x x_q \cos k_x x_p \left[K \sin R_{1n} \sin R_{2n}\right]^2}{ab \sin k l_x \left[K^2 - k_x^2\right]^2} \end{aligned} \tag{2.79}$$

We now turn to the computation of the excitation vector.

2.5 EXCITATION VECTOR FORMULATION

In this section, a surface integral will be set up that provides for evaluating the elements of the excitation vector according to (2.11). This equation may be written as

$$V_q = \int \int_{S_{feed}} \bar{H}_q(x=0) \cdot M_\phi \hat{\phi} \rho d\rho d\phi \tag{2.80}$$

where ρ, and ϕ are cylindrical coordinates referenced to the center of the feeding aperture, as shown in Figure 2.9.

As a first step towards evaluating this integral an expression for M_ϕ will be presented. Second, the magnetic field components parallel to the plane of the aperture (i.e. the $y-z$ plane) will be derived based on the Green's function of Section 2.3.

Finally, the two dimensional numerical approximation used to carry out the integration of (2.80) will be presented. The integration is set up to allow for an arbitrary placement of the feed's center with respect to the substrate surface (see Figure 2.9).

2.5.1 Coaxial feed modeling by an equivalent magnetic surface current

As stated by Chi and Alexopoulos [20], if the radius of the coaxial feed's inner conductor is assumed to be much smaller than the wavelength ($kr_a \ll 1$), and the coaxial feed line is designed to allow only transverse magnetic (TEM) propagation, we can represent the aperture by an equivalent magnetic frill current given by

$$\bar{M}_s = -\frac{V_0}{\ln\left(\frac{r_b}{r_a}\right)\rho}\hat{\phi} \tag{2.81}$$

where

V_0 is the complex voltage present in the coaxial line at the feeding point

r_b is the radius of the coaxial feed's outer conductor

r_a is the radius of the coaxial feed's inner conductor

ρ, ϕ are cylindrical coordinates referenced to the feed's center

Substituting from (2.81) into (2.80) yields (with $ds = \rho d\rho d\phi$)

$$V_q = -\frac{V_0}{\ln\left(\frac{r_b}{r_a}\right)} \int\int_{S_{feed}} H_{q\phi}(x=0) d\rho d\phi \tag{2.82}$$

where the cylindrical coordinates ρ and ϕ are defined in Figure 2.9, and $H^i_{q\phi}$ is the $\hat{\phi}$ component of the magnetic field evaluated in the plane of the aperture ($x = 0$).

2.5.2 Evaluation of the magnetic field at the aperture

To evaluate the magnetic field component $H_{q\phi}$ we will first determine the $\hat{y}$ and $\hat{z}$ components, and then perform a coordinate transformation to the cylindrical coordinates ρ and ϕ.

Determination of $\hat{y}$ and $\hat{z}$ components of $\bar{H}_q$

The magnetic field $\bar{H}_q$ anywhere inside the cavity is given by (2.21)

$$\bar{H}_q^i = \frac{1}{\mu_o}\bar{\nabla} \times \bar{A}_q^i \tag{2.83}$$

where (2.27)

$$\bar{A}_q^i = \mu \int\int\int_V \bar{J}_q \cdot \bar{\bar{G}}^i dv' \,. \tag{2.84}$$

The $\hat{y}$ and $\hat{z}$ components are given by (2.83)

$$H_{qy}^i = \frac{1}{\mu_0}\left(\frac{\partial A_{qx}^i}{\partial z} - \frac{\partial A_{qz}^i}{\partial x}\right) \tag{2.85}$$

$$H_{qz}^i = -\frac{1}{\mu_0}\frac{\partial A_{qx}^i}{\partial y} \tag{2.86}$$

with

$$A_{qx}^i = \mu_0 \int\int_{S_q} \psi(y')\alpha_q(x')G_{xx}^i ds' \tag{2.87}$$

$$A_{qz}^i = \mu_0 \int\int_{S_q} \psi(y')\alpha_q(x')G_{xz}^i ds' \,. \tag{2.88}$$

We now substitute from these equations back into (2.85) and (2.86) to obtain

$$H_{qy}^i = \int\int_{S_q}\left(\frac{\partial G_{xx}^i}{\partial z} - \frac{\partial G_{xz}^i}{\partial x}\right)\psi(y')\alpha_q(x')ds' \tag{2.89}$$

$$H_{qz}^i = -\int\int_{S_q}\frac{\partial G_{xx}^i}{\partial y}\psi(y')\alpha_q(x')ds' \,. \tag{2.90}$$

These components are evaluated in Appendix G (for $i = 1, 2$). Setting $x = 0$ in the resulting expressions yields:

$$H_{qy}^{(1)}(x=0) = H_0 \sum_{m=1}^{\infty}\sum_{n=0}^{\infty} c_{nq}c_{ymn}^{(1)} \sin k_y y \cos k_z^{(1)} z \tag{2.91}$$

$$H_{qz}^{(1)}(x=0) = H_0 \sum_{m=1}^{\infty}\sum_{n=0}^{\infty} c_{nq}c_{zmn}^{(1)} \cos k_y y \sin k_z^{(1)} z \tag{2.92}$$

$$H_{qy}^{(2)}(x=0) = H_0 \sum_{m=1}^{\infty}\sum_{n=0}^{\infty} c_{nq}c_{ymn}^{(2)} \sin k_y y \cos k_z^{(2)}(z-c) \tag{2.93}$$

$$H_{qz}^{(2)}(x=0) = H_0 \sum_{m=1}^{\infty}\sum_{n=0}^{\infty} c_{nq}c_{zmn}^{(2)} \cos k_y y \sin k_z^{(2)}(z-c) \tag{2.94}$$

where

$$H_0 = \frac{k}{ab \sin K l_x} \tag{2.95}$$

$$c_{nq} = \zeta_q \cos k_x x_q \sin R_{1n} \sin R_{2n} \tag{2.96}$$

$$\begin{aligned} c_{ymn}^{(1)} = {} & \frac{\varphi_n \tan k_z^{(2)}(h-c)}{d_{1mn}d_{2mn}d_{3n}\cos k_z^{(1)}h} \Big\{ \Big[(k_z^{(1)})^2 + k_x^2(1-\epsilon_r^*) \Big] \tan k_z^{(1)}h \\ & - k_z^{(1)}k_z^{(2)}\epsilon_r^* \tan k_z^{(2)}(h-c) \Big\} \sin(k_y Y_0) J_0\left(\frac{k_y W}{2}\right) \end{aligned} \tag{2.97}$$

$$c_{zmn}^{(1)} = \frac{\varphi_n \tan k_z^{(2)}(h-c)}{d_{1mn}d_{3n}\cos k_z^{(1)}h} \sin(k_y Y_0) J_0\left(\frac{k_y W}{2}\right) \tag{2.98}$$

$$\begin{aligned} c_{ymn}^{(2)} = {} & \frac{\varphi_n \tan k_z^{(1)}h}{d_{1mn}d_{2mn}d_{3n}\cos k_z^{(2)}(h-c)} \Big\{ k_z^{(2)}k_z^{(1)} \tan k_z^{(1)}h \\ & - \Big[(k_z^{(2)})^2\epsilon_r^* - k_x^2(1-\epsilon_r^*) \Big] \tan k_z^{(2)}(h-c) \Big\} \sin(k_y Y_0) J_0\left(\frac{k_y W}{2}\right) \end{aligned} \tag{2.99}$$

$$c_{zmn}^{(2)} = \frac{\varphi_n \tan k_z^{(1)}h}{d_{1mn}d_{3n}\cos k_z^{(2)}(h-c)} \sin(k_y Y_0) J_0\left(\frac{k_y W}{2}\right) \tag{2.100}$$

and

$$d_{3n} = K^2 - k_x^2 \tag{2.101}$$

$$R_{1n} = \frac{1}{2}(K + k_x) l_x \tag{2.102}$$

$$R_{2n} = \frac{1}{2}(K - k_x) l_x \tag{2.103}$$

$$K = \omega\sqrt{\mu_0\epsilon_0\epsilon_r}\,. \tag{2.104}$$

Coordinate transformation and evaluation of $H_{q\phi}$

Equations (2.91)-(2.94) give the $\hat{y}$ and $\hat{z}$ components of the magnetic field anywhere inside the cavity. To find the $\hat{\phi}$ component we will perform the necessary coordinate transformation in two steps:

Table 2.1: COORDINATE TRANSFORMATION VARIABLES

VARIABLE RELATIONS	UNIT VECTOR RELATIONS
$x'' = x$	$\hat{x}'' = \hat{x}$
$y'' = y - Y_c = \rho\cos\phi$	$\hat{y}'' = \hat{y} = \cos\phi\hat{\rho} - \sin\phi\hat{\phi}$
$z'' = z - h_c = \rho\cos\phi$	$\hat{z}'' = \hat{z} = \sin\phi\hat{\rho} + \cos\phi\hat{\phi}$

1. move the origin from the corner of the cavity to the center of the coaxial feeding aperture.

2. perform a cartesian to cylindrical coordinate transformation.

Referring to Figure 2.9, let us denote a new coordinate system by (x'', y'', z'') whose origin is at the feed's center $(x, y, z) = (0, Y_c, h_c)$. The relationship between the new and old coordinates are outlined in Table 2.1.

Using these relations, we will make the following substitutions in (2.91)-(2.94) to move the origin to the feed's center

$$y \rightarrow y'' + Y_c$$

$$z \rightarrow z'' + h_c$$

This yields:

$$H_{qy}^{(1)}(x=0) = H_0 \sum_{m=1}^{\infty}\sum_{n=0}^{\infty} c_{nq} c_{ymn}^{(1)} \sin k_y(y'' + Y_c)\cos k_z^{(1)}(z'' + h_c) \quad (2.105)$$

$$H_{qz}^{(1)}(x=0) = H_0 \sum_{m=1}^{\infty}\sum_{n=0}^{\infty} c_{nq} c_{zmn}^{(1)} \cos k_y(y'' + Y_c)\sin k_z^{(1)}(z'' + h_c) \quad (2.106)$$

$$H_{qy}^{(2)}(x=0) = H_0 \sum_{m=1}^{\infty}\sum_{n=0}^{\infty} c_{nq} c_{ymn}^{(2)} \sin k_y(y'' + Y_c)\cos k_z^{(2)}(z'' - c'') \quad (2.107)$$

$$H_{qz}^{(2)}(x=0) = H_0 \sum_{m=1}^{\infty}\sum_{n=0}^{\infty} c_{nq} c_{zmn}^{(2)} \cos k_y(y'' + Y_c)\sin k_z^{(2)}(z'' - c'') \quad (2.108)$$

where

$$c'' = c - h_c \, . \tag{2.109}$$

Now, let $\bar{H}^i_{qt}$ represent the projection of $\bar{H}^i_q$ onto the plane of the aperture, then

$$\bar{H}^i_{qt} = H^i_{qy}\hat{y} + H_{qz}\hat{z} = H^i_{q\phi}\hat{\phi} + H_{q\rho^i}\hat{\rho} \tag{2.110}$$

where $H^i_{q\rho}$ and $H^i_{q\phi}$ are the $\hat{\rho}$ and $\hat{\phi}$ components respectively.

From Table 2.1.

$$\begin{aligned} \hat{y} &= \cos\phi\hat{\rho} - \sin\phi\hat{\phi} \\ \hat{y} &= \cos\phi\hat{\rho} - \sin\phi\hat{\phi} \end{aligned}$$

Hence,

$$H^i_{q\phi} = -\sin\phi H^i_{qy} + \cos\phi H^i_{qz} \, . \tag{2.111}$$

If we substitute from (2.105)-(2.108) into the above, and let

$$\begin{aligned} y'' &\rightarrow \rho\cos\phi \\ z'' &\rightarrow \rho\sin\phi \end{aligned}$$

we obtain

$$\begin{aligned} &H^{(1)}_{q\phi}(x=0) = \\ &\quad H_0\Bigg[-\sin\phi\sum_{m=1}^{\infty}\sum_{n=0}^{\infty} c_{nq}c^{(1)}_{ymn}\sin k_y(\rho\cos\phi + Y_c)\cos k^{(1)}_z(\rho\sin\phi + h_c) \\ &\quad + \cos\phi\sum_{m=1}^{\infty}\sum_{n=0}^{\infty} c_{nq}c^{(1)}_{zmn}\cos k_y(\rho\cos\phi + Y_c)\sin k^{(1)}_z(\rho\sin\phi + h_c)\Bigg] \end{aligned} \tag{2.112}$$

$$\begin{aligned} &H^{(2)}_{q\phi}(x=0) = \\ &\quad H_0\Bigg[-sin\phi\sum_{m=1}^{\infty}\sum_{n=0}^{\infty} c_{nq}c^{(2)}_{ymn}\sin k_y(\rho\cos\phi + Y_c)\cos k^{(2)}_z(\rho\sin\phi - c'') \\ &\quad + \cos\phi\sum_{m=1}^{\infty}\sum_{n=0}^{\infty} c_{nq}c^{(2)}_{zmn}\cos k_y(\rho\cos\phi + Y_c)\sin k^{(2)}_z(\rho\sin\phi - c'')\Bigg] \, . \end{aligned} \tag{2.113}$$

2.5.3 Formulation for numerical integration

Consider now the surface integral of (2.82). One factor that complicates the integration is that it must be performed in two regions whose boundaries depend on the feed position as can be seen in Figure 2.9. In other words, the integration can be broken up as follows:

$$\begin{aligned} V_q &= -\frac{V_0}{\ln\left(\frac{r_b}{r_a}\right)} \int\int_{S_{feed}} H_q^i d\rho d\phi \\ &= -\frac{V_0}{\ln\left(\frac{r_b}{r_a}\right)} \left[\int\int_{S_{feed}^{(1)}} H_q^{(1)} d\rho d\phi + \int\int_{S_{feed}^{(2)}} H_q^{(2)} d\rho d\phi \right] \end{aligned} \tag{2.114}$$

where

$S_{feed}^{(1)}$ is the portion of the feed surface lying below the substrate ($z'' = \rho \sin\phi \leq -t$)

$S_{feed}^{(2)}$ is the portion of the feed surface lying above the substrate ($z'' = \rho \sin\phi \geq -t$)

To perform the above integration in the most general form we will make use of a 16 point Product Gauss formula approximation method [21]. Let us define a pair of dummy variables s and u and a function $\mathcal{F}(s,u)$ such that

$$\int_{\phi_{min}=0}^{\phi_{max}=2\pi} \int_{\rho_{min}=r_a}^{\rho_{max}=r_b} H_{q\phi}^i d\rho d\phi = \int_{s_{min}=-1}^{s_{max}=1} \int_{u_{min}=-1}^{u_{max}=1} \mathcal{F}(s,u) ds \tag{2.115}$$

where the correspondence between (u,s) and (ρ,ϕ) is given by the following relations

$$u = \frac{2\rho - (\rho_{max} + \rho_{min})}{\rho_{max} - \rho_{min}} = \frac{2\rho - (r_b - r_a)}{r_b - r_a} \tag{2.116}$$

$$\rho = \frac{1}{2}[u(r_b - r_a) + (r_b + r_a)] \tag{2.117}$$

$$s = \frac{2\phi - (\phi_{max} + \phi_{min})}{\phi_{max} - \phi_{min}} = \phi/\pi - 1 \tag{2.118}$$

$$\phi = \pi(s+1) \tag{2.119}$$

The numerical integration can be carried out by generating a set of 16 pairs of points (u_j, s_j) and adding up their contributions according to

$$\int_{\phi_{min}=0}^{\phi_{max}=2\pi} \int_{\rho_{min}=r_a}^{\rho_{max}=r_b} H_{q\phi}^i d\rho d\phi \doteq \sum_{j=1}^{16} B_j \mathcal{F}(u_j, s_j) \tag{2.120}$$

where

(u_j, s_j) is the j^th pair of integration points, and

B_j is the weighting factor associated with the j^th pair of integration points

$\mathcal{F}(s_j, u_j)$ is the transformed integrand found by performing a coordinate transformation on $H_{q\phi}$.

Alternatively, once we have chosen the 16 points (s_j, u_j), we can find the corresponding values of ρ and ϕ by (2.117) and (2.119) and obtain the same result. That is

$$\int_{\phi_{min}=0}^{\phi_{max}=2\pi} \int_{\rho_{min}=r_a}^{\rho_{max}=r_b} H^i_{q\phi} d\rho d\phi = \sum_{j=1}^{16} B_j \mathcal{H}(\rho_j, \phi_j) \tag{2.121}$$

where

$$\rho_j = \frac{1}{2}[u_j(r_b - r_a) + (r_b + r_a)]$$

$$\phi_j = \pi(s_j + 1)$$

and

$$\mathcal{H}(\rho_j, \phi_j) = \begin{cases} H^{(1)}_{q\phi}(\rho_j, \phi_j) & for \ -h_c \le \rho_j \sin\phi_j \le -t \\ H^{(2)}_{q\phi}(\rho_j, \phi_j) & for \ -t \le \rho_j \sin\phi_j \le c'' = c - h_c \\ error\ condition & \text{else .} \end{cases} \tag{2.122}$$

2.6 MODIFICATIONS FOR ANALYSIS OF TWO PORT STRUCTURES

In the preceeding sections, the theory has been advanced for computing the impedance matrix and excitation vector associated with a one-port network, such as an open circuited transmission line (Figure 2.5). This section will present modifications necessary to extend the theory for treatment of two-port structures. Our approach for computing the network parameters of two-ports, requires simultaneous excitation of the strip conductors from both sides of the cavity. We will refer to this as "dual excitation".

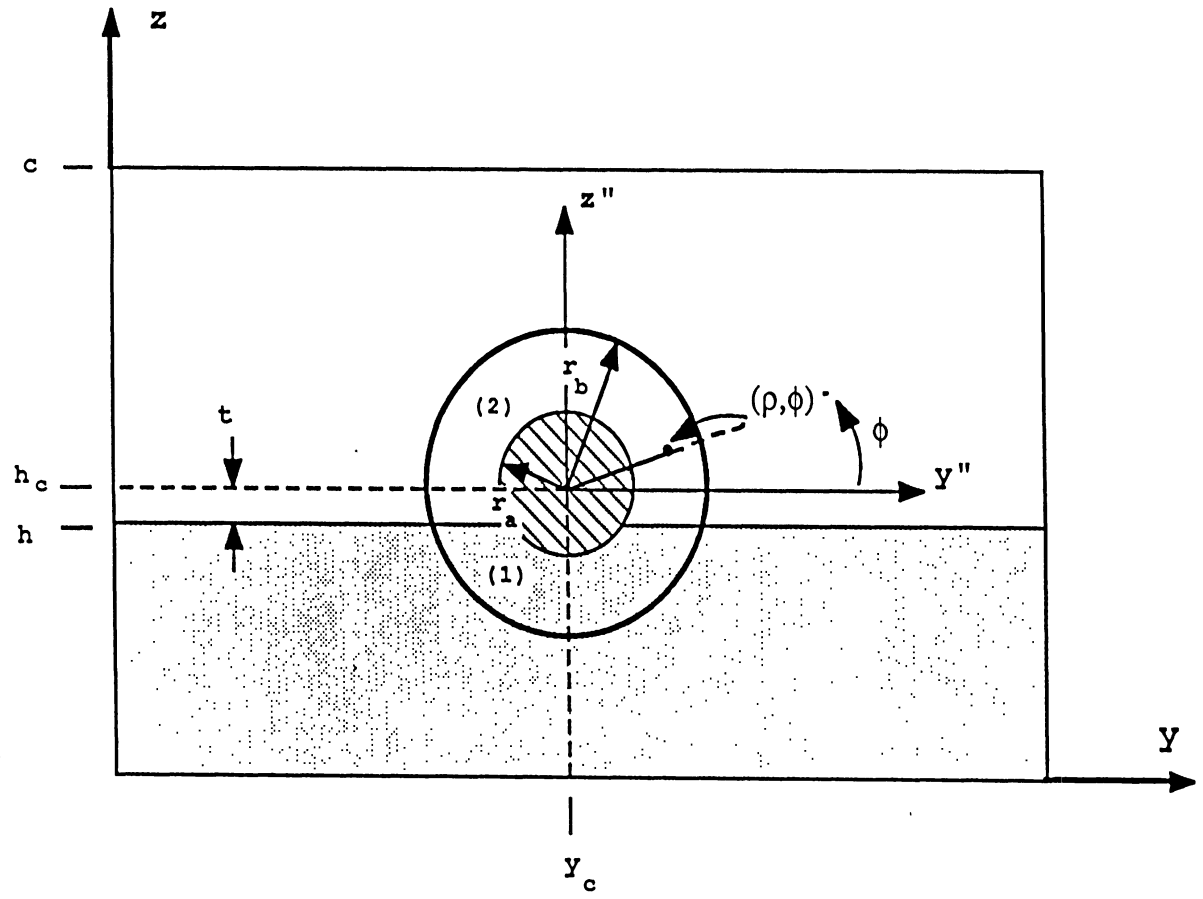

Figure 2.9: Geometry used for numerical integration to compute excitation vector. Note: the relative size of the feed is exaggerated for clarity

2.6.1 Application of reciprocity for dual excitation

In section 2.2.1 an integral equation (2.3) was derived by applying the reciprocity theorem to the one-port network of Figure 2.5. In an analogous fashion, we will now apply the reciprocity theorem to the two- port network of Figure 2.10.

In Figure 2.10, both magnetic current sources $M_{\phi 1}$ and $M_{\phi 2}$ are coupled with the electric current source $\bar{J}_s$ on the conducting strips to produce the total electric field $\bar{E}^{tot}$, and magnetic field $\bar{H}^{tot}$ inside the cavity. As before, we consider an independent test source $\bar{J}_q$ and associated fields $\bar{E}_q$ and $\bar{H}_q$ as shown in Figure 2.6. Applying reciprocity theorem between these two sets of sources yields

$$\begin{aligned} \int\int\int_V (\bar{J}_s \cdot \bar{E}_q - \bar{H}_q \cdot \bar{M}_{s1} - \bar{H}_q \cdot \bar{M}_{s2})\, dv &= \int\int\int_V \bar{J}_q \cdot \bar{E}^{tot} dv \\ &= 0 \end{aligned} \tag{2.123}$$

where the volume V is the interior of the cavity and

$$\bar{M}_{s1} = M_{\phi 1}\hat{\phi} \tag{2.124}$$

$$\bar{M}_{s2} = M_{\phi 2}\hat{\phi}. \tag{2.125}$$

The right hand side of (2.123) vanishes as as described by (2.2). Reducing the remaining volume integrals of (2.123) to the appropriate surface integrals gives

$$\int\int_{S_{strip}} \bar{E}_q(z=h) \cdot \bar{J}_s ds = \int\int_{S_{feed1}} \bar{H}_q(x=0) \cdot \bar{M}_{s1} ds + \int\int_{S_{feed2}} \bar{H}_q(x=a) \cdot \bar{M}_{s2} ds\,. \tag{2.126}$$

Comparing the above to (2.3) it can be seen as a natural extension to the theory for the case of single excitation (one-port analysis).

2.6.2 Expansion of current and modified matrix equation

The current $\bar{J}_s$ is again expanded according to (2.4)

$$\bar{J}_s = \psi(y) \sum_{p=1}^{NSECT} I_p \alpha_p(x)\, \hat{x}$$

The only difference is that we now must consider the basis function for the x-dependence on the last subsection (i.e. closest to the right-most feed) as a special case. This is necessary since at each end of the cavity only a half sinusoidal basis function is required as illustrated in Figure 2.11. Hence, for the right-most subsection we let

$$\alpha_{NSECT}(x) = \begin{cases} \frac{\sin[K(x-a)]}{\sin(Kl_x)} & x_{NSECT-1} \leq x \leq a \\ 0 & else \end{cases} \tag{2.127}$$

where the quantities K and l_x are as defined in section 2.2.2, and NSECT represents the index for the right-most subsection. The rest of the basis function expansion is the same as given by (2.5)-(2.7).

Substituting (2.4) into (2.126) yields

$$\begin{aligned} \sum_{p=1}^{NSECT} \left[\int\int_{S_p} \bar{E}_q(x=h) \cdot \psi(y)\, \alpha_p(x)\, \hat{x} ds \right] I_p = \\ \int\int_{S_{feed1}} \bar{H}_q(x=0) \cdot \bar{M}_{s1} ds \\ + \int\int_{S_{feed2}} \bar{H}_q(x=a) \cdot \bar{M}_{s2} ds \end{aligned} \tag{2.128}$$

which can be expressed as

$$[Z_{qp}][I_p] = [V_{q1}] + [V_{q2}] \tag{2.129}$$

where

S_p is the surface area of the p^{th} subsection

$[Z_{qp}]$ is the impedance matrix, which has the dimensions of NSECT x NSECT

$[I_p]$ is the unknown current vector (NSECT x 1)

$[V_{q1}]$ is the excitation vector of the feed on the left (NSECT x 1)

$[V_{q2}]$ is the excitation vector of the feed on the right (NSECT x 1)

$$V_{q1} = \int\int_{S_{feed1}} \bar{H}_q(x=0) \cdot \bar{M}_{s1} ds \tag{2.130}$$

$$V_{q2} = \int\int_{S_{feed2}} \bar{H}_q(x=a) \cdot \bar{M}_{s2} ds \tag{2.131}$$

We can now solve for the current vector by matrix inversion and multiplication according to

$$[I_p] = [Z_{qp}]^{-1}\,[[V_{q1}] + [V_{q2}]] \; . \tag{2.132}$$

2.6.3 Modifications to impedance matrix

The elements of the impedance matrix for the case of dual excitation are given by the same integral equation as for the one port case, namely (2.10). The difference is in the integration over the last subsection ($p = NSECT$) where $\alpha_p(x)$ is now given by (2.127). The integration for E_{qx} given by (2.65) is also modified for the last subsection ($q = NSECT$) in a similar way. The resulting modifications to the impedance matrix are very straightforward. This is because it can easily be shown that the surface integration over the last subsection (i.e. closest to the feed on the right) is equivalent to the integration over the first subsection (i.e. closest to the feed on the left). Hence, the elements of the impedance matrix are again given by (2.79) the only change being that ζ_q and ζ_p are as redefined below rather than by (2.69) and (2.77)

$$\zeta_p = \begin{cases} 2 & for\ p = 1\ or\ p = NSECT \\ 4 & \text{else} \end{cases} \tag{2.133}$$

$$\zeta_q = \begin{cases} 2 & for\ q = 1\ or\ q = NSECT \\ 4 & \text{else} \; . \end{cases} \tag{2.134}$$

(2.135)

2.6.4 Modifications to excitation vector

We now consider the integrations of (2.130), and (2.131). By analogy with (2.81) we may express the two magnetic currents as follows:

$$\bar{M}_{s1} = -\frac{V_{01}}{\ln\left(\frac{r_b}{r_a}\right)\rho}\hat{\phi} \tag{2.136}$$

$$\bar{M}_{s2} = +\frac{V_{02}}{\ln\left(\frac{r_b}{r_a}\right)\rho}\hat{\phi} \tag{2.137}$$

where the positive sign in the second current source indicates that it is taken to be in the opposite sense (Figure 2.10) and

V_{01} is the complex voltage in the coaxial line at the left-hand feed

V_{02} is the complex voltage in the coaxial line at the right-hand feed

r_b is the radius of the coaxial feed's outer conductor

r_a is the radius of the coaxial feed's inner conductor

ρ, ϕ are cylindrical coordinates referenced to the feed's center

Substituting from (2.136) and (2.137) into (2.130) and (2.131) yields

$$V_{q1} = -\frac{V_{01}}{\ln\left(\frac{r_b}{r_a}\right)} \int\int_{S_{feed}} H_{q\phi}(x=0) d\rho d\phi \tag{2.138}$$

$$V_{q2} = \frac{V_{02}}{\ln\left(\frac{r_b}{r_a}\right)} \int\int_{S_{feed}} H_{q\phi}(x=0) d\rho d\phi \tag{2.139}$$

Now, the integration required for V_{q1} is identical to that carried out in section 2.5 for V_q (single excitation case). The computation of V_{q2} is only slightly modified as we need to shift the origin to $(x', y', z') = (a, Y_c, h_c)$ instead of to $(0, Y_c, h_c)$. After examining the x-dependence of $\bar{H}_q$ given in Appendix G it becomes obvious that we need only multiply the result for V_{q1} by $\cos n\pi$ to get the result for V_{q2}. That is

$$V_{q2} = -\frac{V_{01}}{V_{02}} \cos n\pi \; V_{q1}. \tag{2.140}$$

Let V_{qd} represent the excitation vector elements for dual excitation such that

$$V_{qd} = V_{q1} + V_{q2} \; .$$

Then

$$V_{qd} = \left(1 - \frac{V_{01}}{V_{02}} \cos n\pi\right) V_q \tag{2.141}$$

where V_q represents the excitation vector of section 2.5 with V_0 set equal to unity.

The next step is to find dual excitation vector for even and odd mode excitations. As will be discussed in section 2.7, we will find the two-port scattering parameters for a network by exciting it with even and odd modes.

For the even mode excitation, we let $V_{01} = V_{02} = 1$. In this case from (2.141) we have

$$\begin{aligned} V_{qe} &= V_{q1}(1 - \cos n\pi) \\ &= \begin{cases} 0 & \text{for n even} \\ 2V_q & \text{for n odd .} \end{cases} \end{aligned} \tag{2.142}$$

For the odd mode excitation, we let $V_{01} = -V_{02} = 1$. Now, using (2.141)

$$\begin{aligned} V_{qo} &= V_{q1}(1 + \cos n\pi) \\ &= \begin{cases} 2V_q & \textit{for n even} \\ 0 & \textit{for n odd} \end{cases} \end{aligned} \tag{2.143}$$

where

V_{qe} represents the elements of the even excitation vector

V_{qo} represents the elements of the odd excitation vector .

Using these two excitations, we can compute both the even and odd mode current distributions using the following matrix equations:

$$[I_{pe}] = [Z_{qp}]^{-1}[V_{qe}] \tag{2.144}$$

$$[I_{po}] = [Z_{qp}]^{-1}[V_{qo}] \tag{2.145}$$

where

I_{pe} represents the elements of the current vector for even excitation

I_{po} represents the elements of the current vector for odd excitation.

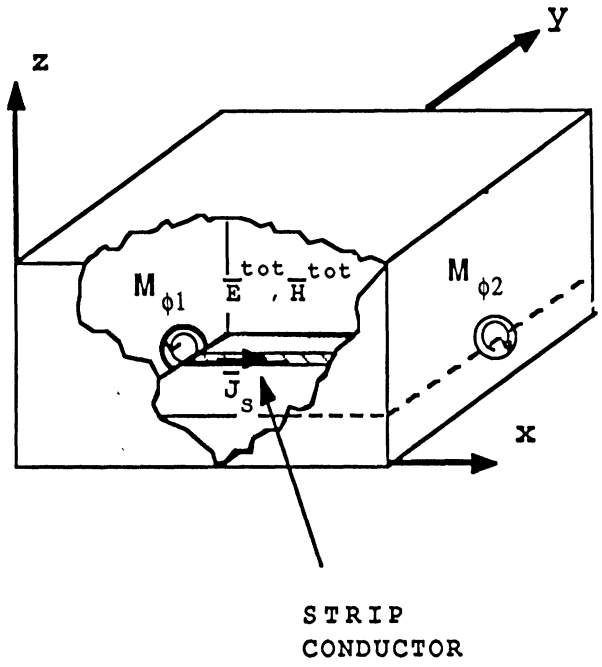

Figure 2.10: Total fields inside cavity $\bar{E}^{tot}, \bar{H}^{tot}$ produced by magnetic currents $M_{\phi 1}$, $M_{\phi 2}$, and electric current $\bar{J}_s$.

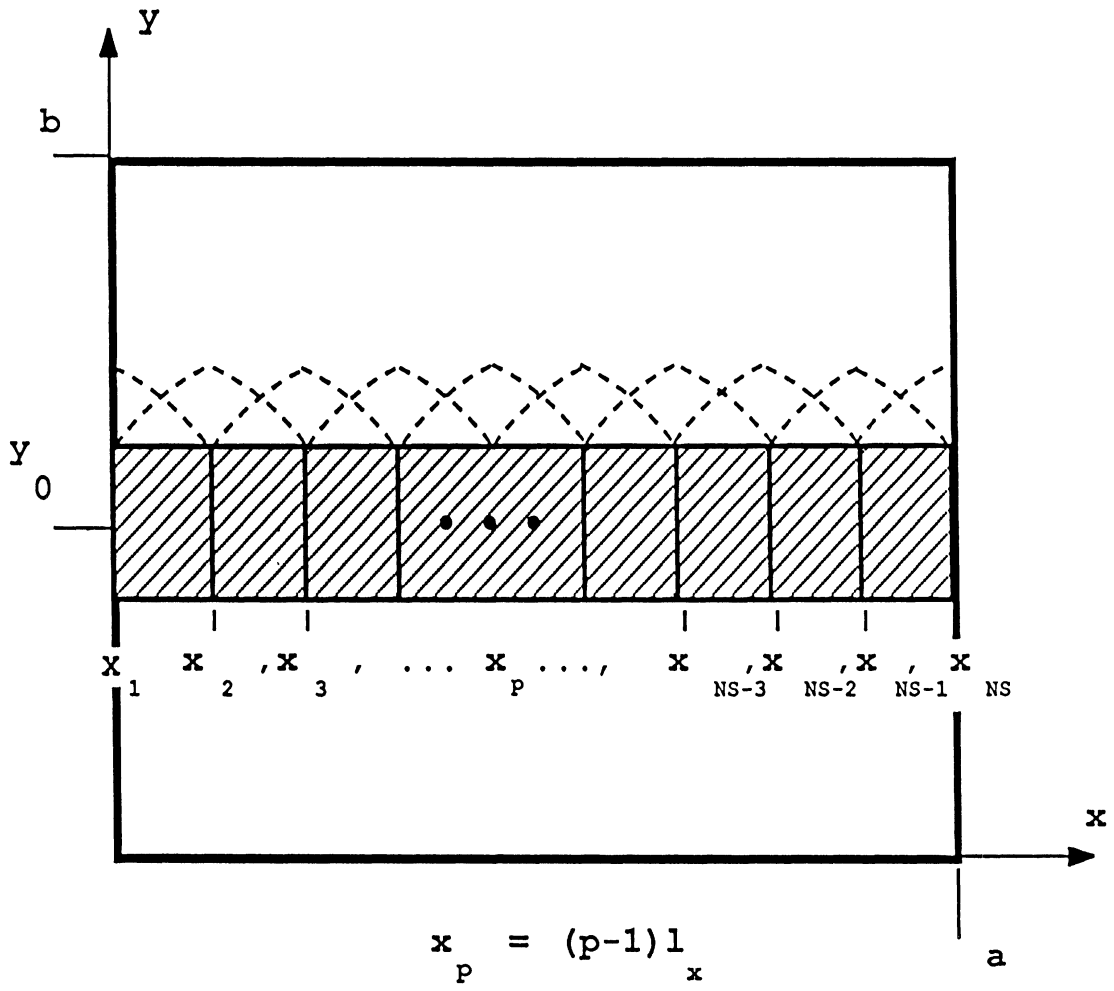

Figure 2.11: Strip geometry for basis function expansion with dual excitation.

CHAPTER III

PRELIMINARY RESULTS

The theoretical methodology described in Chapter 2 has been used as the basis for a computer algorithm which was implemented in a fortran program. This program has, so far, been used to obtain numerical results for the open end and series gap discontinuities. This chapter presents some of these results with comparisons to other numerical solutions and preliminary measured results obtained here at the University of Michigan.

3.1 RESULTS FOR OPEN END DISCONTINUITY

An open end discontinuity in shielded microstrip can be represented as an effective length extension L_{eff}, a shunt capacitance C_{op}, or by the associated reflection coefficient (Γ_{op}) as shown in Figure 3.1. The plot of Figure 3.2 contains the computed effective length for an open end on an alumina substrate (ϵ_r = 9.6, W/H = 1), and Figure 3.3 shows the same for a quartz substrate (ϵ_r = 3.82, W/H = 1.57). Our numerical results are shown compared to results obtained by Jansen et. al. [22] and Itoh [23]. The geometrical parameters of the cavity cross section used in the analysis for each of the above cases are (referring to Figure 2.8): $b = c = .275''$, and $H = .025''$. Also, in both cases the distance from the end of the microstrip line to the end of the cavity was fixed at $.125''$. For both the alumina and quartz cases, our results are seen to fall between the other two numerical results. From this we conclude that our results are at least reasonable.

A comparison with measured results is presented in Figure 3.4, which shows numerical and experimental data for Γ_{op} of an open circuit on an alumina ($\epsilon_r = 9.7, W/H = 1$) substrate. Here, our numerical results are compared with numerical data from *Super Compact* [1] [24] and preliminary measured results. The geometrical parameters for the cavity cross section in this case are: $b = c = .250''$, and $H = .025''$. The measured results are seen to follow our results most closely.

3.2 RESULTS FOR SERIES GAP DISCONTINUITY

A series gap in shielded microstrip may be represented as a pi arrangement of capacitances, or alternatively by a set of scattering parameters as shown in Figure 3.5. Numerical results have been obtained for series gaps on an alumina substrate ($\epsilon_r = 9.7$) with three different gap spacings (G) 5 mil (i.e. .005″), 9 mil, and 15 mil. Results for the scattering parameters of these gaps are shown plotted in Figures 3.6 through 3.13. The geometrical parameters of the cavity cross section are: $b = c = .250''$, and $H = .025''$. For comparison with our numerical results, results obtained using *Super Compact*, and *Touchstone* [25] are also shown plotted along with preliminary measured data.

With one exception, the measured data best follows our numerical results. The one exception was for the magnitude of S21 of the 5 mil gap. In contrast, the Touchstone analysis had the least agreement with the measurements. This may in part be due to the fact that *Touchstone* does not allow for taking either the side walls or the shielding cover into account.

In summary, our numerical results show reasonable agreement with other numerical solutions and, more importantly, demonstrate very good agreement with the measured

[1] It should be noted that *Super Compact* allows for specifying cover height, but does not take the effect of the side walls into account. However, for the given geometry, the effect of the side walls is minimal.

data obtained so far. We are in the process of obtaining another set of improved measurements as the present measured data shown here is not as smooth, as a function of frequency, as it should be.

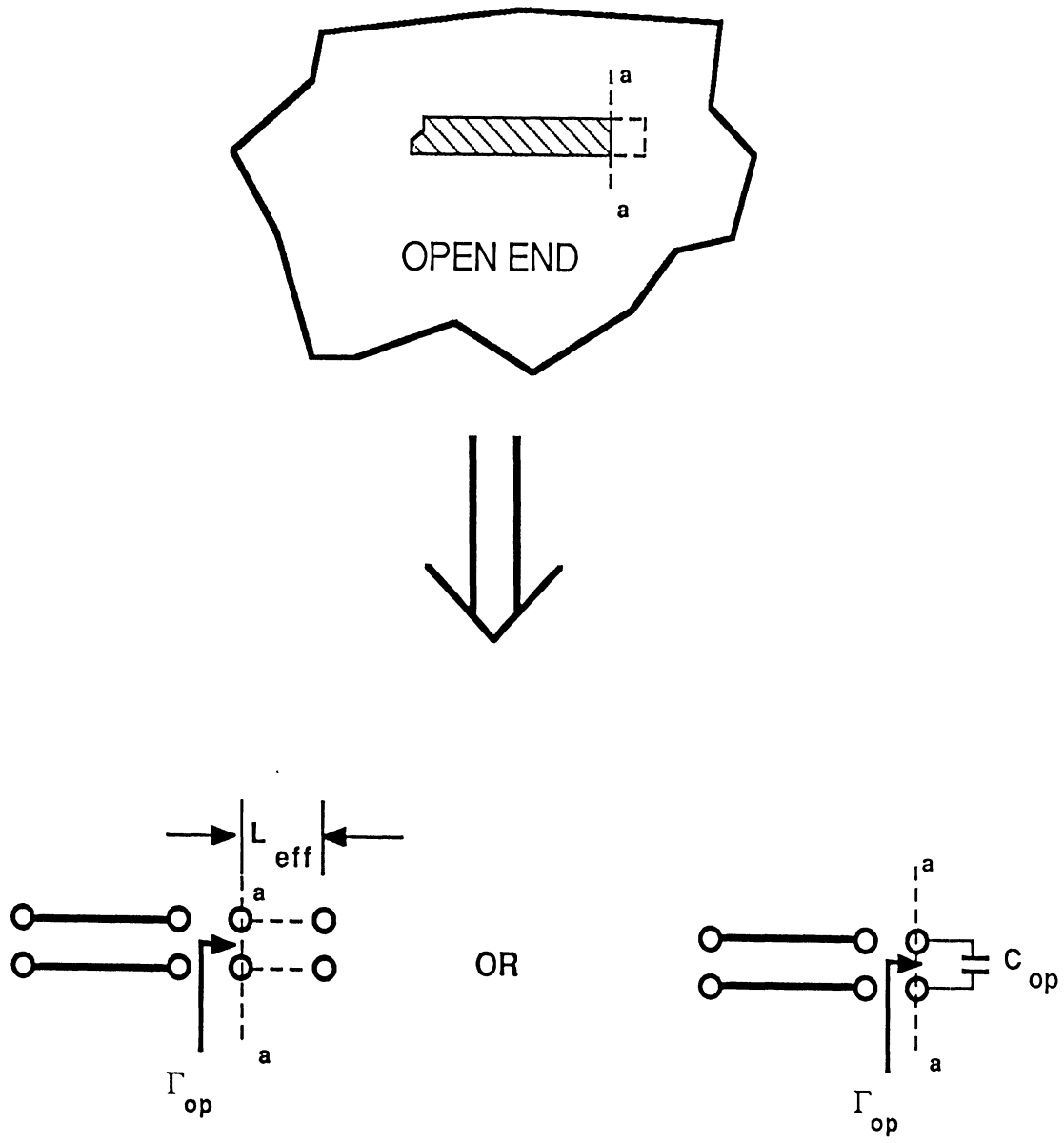

Figure 3.1: Representation for microstrip open end discontinuity

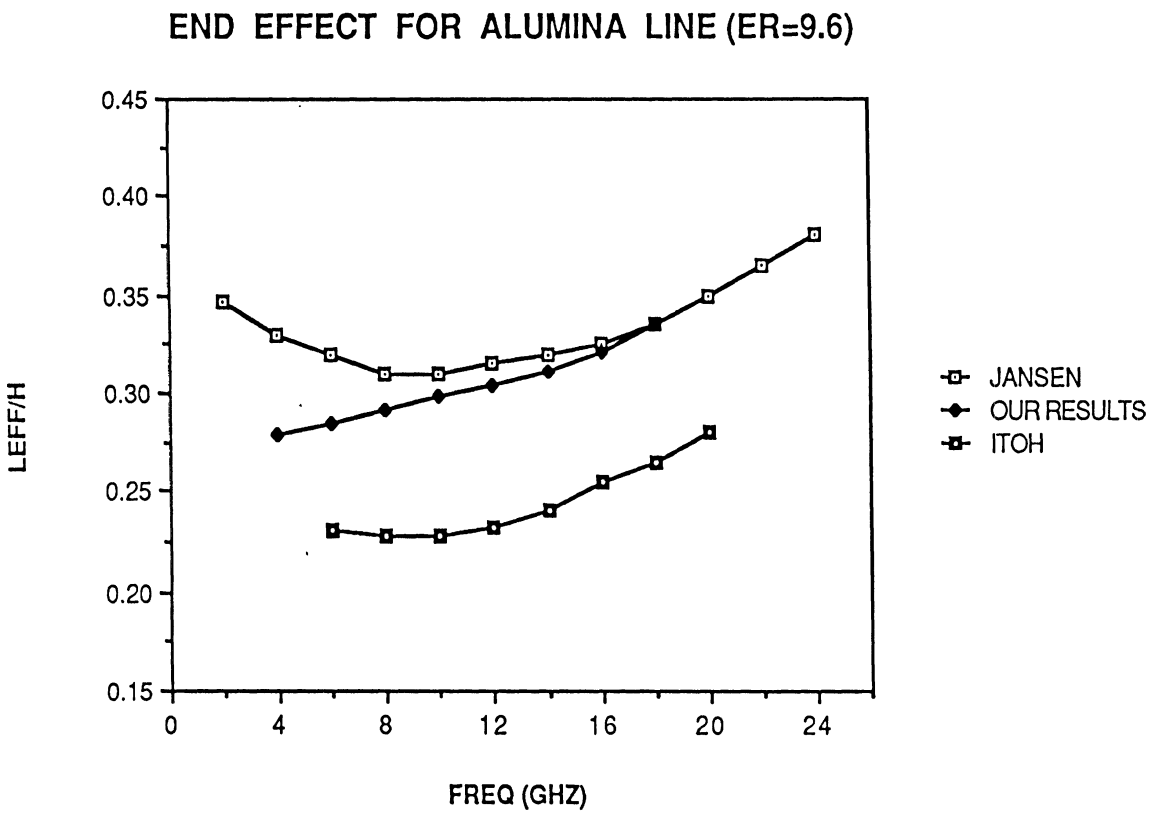

Figure 3.2: Effective length extension of a microstrip open circuit discontinuity on an alumina substrate ($\epsilon_r = 9.6$), as compared to other numerical results

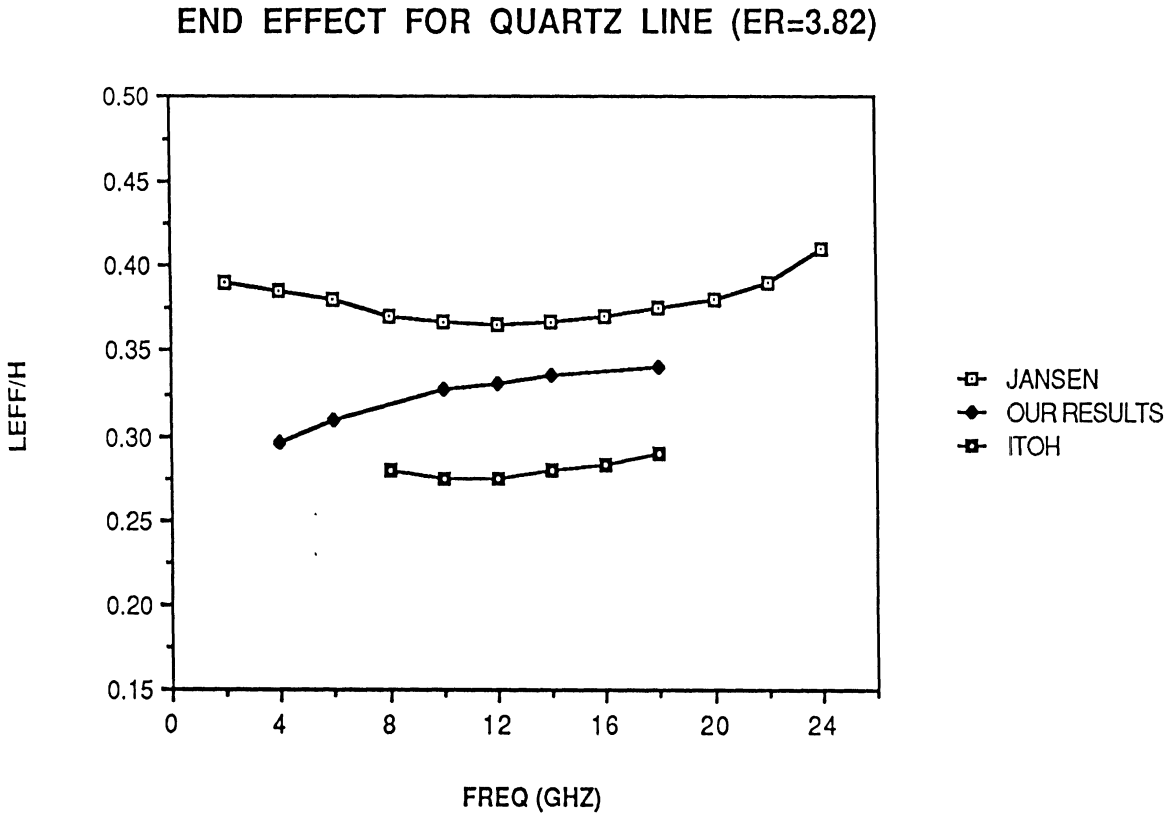

Figure 3.3: Effective length extension of a microstrip open circuit discontinuity on a quartz substrate ($\epsilon_r = 3.82$), as compared to other numerical results.

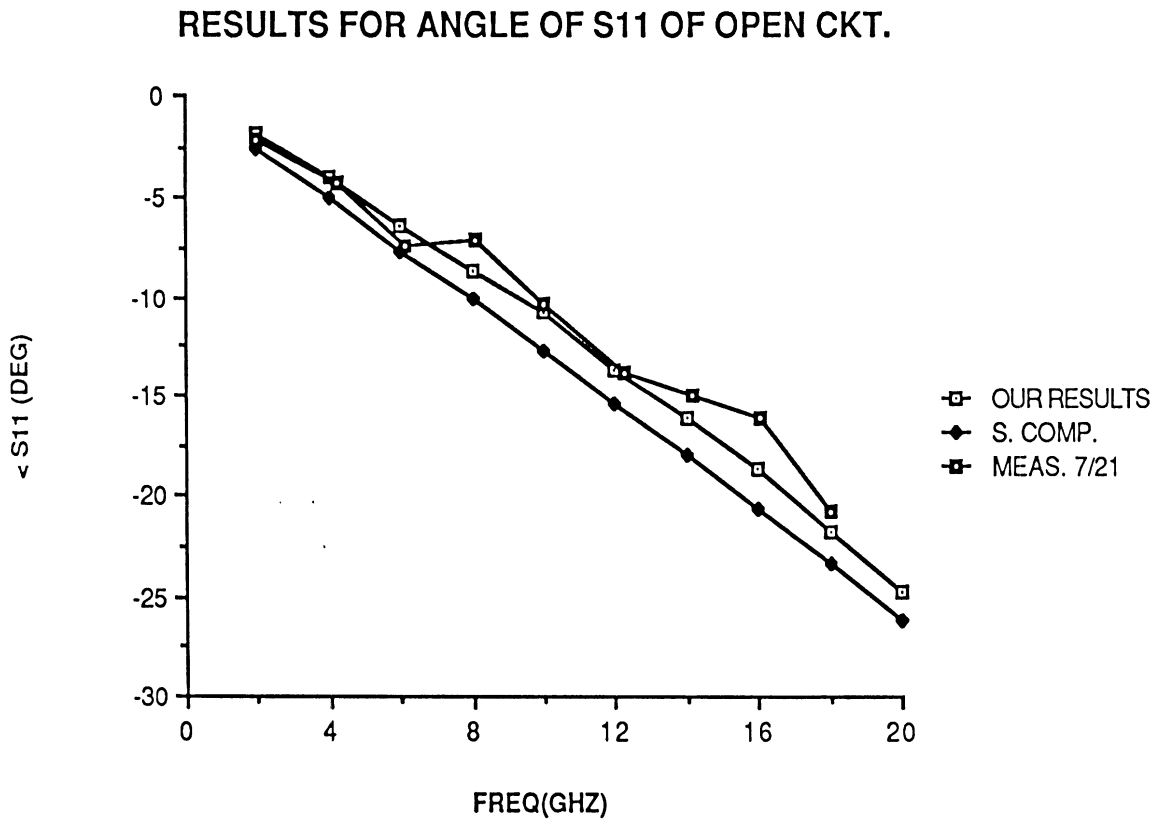

Figure 3.4: Angle of S11 of an open circuit as compared to measurements and *Super Compact* results.

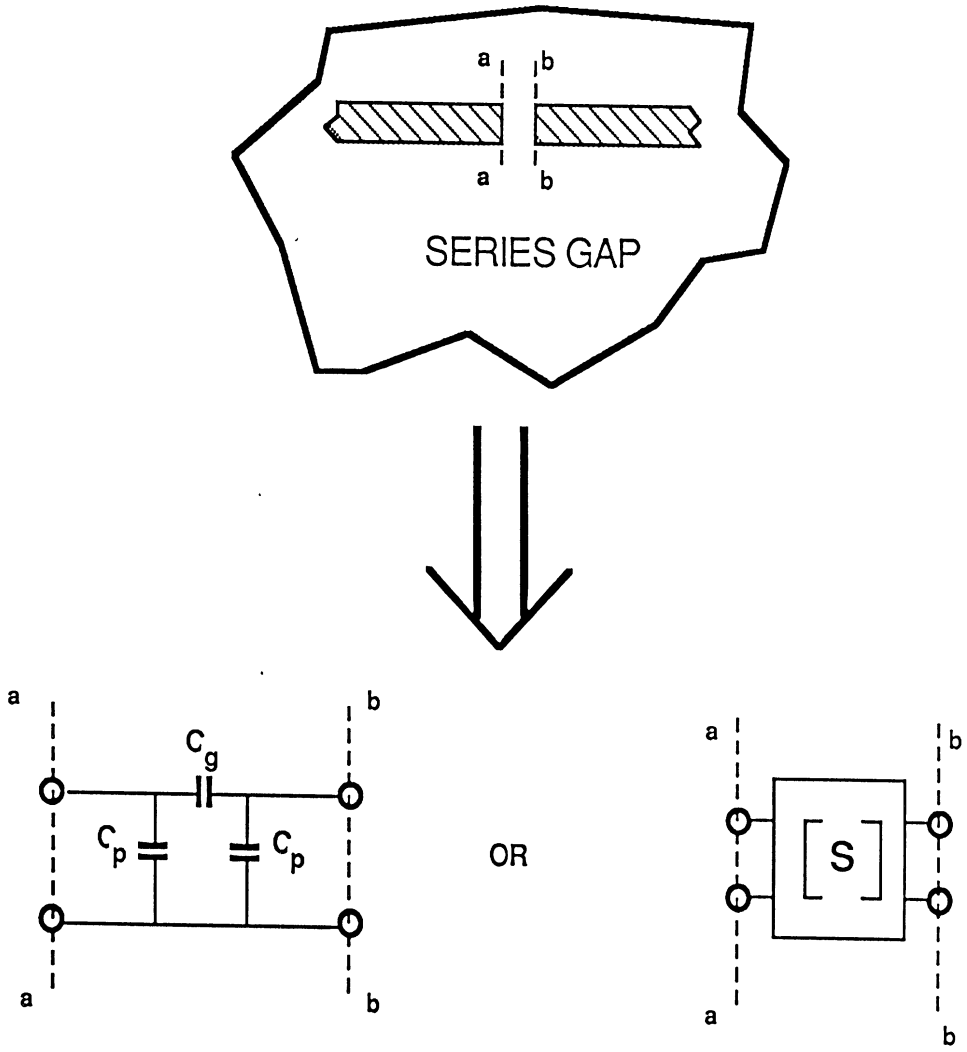

Figure 3.5: Representation for microstrip series gap discontinuity.

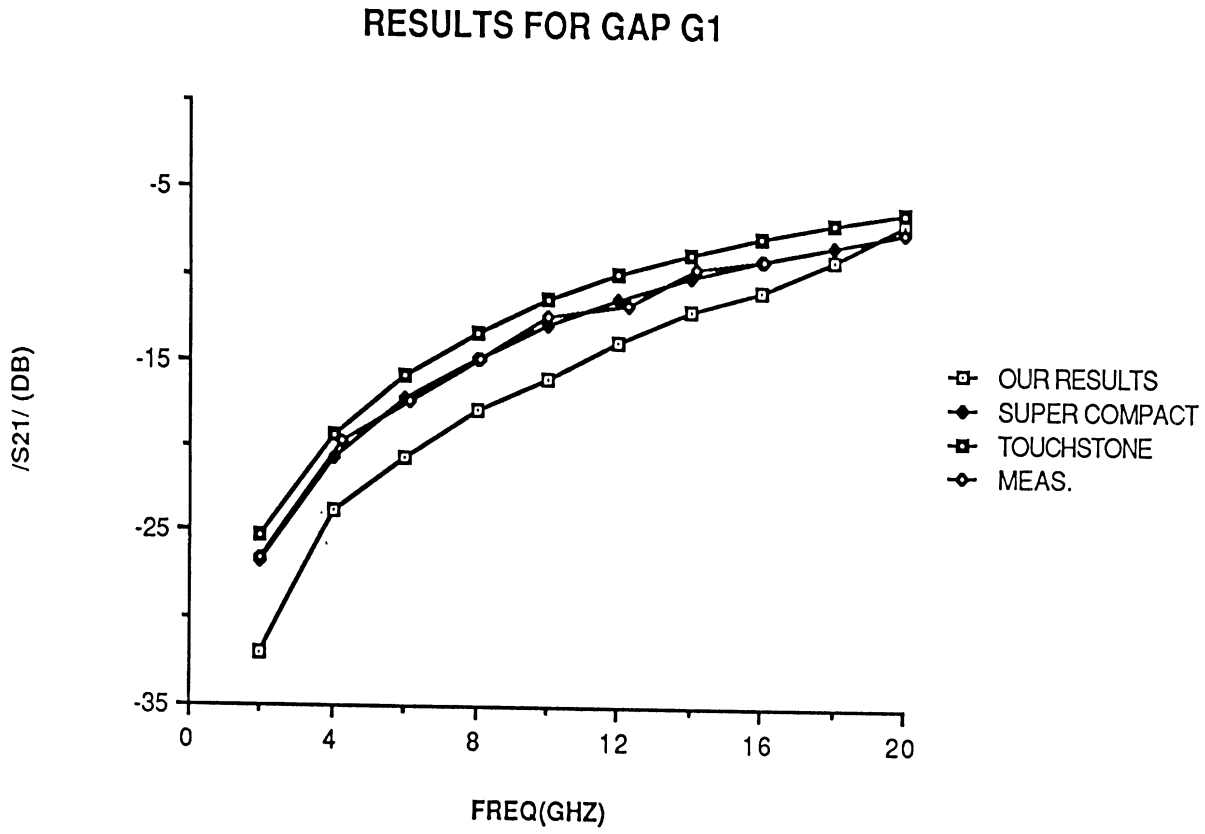

Figure 3.6: Magnitude of S21 for series gap G1 (G = 5 mil) as compared to measurements, *Super Compact*, and *Touchstone*.

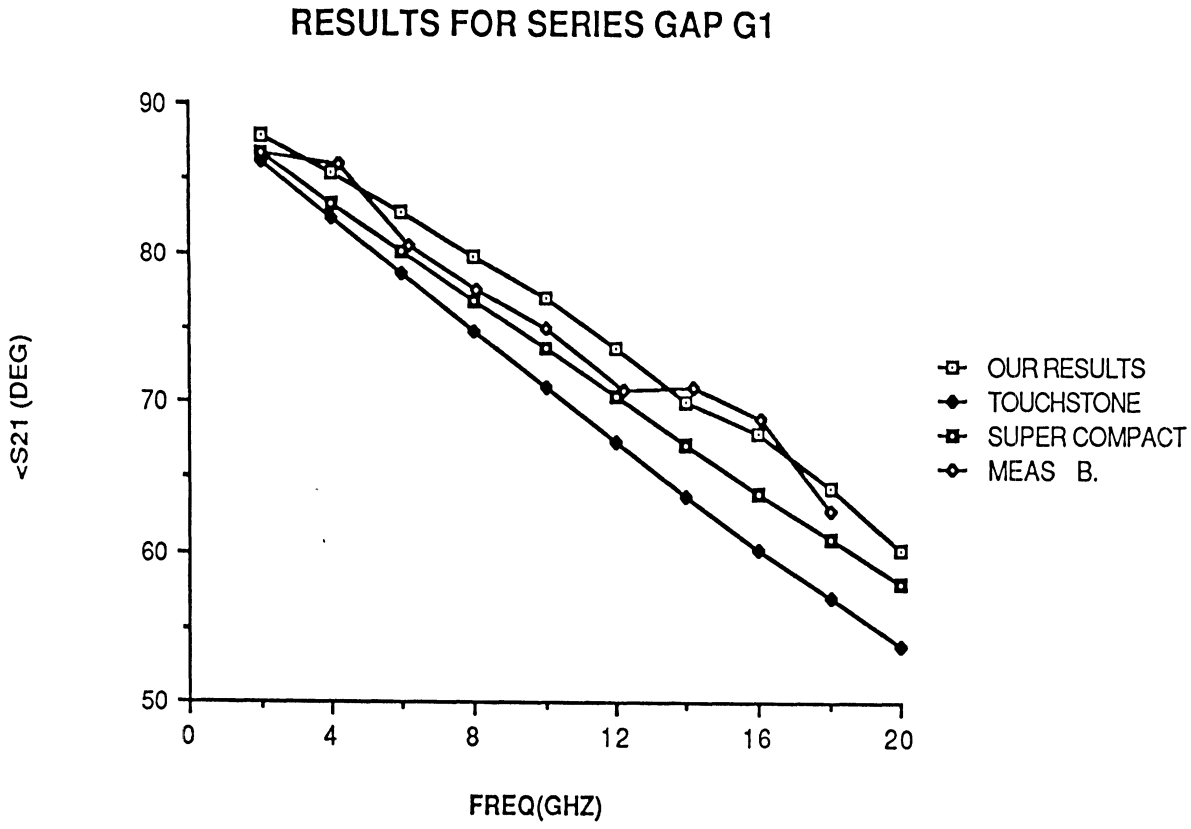

Figure 3.7: Angle of S21 for series gap G1 (G = 5 mil) as compared to measurements, *Super Compact*, and *Touchstone*.

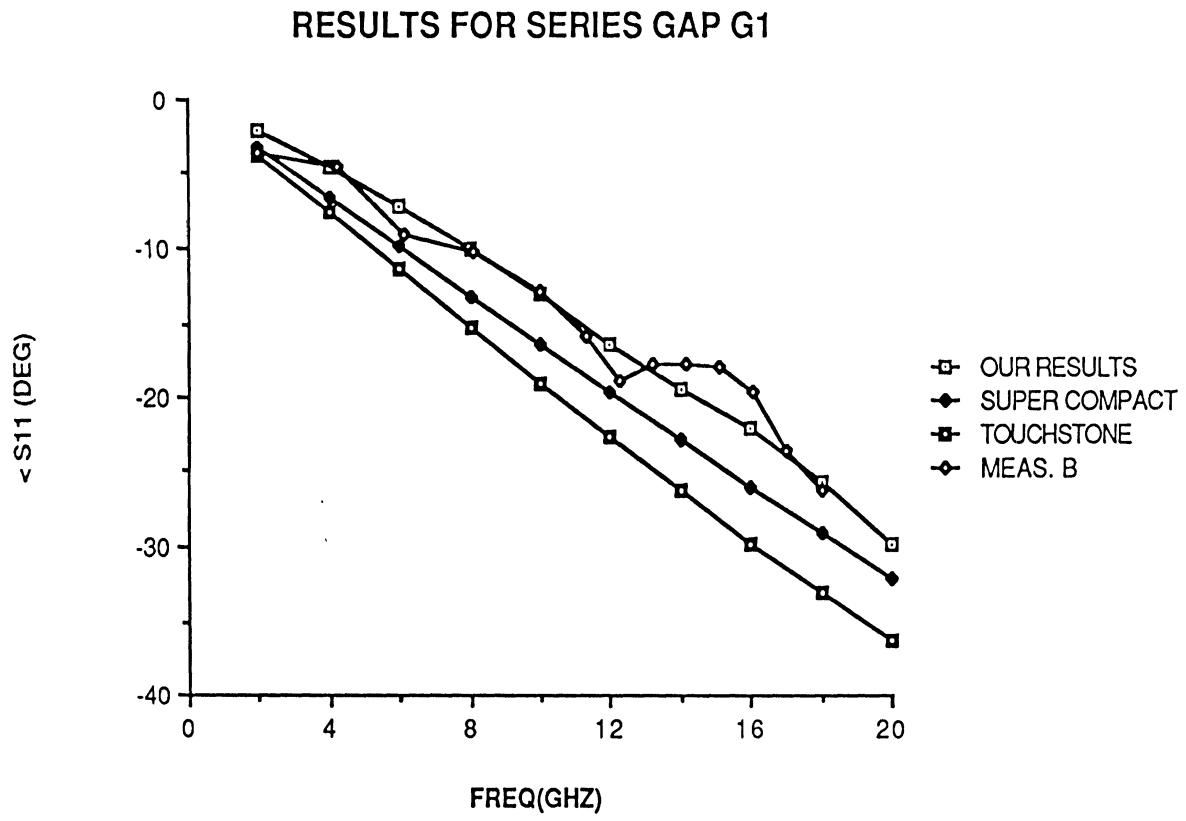

Figure 3.8: Angle of S11 for series gap G1 (G = 5 mil) as compared to measurements, *Super Compact*, and *Touchstone*.

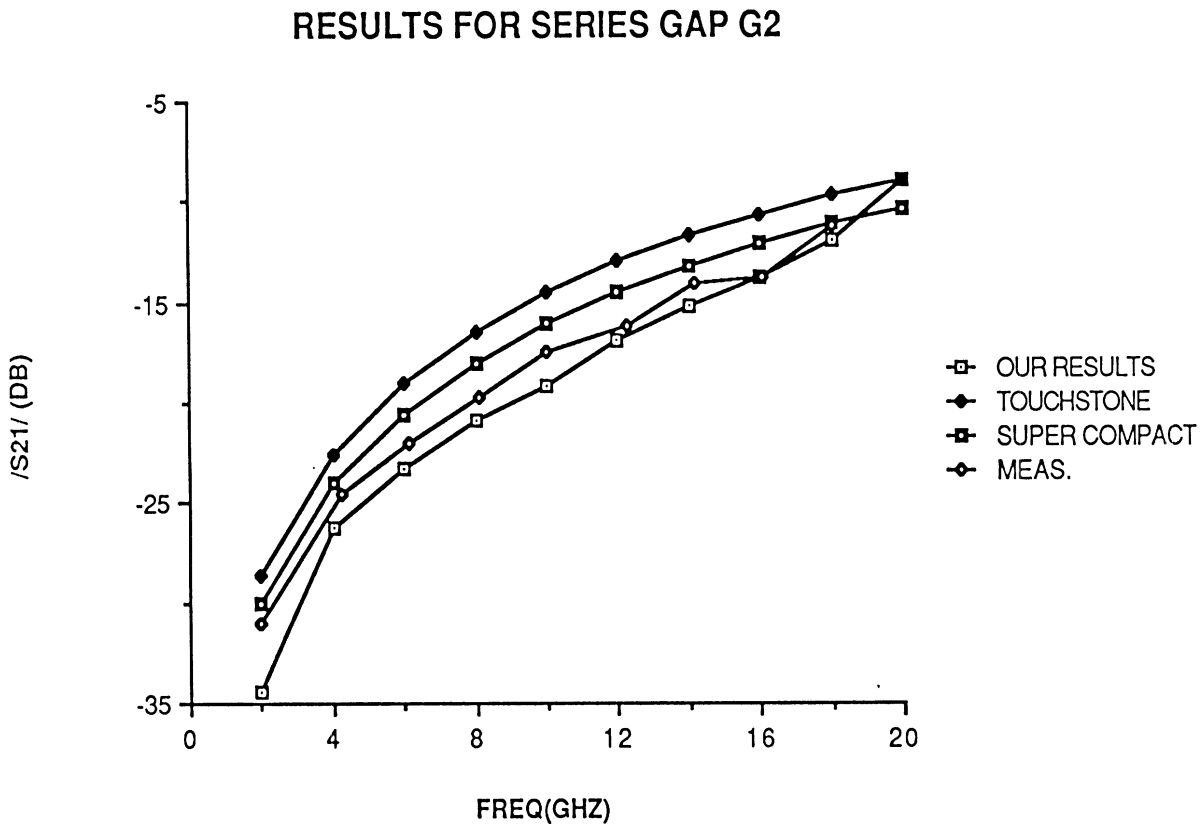

Figure 3.9: Magnitude of S21 for series gap G2 (G = 9 mil) as compared to measurements, *Super Compact*, and *Touchstone*.

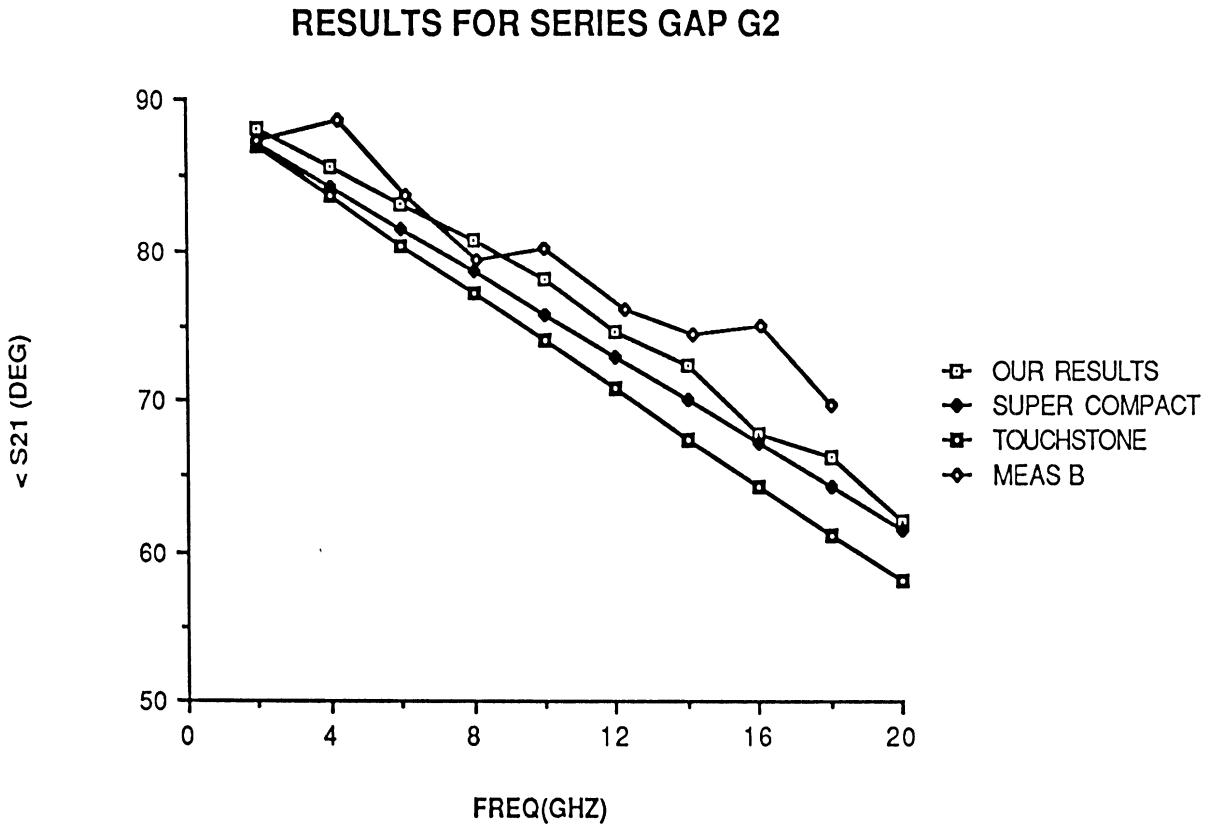

Figure 3.10: Angle of S21 for series gap G2 (G = 9 mil) as compared to measurements, *Super Compact*, and *Touchstone*.

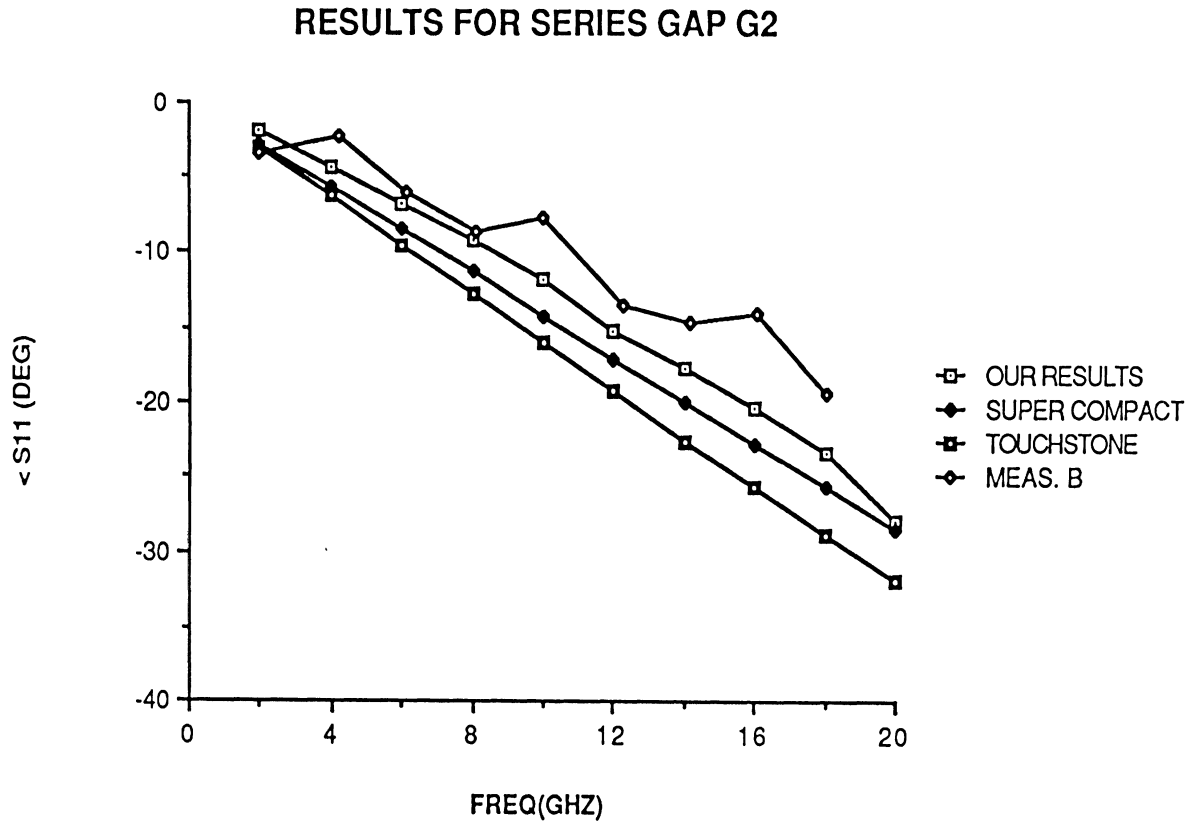

Figure 3.11: Angle of S11 for series gap G2 (G = 9 mil) as compared to measurements, *Super Compact*, and *Touchstone*.

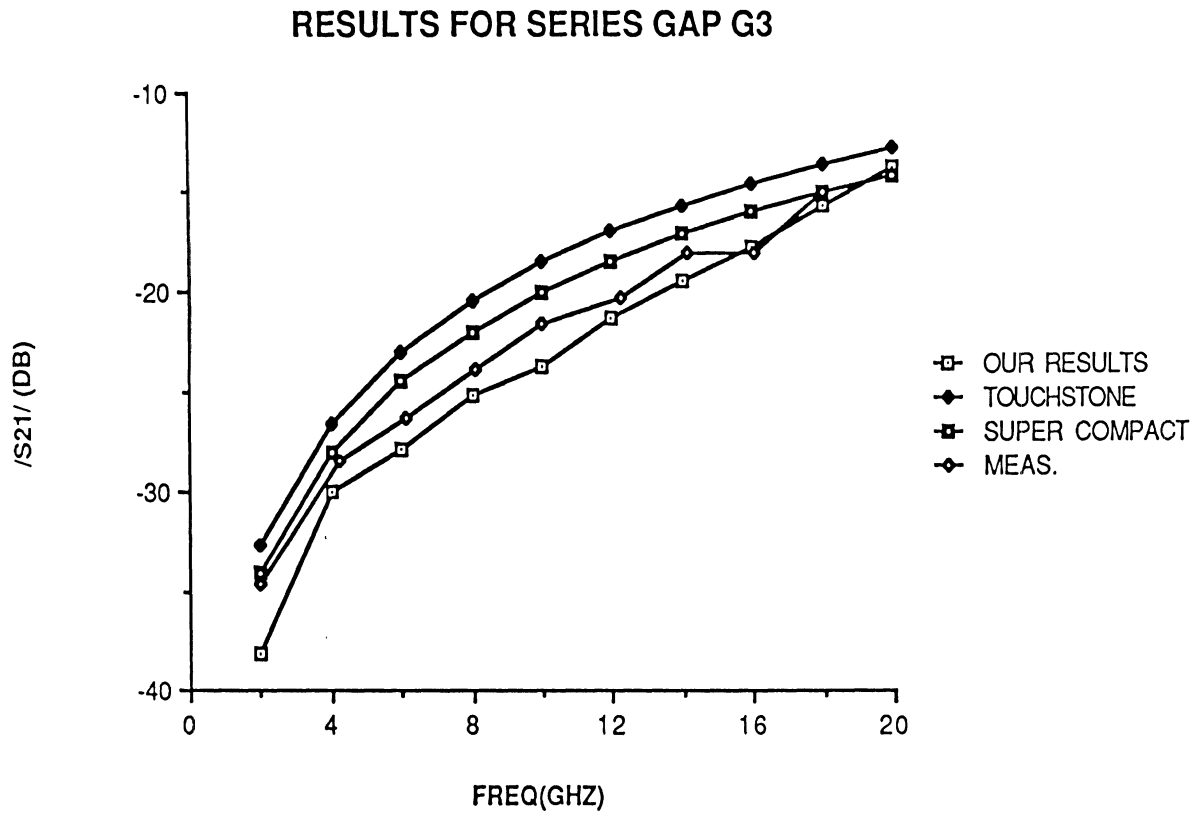

Figure 3.12: Magnitude of S21 for series gap G3 (G = 15 mil) as compared to measurements, *Super Compact*, and *Touchstone*.

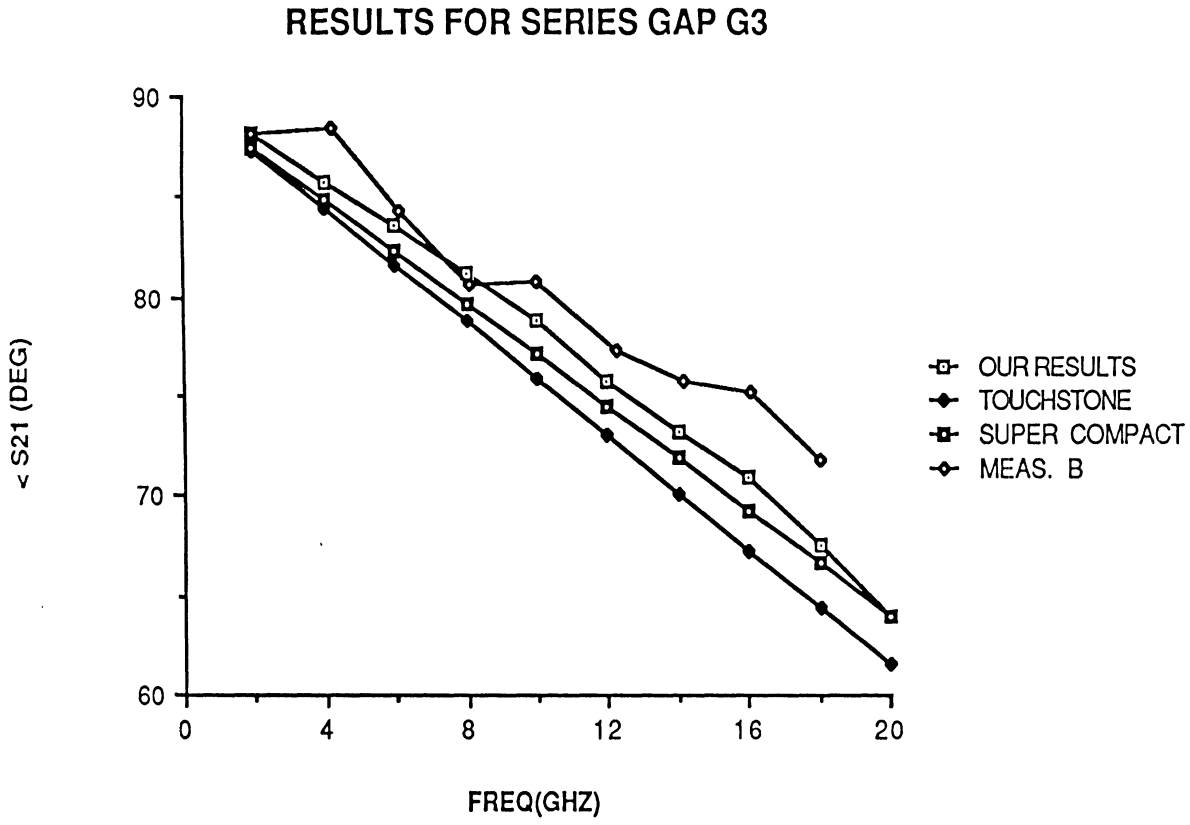

Figure 3.13: Angle of S21 for series gap G3 (G = 15 mil) as compared to measurements, *Super Compact*, and *Touchstone*.

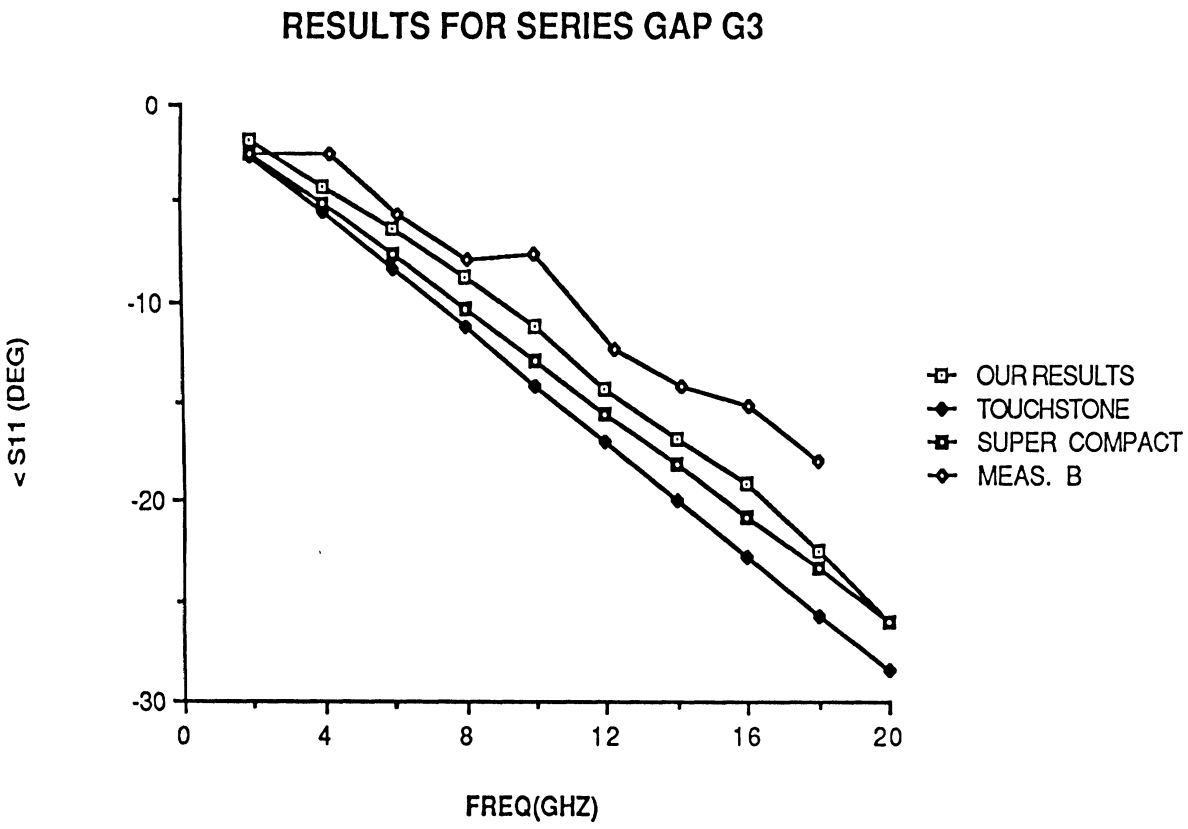

Figure 3.14: Angle of S11 for series gap G3 (G = 15 mil) as compared to measurements, *Super Compact*, and *Touchstone*.

APPENDICES

APPENDIX A

REVIEW OF THE METHOD OF MOMENTS

The general steps involved for in the computation of surface currents using the method of moments can be summarized as follows:

1. Formulate an integral equation for the electric or magnetic field in terms of the surface current density $\bar{J}_s$ on the conductors. It is generally possible to put this equation in the form

$$L_{op}\left(\bar{J}_s\right) = \bar{g}\begin{pmatrix} \bar{E} \\ \\ \bar{H} \end{pmatrix} \tag{A.1}$$

where L_{op} is an integral operator, and $\bar{g}$ is a vector function of either the electric field $\bar{E}$ or magnetic field $\bar{H}$ associated with $\bar{J}_s$.

2. Expand $\bar{J}_s$ into a series of basis functions $\bar{J}_p$ so that

$$\bar{J}_s = \sum_{p=1}^{NSECT} I_p \bar{J}_p \tag{A.2}$$

where the I_p's are complex coefficients and $NSECT$ is the number of sections the conductor is divided into.

3. Determine a suitable inner product and define a set of test (or weighting) functions $\bar{W}_q$. The result may be expressed as

$$\sum_{p=1}^{NSECT} I_p \left\langle \bar{W}_q, L_{op}\left(\bar{J}_p\right)\right\rangle = \left\langle \bar{W}_q, \bar{g}\right\rangle \tag{A.3}$$

where the inner product is defined as

$$\langle \bar{a}, \bar{b} \rangle = \int_S \int \bar{a} \cdot \bar{b} dS$$

In Galerkin's method, the weighting functions are taken to be test currents $\bar{J}_q$ which are identical in form to the basis functions $\bar{J}_p$.

4. Solve the inner product equation (.3) and form a matrix equation of the form

$$[Z_{qp}][I_p] = [V_q] \tag{A.4}$$

where $[Z_{qp}]$ is termed the impedance matrix, and $[V_q]$ is called the excitation vector.

5. Solve for the current coefficient vector by matrix inversion and multiplication according to

$$[I_p] = [Z_{qp}]^{-1}[V_q]. \tag{A.5}$$

APPENDIX B

DERIVATION OF INTEGRAL EQUATION FOR ELECTRIC FIELD

Starting with Maxwell's equations

$$\bar{\nabla} \times \bar{E} = -j\omega\mu\bar{H} \tag{B.1}$$

$$\bar{\nabla} \times \bar{H} = j\omega\epsilon\bar{E} + \bar{J} \tag{B.2}$$

$$\bar{\nabla} \cdot \bar{J} = -j\omega\rho \tag{B.3}$$

$$\bar{\nabla} \cdot (\epsilon\bar{E}) = \rho \tag{B.4}$$

$$\bar{\nabla} \cdot (\mu\bar{H}) = 0 \tag{B.5}$$

we define $\bar{A}$ such that

$$\bar{H} = \frac{1}{\mu}\bar{\nabla} \times \bar{A} \,. \tag{B.6}$$

Substituting (B.6) into (B.1) yields

$$\bar{\nabla} \times (\bar{E} + j\omega\bar{A}) = 0 \,. \tag{B.7}$$

Since $\bar{\nabla} \times \bar{\nabla}\phi = 0$ for any arbitrary vector function ϕ, we let

$$\bar{E} + j\omega\bar{A} = -\bar{\nabla}\phi \,. \tag{B.8}$$

Making use of (B.6) and (B.8) in (B.2) yields

$$\bar{\nabla} + \frac{1}{\mu}\bar{\nabla} \times \bar{A} = -j\omega\epsilon(j\omega\bar{A} + \bar{\nabla}\phi) + \bar{J} \tag{B.9}$$

or

$$-\nabla^2\bar{A} + \bar{\nabla}(\bar{\nabla} \cdot \bar{A}) = \omega^2\mu\epsilon\bar{A} - j\omega\mu\epsilon\bar{\nabla}\phi + \mu\bar{J} \,. \tag{B.10}$$

We use the Lorentz condition

$$\bar{\nabla}(\bar{\nabla}\cdot\bar{A}) = -j\omega\mu\epsilon\bar{\nabla}\phi \tag{B.11}$$

in (B.10) to obtain

$$\nabla^2\bar{A} + k^2\bar{A} = -\mu\bar{J} \tag{B.12}$$

where $k^2 = \omega^2\mu\epsilon$. From (B.9) and (B.11) the electric field may be expressed as

$$\begin{aligned}\bar{E} &= -j\omega\bar{A} + \frac{1}{j\omega\mu\epsilon}\bar{\nabla}(\bar{\nabla}\cdot\bar{A}) \\ &= -j\omega(1 + \frac{1}{k^2}\bar{\nabla}\bar{\nabla}\cdot)\bar{A}\end{aligned} \tag{B.13}$$

We now define a dyadic Green's function $\bar{\bar{G}}$ to be a solution of

$$\nabla^2\bar{\bar{G}} + k^2\bar{\bar{G}} = -\bar{\bar{I}}\delta(\bar{r} - \bar{r}')\,. \tag{B.14}$$

After some manipulation, the vector dyadic Green's theorem [26] can be put in the following form (an appendix will be added later to give the details of this derivation)

$$\begin{aligned}&\int\int\int_V(\nabla^2\bar{A}\cdot\bar{\bar{G}} - \bar{A}\cdot\nabla^2\bar{\bar{G}})dV = \\ &\quad\int\int_{S_w+S_s}\Big\{(\hat{n}'\times\bar{A})\cdot\bar{\nabla}\times\bar{\bar{G}} \\ &\quad+(\hat{n}'\times\bar{\nabla}\times\bar{A})\cdot\bar{\bar{G}} + \hat{n}'\cdot\Big[\bar{A}(\bar{\nabla}\cdot\bar{\bar{G}})\Big] \\ &\quad-\hat{n}'\cdot\Big[(\bar{\nabla}\cdot\bar{A})\bar{\bar{G}}\Big]\Big\}\,dS\end{aligned} \tag{B.15}$$

where, for our shielded microstrip cavity problem, the volume V is the interior of the cavity, and S_w and S_s are the surface of the cavity walls, and the surface of a small volume enclosing the source region respectively. We will require that the components of $\bar{A}$ and $\bar{\bar{G}}$ satisfy the same boundary conditions on S_w and S_s. In this case, it can be shown that the entire surface integral on the right hand side of (B.15) vanishes. If we now substitute from (B.12) and (B.14) for $\nabla^2\bar{A}$ and $\nabla^2\bar{\bar{G}}$ we obtain

$$\int\int\int_V(\nabla^2\bar{A}\cdot\bar{\bar{G}} - \bar{A}\cdot\nabla^2\bar{\bar{G}})dV = \int\int\int_V\Big\{(-\mu\bar{J} - k^2\bar{A})\cdot\bar{\bar{G}}$$

$$
\begin{aligned}
& -\bar{A}\cdot\left[-\bar{\bar{I}}\delta(\bar{r}-\bar{r}')-k^2\cdot\bar{\bar{G}}\right]\Big\}\,dV \\
= \; & -\mu\int\int\int_V \bar{J}\cdot\bar{\bar{G}}dV+\bar{A}(\bar{r}) \\
= \; & 0\,. \qquad\qquad (B.16)
\end{aligned}
$$

Hence,

$$\bar{A}=\mu\int\int\int_V \bar{J}\cdot\bar{\bar{G}}dV \qquad (B.17)$$

Finally, substituting from (B.17) into (B.13) produces the following integral equation for the electric field

$$
\begin{aligned}
\bar{E} &= -j\omega\mu(1+\frac{1}{k^2}\bar{\nabla}\bar{\nabla}\cdot)\int\int\int_V \bar{J}\cdot\bar{\bar{G}}dV \\
&= -j\omega\mu\int\int\int_V\left[(1+\frac{1}{k^2}\bar{\nabla}\bar{\nabla}\cdot)(\bar{\bar{G}})^T\right] \qquad (B.18)
\end{aligned}
$$

where $(\bar{\bar{G}})^T$ represents the transpose of $\bar{\bar{G}}$.

APPENDIX C

EIGENFUNCTION SOLUTION FOR GREEN'S FUNCTION

The boundary conditions on the cavity walls are applied here in order to derive the functional form of the Green's function. First, the general solution to the homogeneous differential equations for the components of the Green's function is presented. Then, the boundary conditions on the walls are used to arrive at an eigenfunction expansion for each of the Green's function components. The particular solution for the Green's function is found by integrating the inhomogeneous differential equation across the source region.

GENERAL SOLUTION TO HOMOGENEOUS D.E.'s FOR GREEN'S FUNCTION

Consider the homogeneous forms of equations (2.23) and (2.25)

$$\nabla^2 \bar{A}^i + k_i^2 \bar{A}^i = 0 \tag{C.1}$$

$$\nabla^2 \bar{\bar{G}}^i + k_i^2 \bar{\bar{G}}^i = 0 \tag{C.2}$$

where $i = 1, 2$ denotes that these equations hold in each region respectively.

With $\bar{\bar{G}}^i$ given by (2.30), it can readily be shown that (C.2) implies

$$\nabla^2 G_{xx}^i + k_i^2 G_{xx}^i = 0 \tag{C.3}$$

$$\nabla^2 G_{xz}^i + k_i^2 G_{xz}^i = 0\,. \tag{C.4}$$

We now apply the method of separation of variables. Let

$$G_{xx}^i = X_x^i(x) Y_x^i(y) Z_x^i(z) \tag{C.5}$$

$$G^i_{xz} = X^i_z(x)Y^i_z(y)Z^i_z(z)\,. \tag{C.6}$$

Substituting from (C.5) into (C.4) produces the following differential equations for Gxx:

$$\frac{d^2X^i_x}{dx^2} + k^{i^2}_x X^i_x = 0 \tag{C.7}$$

$$\frac{d^2Y^i_x}{dy^2} + k^{i^2}_y Y^i_x = 0 \tag{C.8}$$

$$\frac{d^2Z^i_x}{dz^2} + k^{i^2}_z Z^i_x = 0\,. \tag{C.9}$$

Similarly, substituting from (C.6) into (C.4) yields for Gxz

$$\frac{d^2X^i_z}{dx^2} + k^{i^2}_x X^i_z = 0 \tag{C.10}$$

$$\frac{d^2Y^i_z}{dy^2} + k^{i^2}_y Y^i_z = 0 \tag{C.11}$$

$$\frac{d^2Z^i_z}{dz^2} + k^{i^2}_z Z^i_z = 0 \tag{C.12}$$

where

$$k^2_i = k^{i^2}_x + k^{i^2}_y + k^{i^2}_z\,. \tag{C.13}$$

The well known general solution of each of the above differential equations may be put in the form

$$\psi = A_1 \cos k^i_t t + A_2 \sin k^i_t t \tag{C.14}$$

where $t = x, y,$ or $z; \psi = X^i_s, Y^i_s,$ or Z^i_s (where $s = x$ or z) and k^i_t is complex in general.

The next step is to consider the boundary conditions on the cavity walls.

APPLICATION OF BOUNDARY CONDITIONS ON THE CAVITY WALLS

In the application of Green's theorem (Appendix B) it is required that the components of $\bar{A}^i$ and $\bar{\bar{G}}^i$ must satisfy the same boundary conditions. Hence, the following correspondences apply

$$A^i_x \leftrightarrow G^i_{xx} \quad ; \quad A^i_z \leftrightarrow G^i_{xz} \tag{C.15}$$

That is, A_x^i and G_{xx}^i must satisfy the same boundary conditions on the waveguide walls and on the substrate/air interface and, hence, must have the same functional form in terms of spatial variation. The same holds true for A_z^i and G_{xz}^i.

In order to establish what conditions $\bar{A}^i$ (and correspondingly $\bar{\bar{G}}^i$) must satisfy at the walls, we need first to establish more explicit relations between $\bar{A}^i$ and $\bar{E}^i$. From (B.13)

$$\bar{E}^i = -j\omega\bar{A}^i + \frac{1}{j\omega\epsilon\mu}\bar{\nabla}(\bar{\nabla}\cdot\bar{A}^i)\,. \tag{C.16}$$

Now, from (2.26)

$$\bar{A}^i = A_x^i\hat{x} + A_z^i\hat{z} \tag{C.17}$$

hence,

$$\bar{\nabla}\cdot\bar{A}^i = \frac{\partial A_x^i}{\partial x} + \frac{\partial A_z^i}{\partial z} \tag{C.18}$$

and

$$\begin{aligned}\bar{\nabla}(\bar{\nabla}\cdot\bar{A}^i) = \\ &\frac{\partial}{\partial x}(\frac{\partial A_x^i}{\partial x} + \frac{\partial A_z^i}{\partial z})\hat{x} \\ +&\frac{\partial}{\partial y}(\frac{\partial A_x^i}{\partial x} + \frac{\partial A_z^i}{\partial z})\hat{y} \\ +&\frac{\partial}{\partial z}(\frac{\partial A_x^i}{\partial x} + \frac{\partial A_z^i}{\partial z})\hat{z}\,.\end{aligned} \tag{C.19}$$

Using (C.17) and (C.19) in (C.16) yields the following expressions for the electric field components:

$$\begin{aligned}E_x^i &= -j\omega\left[A_x^i + \frac{1}{k_i^2}\frac{\partial}{\partial x}(\bar{\nabla}\cdot\bar{A}^i)\right] \\ &= -j\omega\left[A_x^i + \frac{1}{k_i^2}\frac{\partial}{\partial x}(\frac{\partial A_x^i}{\partial x} + \frac{\partial A_z^i}{\partial z})\right]\end{aligned} \tag{C.20}$$

$$E_y^i = \frac{-j\omega}{k_i^2}\frac{\partial}{\partial y}(\frac{\partial A_x^i}{\partial x} + \frac{\partial A_z^i}{\partial z}) \tag{C.21}$$

$$E_z^i = -j\omega\left[A_z^i + \frac{1}{k_i^2}\frac{\partial}{\partial z}(\frac{\partial A_x^i}{\partial x} + \frac{\partial A_z^i}{\partial z})\right]\,. \tag{C.22}$$

We now consider the boundary conditions at each of the cavity walls.

Boundary conditions at $x = 0,\ a$

Since the cavity walls are assumed to be perfectly conducting, the tangential components of the electric field must vanish at the walls. Therefore, for the walls at $x = 0$ and a

$$E_y^i(x = 0, a) = 0 \tag{C.23}$$

$$E_z^i(x = 0, a) = 0 . \tag{C.24}$$

In view of these two equations, (C.20) and (C.22) lead to

$$E_y^i(x = 0, a) = \left[\frac{\partial}{\partial y}\left(\frac{\partial A_x^i}{\partial x} + \frac{\partial A_z^i}{\partial z}\right)\right] |_{x=0,a} = 0 . \tag{C.25}$$

$$E_z^i(x = 0, a) = -j\omega \left[A_z^i + \frac{1}{k_i^2}\frac{\partial}{\partial z}\left(\frac{\partial A_x^i}{\partial x} + \frac{\partial A_z^i}{\partial z}\right)\right] |_{x=0,a} = 0 . \tag{C.26}$$

Now, (C.25) is satisfied if the following condition is imposed:

$$\left(\frac{\partial A_x^i}{\partial x} + \frac{\partial A_z^i}{\partial z}\right) |_{x=0,a} = 0 \tag{C.27}$$

in which case (C.26) leads to

$$A_z^i(x = 0, a) = 0 . \tag{C.28}$$

If we use the correspondences of (C.15) and the representation of (C.6) we may deduce that

$$X_z^i(x = 0, a) = 0 . \tag{C.29}$$

If (C.28) is placed into (C.27) it is seen that

$$\frac{\partial A_x^i}{\partial x} |_{x=0,a} = 0 . \tag{C.30}$$

then (C.15) and the representation of (C.5) leads us to conclude that

$$\frac{\partial X_x^i}{\partial x} |_{x=0,a} = 0 . \tag{C.31}$$

The boundary conditions of (C.29) and (C.31) can be satisfied by choosing the following eigenfunction solutions for the x-dependence:

$$X_x^i = \cos k_x^i x \tag{C.32}$$

$$X_z^i = \sin k_x^i x \,. \tag{C.33}$$

for $i = 1, 2$, where

$$k_x^{(1)} = k_x^{(2)} = k_x = \frac{n\pi}{a} \qquad for\ n = 0, 1, 2, \ldots \tag{C.34}$$

Boundary conditions at $y = 0,\ b$

The tangential component of the electric field must vanish on the walls $y = 0$ and b; hence,

$$E_x^i(y = 0, b) = 0 \tag{C.35}$$

$$E_z^i(y = 0, b) = 0 \,. \tag{C.36}$$

From (C.20) and (C.21)

$$E_x^i(y = 0, b) = -j\omega \left[A_x^i + \frac{1}{k_i^2} \frac{\partial}{\partial x} \left(\frac{\partial A_x^i}{\partial x} + \frac{\partial A_z^i}{\partial z} \right) \right] |_{y=0,b} = 0 \tag{C.37}$$

$$E_z^i(y = 0, b) = -j\omega \left[A_z^i + \frac{1}{k_i^2} \frac{\partial}{\partial z} \left(\frac{\partial A_x^i}{\partial x} + \frac{\partial A_z^i}{\partial z} \right) \right] |_{y=0,b} = 0 \,. \tag{C.38}$$

If we impose (C.27) at $y = 0$ and b, we obtain

$$\left(\frac{\partial A_x^i}{\partial x} + \frac{\partial A_z^i}{\partial z} \right) |_{y=0,b} = 0 \,, \tag{C.39}$$

and when this is combined with (C.37) and (C.38) the result is

$$A_x^i(y = 0, b) = 0 \tag{C.40}$$

$$A_z^i(y = 0, b) = 0 \tag{C.41}$$

from which it follows that the eigenfunction solution for the y-dependence is given by

$$Y_x^i = \sin k_y^i y \tag{C.42}$$

$$Y_z^i = \sin k_y^i y \tag{C.43}$$

(for $i = 1, 2$), where

$$k_y^{(1)} = k_y^{(2)} = k_y = \frac{m\pi}{b} \qquad for\ m = 1, 2, 3, \ldots \ . \tag{C.44}$$

Note that it is easily shown that $m = 0$ leads to a trivial solution for the y-dependence of both components.

Boundary conditions at $z = 0,\ c$

Similarly at the walls $z = 0$ and c we have

$$E_x^i(z = 0, c) = 0 \tag{C.45}$$

$$E_y^i(z = 0, c) = 0 \ . \tag{C.46}$$

Making use of (C.20) and (C.21) yields

$$E_x^i(z = 0, c) = -j\omega \left[A_x^i + \frac{1}{k_i^2} \frac{\partial}{\partial x} \left(\frac{\partial A_x^i}{\partial x} + \frac{\partial A_z^i}{\partial z} \right) \right] |_{z=0,c} = 0 \tag{C.47}$$

$$E_y^i(z = 0, c) = \left[\frac{-j\omega}{k_i^2} \frac{\partial}{\partial y} \left(\frac{\partial A_x^i}{\partial x} + \frac{\partial A_z^i}{\partial z} \right) \right] |_{z=0,c} = 0 \ . \tag{C.48}$$

Again we impose (C.27) this time at $z = 0$ and c

$$\left(\frac{\partial A_x^i}{\partial x} + \frac{\partial A_z^i}{\partial z} \right) |_{z=0,c} = 0 \tag{C.49}$$

which results in

$$A_x^i(z = 0, c) = 0 \ . \tag{C.50}$$

If we substitute (C.50) back into (C.49) we deduce

$$\frac{\partial A_z^i}{\partial z} |_{z=0,c} = 0 \tag{C.51}$$

Finally, from the correspondence of (C.15), the separation of variables representation of (C.5) and (C.6), and the conditions imposed by (C.50) and (C.51) the eigenfunction solution for the z-dependence can be written as

$$Z_x^{(1)} = \sin k_z^{(1)} z \tag{C.52}$$

$$Z_z^{(1)} = \cos k_z^{(1)} z \tag{C.53}$$

$$Z_x^{(2)} = \sin k_z^{(2)} (z-c) \tag{C.54}$$

$$Z_z^{(2)} = \cos k_z^{(2)} (z-c) \tag{C.55}$$

where —from (C.13), (C.34), and (C.44)— $k_z^{(1)}$ and $k_z^{(2)}$ are given explicitly by

$$k_z^{(1)} = \sqrt{k_1^2 - (\frac{n\pi}{a})^2 - (\frac{m\pi}{b})^2} \tag{C.56}$$

$$k_z^{(2)} = \sqrt{k_0^2 - (\frac{n\pi}{a})^2 - (\frac{m\pi}{b})^2} \tag{C.57}$$

and

$$k_1 = \omega\sqrt{\mu\epsilon_1} \tag{C.58}$$

$$k_0 = \omega\sqrt{\mu\epsilon_0}\,. \tag{C.59}$$

REPRESENTATION OF GREEN'S FUNCTION BY EIGENFUNCTION SERIES

We will now combine the results obtained above, so that the Green's function may be written in series expansion form. Substituting from (C.32), (C.42),(C.52), and (C.54) into (C.5) and taking the summation over all the possible modes, results in the following for G_{xx}^i:

$$G_{xx}^{(1)} = \sum_{m=1}^{\infty}\sum_{n=0}^{\infty} A_{mn}^{(1)} \cos k_x x \sin k_y y \sin k_z^{(1)} z \tag{C.60}$$

$$G_{xz}^{(2)} = \sum_{m=1}^{\infty}\sum_{n=0}^{\infty} B_{mn}^{(2)} \sin k_x x \sin k_y y \cos k_z^{(2)} (z-c)\,. \tag{C.61}$$

Similarly, if we substitute from (C.33),(C.43),(C.53), and (C.55) into (C.6) we obtain the following for G^i_{xz}

$$G^{(1)}_{xz} = \sum_{m=1}^{\infty}\sum_{n=0}^{\infty} B^{(1)}_{mn} \sin k_x x \sin k_y y \cos k^{(1)}_z z \tag{C.62}$$

$$G^{(2)}_{xx} = \sum_{m=1}^{\infty}\sum_{n=0}^{\infty} A^{(2)}_{mn} \cos k_x x \sin k_y y \sin k^{(2)}_z (z-c)\,. \tag{C.63}$$

The complex coefficients A^i_{mn} and B^i_{mn} $(i = 1,2)$ are determined in Appendix D by the application of boundary conditions at the substrate/air interface $(z = h)$.

APPENDIX D

BOUNDARY CONDITIONS AT SUBSTRATE/AIR INTERFACE

The complex coefficients A^i_{mn}, and B^i_{mn} (for $i = 1, 2$) for the Green's function components given by (2.31)-(2.34) are found here by applying boundary conditions at the substrate/air interface ($z = h$).

Figure D.1 shows a cross section of the cavity in the $x-z$ plane. The application of boundary conditions at the interface is made difficult by the presence of the infinitesimal current source on the substrate surface. We will avoid this difficulty by first solving a similar problem with the current source raised a distance Δh above the substrate. After solving for the boundary conditions at $z = h$ and $z = h + \Delta h$, the equations required to determine the coefficients A^i_{mn}, and B^i_{mn} are obtained by letting Δh go to zero.

FORMULATION

From the consideration of the boundary conditions on the waveguide walls the components of the Green's function are given as

$$G^{(1)}_{xx} = \sum_{m=1}^{\infty}\sum_{n=0}^{\infty} A^{(1)}_{mn} \cos k_x x \sin k_y y \sin k^{(1)}_z z \tag{D.1}$$

$$G^{(1)}_{xz} = \sum_{m=1}^{\infty}\sum_{n=0}^{\infty} B^{(1)}_{mn} \sin k_x x \sin k_y y \cos k^{(1)}_z z \tag{D.2}$$

$$G^{(2)}_{xx} = \sum_{m=1}^{\infty}\sum_{n=0}^{\infty} A^{(2)}_{mn} \cos k_x x \sin k_y y \sin k^{(2)}_z (z-c) \tag{D.3}$$

$$G^{(2)}_{xz} = \sum_{m=1}^{\infty}\sum_{n=0}^{\infty} B^{(2)}_{mn} \sin k_x x \sin k_y y \cos k^{(2)}_z (z-c) \tag{D.4}$$

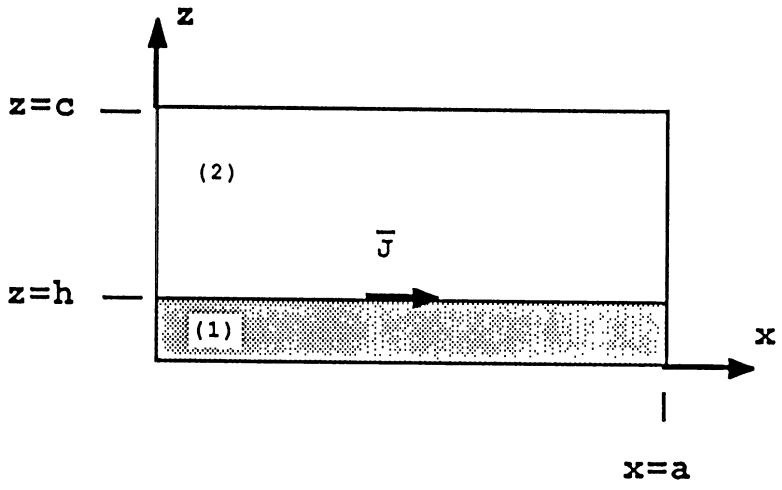

a) Actual position of current source

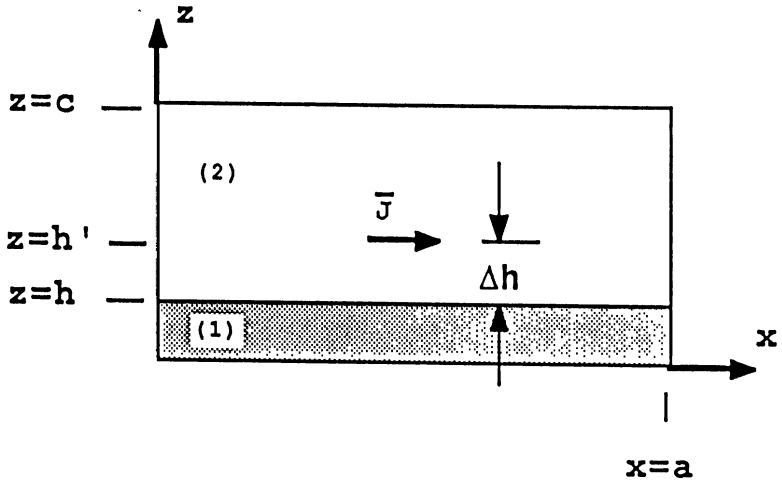

b) Current source raised above interface

Figure D.1: The current source is raised above the substrate/air interface to apply boundary conditions.

For region 3, the Green's function must satisfy the same differential equation (2.25) as in the other two regions. We will use the form of the general solution given by

$$G_{xx}^{(3)} = \sum_{m=1}^{\infty}\sum_{n=0}^{\infty} \cos k_x x \sin k_y y \left[A_{mn}^{(3)} e^{jk_z^{(3)}z} + B_{mn}^{(3)} e^{-jk_z^{(3)}z}\right] \tag{D.5}$$

$$G_{xz}^{(3)} = \sum_{m=1}^{\infty}\sum_{n=0}^{\infty} \sin k_x x \sin k_y y \left[C_{mn}^{(3)} e^{jk_z^{(3)}z} + D_{mn}^{(3)} e^{-jk_z^{(3)}z}\right] \tag{D.6}$$

where,

$$k_x = n\pi/a \tag{D.7}$$

$$k_y = m\pi/b \tag{D.8}$$

$$k_z^{(1)} = \sqrt{k_1^2 - k_x^2 - k_y^2} \tag{D.9}$$

$$k_z^{(2)} = \sqrt{k_0^2 - k_x^2 - k_y^2} \tag{D.10}$$

$$k_z^{(3)} = k_z^{(2)} \tag{D.11}$$

$$k = \omega\sqrt{\mu_0\epsilon_1} \tag{D.12}$$

$$k_0 = \omega\sqrt{\mu_0\epsilon_0}\,. \tag{D.13}$$

Recall, the electric field solution in terms of the vector potential components (C.20)-(C.22)

$$\begin{aligned} E_x^i &= -j\omega\left[A_x^i + \frac{1}{k_i^2}\frac{\partial}{\partial x}(\bar{\nabla}\cdot\bar{A}^i)\right] \\ &= -j\omega\left[A_x^i + \frac{1}{k_i^2}\frac{\partial}{\partial x}(\frac{\partial A_x^i}{\partial x} + \frac{\partial A_z^i}{\partial z})\right] \end{aligned} \tag{D.14}$$

$$E_y^i = \frac{-j\omega}{k_i^2}\frac{\partial}{\partial y}(\frac{\partial A_x^i}{\partial x} + \frac{\partial A_z^i}{\partial z}) \tag{D.15}$$

$$E_z^i = -j\omega\left[A_z^i + \frac{1}{k_i^2}\frac{\partial}{\partial z}(\frac{\partial A_x^i}{\partial x} + \frac{\partial A_z^i}{\partial z})\right]\,. \tag{D.16}$$

These equations hold in each region respectively (i.e. for $i = 1, 2, 3$).

The solution for the magnetic field can be written using (2.21) and (2.26) as follows:

$$\bar{H}^i = \frac{1}{\mu_o}\bar{\nabla}\times\bar{A}^i = \frac{1}{\mu_o}[\bar{\nabla}\times(A_x^i\hat{x} + A_z^i\hat{z})]\,. \tag{D.17}$$

Separating this into x, y, and z components gives

$$H_x^i = \frac{1}{\mu_0}\frac{\partial A_z^i}{\partial y} \tag{D.18}$$

$$H_y^i = \frac{1}{\mu_0}\left(\frac{\partial A_x^i}{\partial z} - \frac{\partial A_z^i}{\partial x}\right) \tag{D.19}$$

$$H_z^i = -\frac{1}{\mu_0}\frac{\partial A_x^i}{\partial y}\,. \tag{D.20}$$

APPLICATION OF BOUNDARY CONDITIONS

Recall from Appendix C (C.15) that the following direct correspondences can be made as far as boundary conditions are concerned

$$A_x^i \leftrightarrow G_{xx}^i \quad ; \quad A_z^i \leftrightarrow G_{xz}^i\,. \tag{D.21}$$

Boundary conditions at $z = h$

At $z = h$, the following boundary conditions apply:

$$E_x^{(1)} = E_x^{(3)} \tag{D.22}$$

$$E_y^{(1)} = E_y^{(3)} \tag{D.23}$$

$$H_x^{(1)} = H_x^{(3)} \tag{D.24}$$

$$H_y^{(1)} = H_y^{(3)} \tag{D.25}$$

$$\mu_0 H_z^{(1)} = \mu_0 H_z^{(3)} \Longrightarrow H_z^{(1)} = H_z^{(3)} \tag{D.26}$$

$$\epsilon_1 E_z^{(1)} = \epsilon_0 E_z^{(3)}\,. \tag{D.27}$$

We will make use of (D.23)-(D.26) to formulate four of the eight equations needed to solve for the complex coefficients in (D.1)-(D.6). We start with (D.26), then substitute from

(D.20), and recall the correspondences of (D.21) to obtain

$$\frac{\partial G_{xx}^{(1)}}{\partial y}|_{z=h} = \frac{\partial G_{xx}^{(3)}}{\partial y}|_{z=h} . \tag{D.28}$$

When (D.1) is placed in (D.5) and orthogonality is applied, the following result is obtained

$$A_{mn}^{(1)} \sin k_z^{(1)} h = A_{mn}^{(3)} e^{jk_z^{(2)}h} + B_{mn}^{(3)} e^{-jk_z^{(2)}h} \tag{D.29}$$

where $k_z^{(2)}$ has been substituted for $k_z^{(3)}$ in accordance with (D.11).

Next, from (D.24),(D.18), and (D.21)

$$\frac{\partial G_{xz}^{(1)}}{\partial y} = \frac{\partial G_{xz}^{(3)}}{\partial y} . \tag{D.30}$$

From (D.2) and (D.6)

$$B_{mn}^{(1)} \cos k_z^{(1)} h = C_{mn}^{(3)} e^{jk_z^{(2)}h} + D_{mn}^{(3)} e^{-jk_z^{(2)}h} . \tag{D.31}$$

The combination of (D.25), (D.19) and (D.21) yields

$$\left(\frac{\partial G_{xx}^{(1)}}{\partial z} - \frac{\partial G_{xz}^{(1)}}{\partial x} \right) |_{z=h} = \left(\frac{\partial G_{xx}^{(3)}}{\partial z} - \frac{\partial G_{xz}^{(3)}}{\partial x} \right) |_{z=h} . \tag{D.32}$$

Making substitutions from (D.1),(D.2),(D.5) and (D.6) in this expression leads to

$$\begin{aligned} \left[A_{mn}^{(1)} k_z^{(1)} - B_{mn}^{(1)} k_x \right] \cos k_z^{(1)} h &= jk_z^{(2)} \left[A_{mn}^{(3)} e^{jk_z^{(2)}h} - B_{mn}^{(3)} e^{-jk_z^{(2)}h} \right] \\ &\quad -k_x \left[C_{mn}^{(3)} e^{jk_z^{(2)}h} + D_{mn}^{(3)} e^{-jk_z^{(2)}h} \right] . \end{aligned} \tag{D.33}$$

We now substitute for $B_{mn}^{(1)} \cos k_z^{(1)} h$ from (D.31) to reduce the above to

$$A_{mn}^{(1)} k_z^{(1)} \cos k_z^{(1)} h = jk_z^{(2)} \left[A_{mn}^{(3)} e^{jk_z^{(2)}h} - B_{mn}^{(3)} e^{-jk_z^{(2)}h} \right] . \tag{D.34}$$

Now consider (D.23). From (D.15) and (D.21)

$$\frac{1}{\epsilon_r^*} \frac{\partial}{\partial y} \left(\frac{\partial G_{xx}^{(1)}}{\partial x} + \frac{\partial G_{xz}^{(1)}}{\partial z} \right) |_{z=h} = \frac{\partial}{\partial y} \left(\frac{\partial G_{xx}^{(3)}}{\partial x} + \frac{\partial G_{xz}^{(3)}}{\partial z} \right) |_{z=h} . \tag{D.35}$$

Substituting from (D.1),(D.3),(D.5), and (D.6), produces, after simplification,

$$\begin{aligned} \frac{1}{\epsilon_r^*} \left(A_{mn}^{(1)} k_x + B_{mn}^{(1)} k_z^{(1)} \right) \sin k_z^{(1)} h &= k_x \left(A_{mn}^{(3)} e^{jk_z^{(2)}h} + B_{mn}^{(3)} e^{-jk_z^{(2)}h} \right) \\ &\quad -jk_z^{(2)} \left(C_{mn}^{(3)} e^{jk_z^{(2)}h} - D_{mn}^{(3)} e^{-jk_z^{(2)}h} \right) . \end{aligned} \tag{D.36}$$

Next, we use the expression from (D.29) to replace $A_{mn}^{(3)}e^{jk_z^{(2)}h} + B_{mn}^{(3)}e^{-jk_z^{(2)}h}$. This yields

$$A_{mn}^{(1)}(1-\epsilon_r^*)k_x \sin k_z^{(1)}h + B_{mn}^{(1)}k_z^{(1)} \sin k_z^{(1)}h =$$
$$-jk_z^{(2)}\epsilon_r^* \left[C_{mn}^{(3)}e^{jk_z^{(2)}h} - D_{mn}^{(3)}e^{-jk_z^{(2)}h}\right] . \tag{D.37}$$

Equations (D.29), (D.31), (D.34), and (D.37) represent 4 of the 8 equations we need.

Boundary conditions at $z = h'$

We now proceed to the boundary conditions at $z = h'$ (see Figure D.1) we have

$$E_x^{(2)} = E_x^{(3)} \tag{D.38}$$

$$E_y^{(2)} = E_y^{(3)} \tag{D.39}$$

$$E_z^{(2)} - E_z^{(3)} = \sigma_s \tag{D.40}$$

$$H_z^{(2)} = H_z^{(3)} \tag{D.41}$$

$$\hat{z} \times (\bar{H}^{(2)} - \bar{H}^{(3)} = J_s\hat{x} \Longrightarrow$$

$$H_x^{(2)} = H_x^{(3)} \tag{D.42}$$

$$-(H_y^{(2)} - H_y^{(3)}) = J_s . \tag{D.43}$$

Of the above, we will use (D.38), (D.41), and (D.42) to derive three more equations for the complex coefficients.

We start with (D.42) and use (D.18) and (D.21) to obtain

$$\frac{\partial G_{xz}^{(2)}}{\partial y}|_{z=h'} = \frac{\partial G_{xz}^{(3)}}{\partial y}|_{z=h'} \tag{D.44}$$

which yields after substituting from (D.4) and (D.6)

$$B_{mn}^{(2)} \cos k_z^{(2)}(h'-c) = C_{mn}^{(3)}e^{jk_z^{(2)}h'} + D_{mn}^{(3)}e^{-jk_z^{(2)}h'} . \tag{D.45}$$

Next, consider the boundary condition of (D.41). This leads to

$$\frac{\partial G_{xx}^{(2)}}{\partial y}|_{z=h'} = \frac{\partial G_{xx}^{(3)}}{\partial y}|_{z=h'} \tag{D.46}$$

after the use of (D.20) and (D.21). Substitution from (D.3) and (D.5) yields

$$A_{mn}^{(2)} \sin k_z^{(2)}(h' - c) = A_{mn}^{(3)} e^{jk_z^{(2)}h'} + B_{mn}^{(3)} e^{-jk_z^{(2)}h'} . \tag{D.47}$$

This equation, when combined with (D.3) and (D.5) , shows that

$$G_{xx}^{(2)}(z = h') = G_{xx}^{(3)}(z = h') . \tag{D.48}$$

With the above equality, we can substitute from (D.14) into the boundary condition of (D.38), and make use of (D.21) to produce

$$\frac{\partial}{\partial x}\left(\frac{\partial G_{xx}^{(2)}}{\partial x} + \frac{\partial G_{xz}^{(2)}}{\partial z}\right) = \frac{\partial}{\partial x}\left(\frac{\partial G_{xx}^{(3)}}{\partial x} + \frac{\partial G_{xz}^{(3)}}{\partial z}\right) . \tag{D.49}$$

Substitution in the above from (D.3), (D.4),(D.5), and (D.6) yields

$$\begin{aligned} &\left[A_{mn}^{(2)} k_x^2 + B_{mn}^{(2)} k_x k_z^{(2)}\right] \sin k_z^{(2)}(h' - c) = \\ &\quad k_x^2 \left[A_{mn}^{(3)} e^{jk_z^{(2)}h'} + B_{mn}^{(3)} e^{-jk_z^{(2)}h'}\right] \\ &\quad -jk_x k_z^{(2)} \left[C_{mn}^{(3)} e^{jk_z^{(2)}h'} - D_{mn}^{(3)} e^{-jk_z^{(2)}h'}\right] . \end{aligned} \tag{D.50}$$

Now, replace $[A_{mn}^{(3)} e^{jk_z^{(2)}h'} + B_{mn}^{(3)} e^{-jk_z^{(2)}h'}]$ with $A_{mn}^{(2)} \sin k_z^{(2)}(h' - c)$ from (D.47) and we may write

$$B_{mn}^{(2)} \sin k_z^{(2)}(h' - c) = -j \left[C_{mn}^{(3)} e^{jk_z^{(2)}h'} - D_{mn}^{(3)} e^{-jk_z^{(2)}h'}\right] . \tag{D.51}$$

At this point we have 7 independent equations —(D.29), (D.31),(D.34), (D.37),(D.45),-(D.47), and (D.51)— and we have 8 unknown complex coefficients. The other required equation is obtained by integrating the differential equation of (2.25) across the boundary at $z = h'$.

Integration of the differential equation for $\bar{\bar{G}}^i$ across the source region at z=h'

From (2.25) we have

$$\nabla^2 \bar{\bar{G}}^i + k_i^2 \bar{\bar{G}}^i = -\bar{\bar{I}}\delta(\bar{r} - \bar{r}') . \tag{D.52}$$

we then substitute from (2.30) to yield

$$(\nabla^2 + k_i^2)\left(G_{xx}^i \hat{x}\hat{x} + G_{xz}^i \hat{x}\hat{z}\right) = -\delta(\bar{r} - \bar{r}')\hat{x}\hat{x} \; . \tag{D.53}$$

Hence,

$$(\nabla^2 + k_i^2)G_{xx}^i = -\delta(\bar{r} - \bar{r}') = -\delta(x - x')\delta(y - y')\delta(z - z') \; . \tag{D.54}$$

We now integrate both sides of this equation over a line passing through the source point $\bar{r}'$, and then take the limit as the length of this line vanishes

$$\lim_{\alpha \to 0} \int_{h'-\alpha}^{h'+\alpha} (\nabla^2 + k_i^2)G_{xx}^i dz = -\delta(x - x')\delta(y - y') \; . \tag{D.55}$$

This may be written as

$$\lim_{\alpha \to 0} \left[\left(\frac{\partial}{\partial x^2} + \frac{\partial}{\partial y^2} + k_i^2 \right) \int_{h'-\alpha}^{h'+\alpha} G_{xx}^i dz + \int_{h'-\alpha}^{h'+\alpha} \frac{\partial}{\partial z^2} G_{xx}^i dz \right] = -\delta(x-x')\delta(y-y') \tag{D.56}$$

If we make use of (D.3) and (D.5), we can show that the first integral vanishes as follows:

$$\begin{aligned}
\lim_{\alpha \to 0} \int_{h'-\alpha}^{h'+\alpha} G_{xx}^i dz &= \lim_{\alpha \to 0} \left[\int_{h'-\alpha}^{h'} G_{xx}^{(3)} dz + \int_{h'}^{h'+\alpha} G_{xx}^{(2)} dz \right] \\
&= \lim_{\alpha \to 0} \left[\sum_{m=1}^{\infty} \sum_{n=0}^{\infty} \left(\frac{1}{jk_z^{(2)}} \right) \cos k_x x \sin k_y y \left(A_{mn}^{(3)} e^{jk_z^{(2)} z} - B_{mn}^{(3)} e^{-jk_z^{(2)} z} \right) \right] \Bigg|_{z=h'-\alpha}^{z=h'} \\
&\quad + \lim_{\alpha \to 0} \left[\sum_{m=1}^{\infty} \sum_{n=0}^{\infty} \left(\frac{-1}{k_z^{(2)}} \right) A_{mn}^{(2)} \cos k_x x \sin k_y y \cos k_z^{(2)}(z - c) \right] \Bigg|_{z=h'}^{z=h'+\alpha} \\
&= 0
\end{aligned} \tag{D.57}$$

(since each of the limits on the right hand side vanish individually.)

Therefore, (D.56) can be reduced to

$$\lim_{\alpha \to 0} \int_{h'-\alpha}^{h'+\alpha} \frac{\partial}{\partial z^2} G_{xx}^i dz = -\delta(x - x')\delta(y - y') \tag{D.58}$$

From which we obtain

$$\lim_{\alpha \to 0} \frac{\partial G_{xx}^i}{\partial z} \Big|_{h'-\alpha}^{h'+\alpha} = -\delta(x - x')\delta(y - y'), \tag{D.59}$$

or

$$\frac{\partial G_{xx}^{(2)}}{\partial z} - \frac{\partial G_{xx}^{(3)}}{\partial z} = -\delta(x - x')\delta(y - y'). \tag{D.60}$$

Substitution in the above from (D.3) and (D.5), and simplifying (with the use orthogonality principles) yields

$$\frac{ab}{\varphi_n}\left\{A_{mn}^{(2)}k_z^{(2)}\cos k_z^{(2)}(h'-c) \quad -jk_z^{(2)}(A_{mn}^{(3)}e^{jk_z^{(2)}z} - B_{mn}^{(3)}e^{-jk_z^{(2)}z})\right\} = -\cos k_x x' \sin k_y y' \qquad \text{(D.61)}$$

where

$$\varphi_n = \begin{cases} 2 & for\ n = 0 \\ 4 & for\ n \neq 0 \end{cases} \qquad \text{(D.62)}$$

The above represents the final equation needed to evaluate the complex coefficients.

EVALUATION OF THE COMPLEX COEFFICIENTS OF THE GREEN'S FUNCTION

To evaluate the complex coefficients, we will make use of the equations derived above involving A_{mn}^{i}, B_{mn}^{i} $(i = 1,3)$, and $C_{mn}^{(3)}$ and $D_{mn}^{(3)}$. Since we are only interested in $A_{mn}^{(1)}$, $B_{mn}^{(1)}$, $A_{mn}^{(2)}$, and $B_{mn}^{(2)}$ these will be evaluated by eliminating the other complex coefficients along the way.

Now, recall that $h' = h + \Delta h$. If $\Delta h \to 0$ then $h' \to h$ in equations (D.45), (D.47), (D.51), and (D.61).

Starting with (D.45) with $h' \to h$ we can substitute from (D.31) to obtain

$$B_{mn}^{(1)}\cos k_z^{(1)}h = B_{mn}^{(2)}\cos k_z^{(2)}(h-c)\,. \qquad \text{(D.63)}$$

Similarly, (D.29) and (D.47) yield

$$A_{mn}^{(2)}\sin k_z^{(2)}(h-c) = A_{mn}^{(1)}\sin k_z^{(1)}h\,. \qquad \text{(D.64)}$$

From (D.37) and (D.51) we get

$$B_{mn}^{(2)}\sin k_z^{(2)}(h-c) = \frac{1}{k_z^{(2)}}\left[A_{mn}^{(1)}\left(\frac{1}{\epsilon_r^*}-1\right)k_x \sin k_z^{(1)}h + \frac{B_{mn}^{(1)}k_z^{(1)}}{\epsilon_r^*}\sin k_z^{(1)}h\right]. \qquad \text{(D.65)}$$

From (D.34) and (D.61)

$$\frac{ab}{\varphi_n}\left[A_{mn}^{(2)}k_z^{(2)}\cos k_z^{(2)}(h'-c) - A_{mn}^{(1)}k_z^{(1)}\cos k_z^{(1)}h\right] = -\cos k_x x' \sin k_y y' \,. \tag{D.66}$$

The combination of (D.64) and (D.66) yields

$$\frac{ab}{\varphi_n}\left[\frac{A_{mn}^{(1)}\sin k_z^{(1)}h}{\sin k_z^{(2)}(h-c)}k_z^{(2)}\cos k_z^{(2)}(h-c) - A_{mn}^{(1)}k_z^{(1)}\cos k_z^{(1)}h\right] = -\cos k_x x' \sin k_y y' \,. \tag{D.67}$$

Solving for $A_{mn}^{(1)}$

$$A_{mn}^{(1)} = \frac{-\varphi_n \cos k_x x' \sin k_y y' \tan k_z^{(2)}(h-c)}{abd_{1mn}\cos k_z^{(1)}h} \tag{D.68}$$

where

$$d_{1mn} = k_z^{(2)}\tan k_z^{(1)}h - k_z^{(1)}\tan k_z^{(2)}(h-c) \tag{D.69}$$

and φ_n is given by (D.62) $A_{mn}^{(2)}$ is found by substitution from (D.68) into (D.64)

$$A_{mn}^{(2)} = \frac{-\varphi_n \cos k_x x' \sin k_y y' \tan k_z^{(1)}h}{abd_{1mn}\cos k_z^{(2)}(h-c)} \,. \tag{D.70}$$

Next, we combine (D.63) and (D.65) to get

$$\begin{aligned}\frac{B_{mn}^{(1)}\cos k_z^{(1)}h \sin k_z^{(2)}(h-c)}{\cos k_z^{(2)}(h-c)} &= \frac{1}{k_z^{(2)}}\left[A_{mn}^{(1)}\left(\frac{1}{\epsilon_r^*}-1\right)k_x \sin k_z^{(1)}h \right.\\ &\left. + \frac{B_{mn}^{(1)}k_z^{(1)}}{\epsilon_r^*}\sin k_z^{(1)}h\right],\end{aligned} \tag{D.71}$$

which, by substituting for $A_{mn}^{(1)}$ from (D.68), can be rearranged to find $B_{mn}^{(1)}$ as

$$B_{mn}^{(1)} = \frac{-\varphi_n(1-\epsilon_r^*)k_x \cos k_x x' \sin k_y y' \tan k_z^{(1)}h \tan k_z^{(2)}(h-c)}{abd_{1mn}d_{2mn}\cos k_z^{(1)}h} \tag{D.72}$$

where

$$d_{2mn} = k_z^{(2)}\epsilon_r^* \tan k_z^{(2)}(h-c) - k_z^{(1)}\tan k_z^{(1)}h \,. \tag{D.73}$$

Finally, place (D.72) in (D.63), and $B_{mn}^{(2)}$ can be expressed as:

$$B_{mn}^{(2)} = \frac{-\kappa_{ab}(1-\epsilon_r^*)k_x \cos k_x x' \sin k_y y' \tan k_z^{(1)}h \tan k_z^{(2)}(h-c)}{d_{1mn}d_{2mn}\cos k_z^{(2)}(h-c)} \,. \tag{D.74}$$

We now have derived explicit relations for the desired complex coefficients $A_{mn}^{(1)}$, $A_{mn}^{(2)}$, $B_{mn}^{(1)}$, $B_{mn}^{(2)}$. It can be shown that the same relations can be obtained by moving the current source of Figure D.1 into the dielectric region and then bringing it back to the substrate surface.

APPENDIX E

EVALUATION OF THE MODIFIED DYADIC GREENS FUNCTION $\bar{\bar{\Gamma}}^i$

The modified dyadic Greens function was defined in (2.53) as

$$\bar{\bar{\Gamma}}^i = -j\omega\mu_0 \left[\left(1 + \frac{1}{k_i^2} \bar{\nabla}\bar{\nabla}\cdot \right) (\bar{\bar{G}}^i)^T \right] . \tag{E.1}$$

From (2.30)

$$\bar{\bar{G}}^i = G^i_{xx}\hat{x}\hat{x} + G^i_{xz}\hat{x}\hat{z} .$$

The dyadic transpose is

$$(\bar{\bar{G}}^i)^T = G^i_{xx}\hat{x}\hat{x} + G^i_{xz}\hat{z}\hat{x} \tag{E.2}$$

The divergence of E.2) yields

$$\bar{\nabla} \cdot (\bar{\bar{G}}^i)^T = \left(\frac{\partial G^i_{xx}}{\partial x} + \frac{\partial G^i_{xz}}{\partial z} \right) \hat{x} .$$

Forming the gradient of this

$$\begin{aligned} \bar{\nabla}\bar{\nabla} \cdot (\bar{\bar{G}}^i)^T \;=\; & \frac{\partial}{\partial x} \left(\frac{\partial G^i_{xx}}{\partial x} + \frac{\partial G^i_{xz}}{\partial z} \right) \hat{x}\hat{x} \\ & + \frac{\partial}{\partial y} \left(\frac{\partial G^i_{xx}}{\partial x} + \frac{\partial G^i_{xz}}{\partial z} \right) \hat{y}\hat{x} \\ & + \frac{\partial}{\partial z} \left(\frac{\partial G^i_{xx}}{\partial x} + \frac{\partial G^i_{xz}}{\partial z} \right) \hat{z}\hat{x} . \end{aligned} \tag{E.3}$$

We can now substitute from (E.2) and (E.3) into (E.1) to yield

$$\bar{\bar{\Gamma}}^i \;=\; -j\omega\mu_0 \left\{ \left[G^i_{xx} + \frac{1}{k_i^2} \frac{\partial}{\partial x} \left(\frac{\partial G^i_{xx}}{\partial x} + \frac{\partial G^i_{xz}}{\partial z} \right) \right] \hat{x}\hat{x} \right.$$

$$+\left[\frac{1}{k_i^2}\frac{\partial}{\partial y}\left(\frac{\partial G_{xx}^i}{\partial x}+\frac{\partial G_{xz}^i}{\partial z}\right)\right]\hat{y}\hat{x}$$
$$+\left[G_{xz}^i+\frac{1}{k_i^2}\frac{\partial}{\partial z}\left(\frac{\partial G_{xx}^i}{\partial x}+\frac{\partial G_{xz}^i}{\partial z}\right)\right]\hat{z}\hat{x}\Bigg\}\ . \tag{E.4}$$

Hence, the xx component of the modified Green's function is given by

$$\Gamma_{xx}^i=-j\omega\mu_0\left[G_{xx}^i+\frac{1}{k_i^2}\frac{\partial}{\partial x}\left(\frac{\partial G_{xx}^i}{\partial x}+\frac{\partial G_{xz}^i}{\partial z}\right)\right]\ . \tag{E.5}$$

From (2.31) and (2.32)

$$G_{xx}^{(1)} = \sum_{m=1}^{\infty}\sum_{n=0}^{\infty}A_{mn}^{(1)}\cos k_x x\sin k_y y\sin k_z^{(1)}z \tag{E.6}$$
$$\frac{\partial G_{xx}^{(1)}}{\partial x} = -\sum_{m=1}^{\infty}\sum_{n=0}^{\infty}k_x A_{mn}^{(1)}\sin k_x x\sin k_y y\sin k_z^{(1)}z$$
$$\frac{\partial^2 G_{xx}^{(1)}}{\partial x^2} = -\sum_{m=1}^{\infty}\sum_{n=0}^{\infty}A_{mn}^{(1)}k_x^2\cos k_x x\sin k_y y\sin k_z^{(1)}z \tag{E.7}$$
$$G_{xz}^{(1)} = \sum_{m=1}^{\infty}\sum_{n=0}^{\infty}B_{mn}^{(1)}\sin k_x x\sin k_y y\cos k_z^{(1)}z \tag{E.8}$$
$$\frac{\partial G_{xz}^{(1)}}{\partial z} = -\sum_{m=1}^{\infty}\sum_{n=0}^{\infty}k_z^{(1)}B_{mn}^{(1)}\sin k_x x\sin k_y y\sin k_z^{(1)}z$$
$$\frac{\partial^2 G_{xz}^{(1)}}{\partial x\partial z} = -\sum_{m=1}^{\infty}\sum_{n=0}^{\infty}k_x k_z^{(1)}B_{mn}^{(1)}\cos k_x x\sin k_y y\sin k_z^{(1)}z\ . \tag{E.9}$$

Substitution from (E.6)-(E.9) into (E.5) results in

$$\Gamma_{xx}^{(1)}=-j\omega\mu_0\sum_{m=1}^{\infty}\sum_{n=0}^{\infty}\cos k_x x\sin k_y y\sin k_z^{(1)}z\left[A_{mn}^{(1)}\left(1-\frac{k_x^2}{k_1^2}\right)-\frac{k_x k_z^{(1)}}{k_1^2}B_{mn}^{(1)}\right]$$

Replace the expressions for $A_{mn}^{(1)}$ and $B_{mn}^{(1)}$ from (2.41) and (2.43). The result is

$$\Gamma_{xx}^{(1)} = +j\omega\mu_0\sum_{m=1}^{\infty}\sum_{n=0}^{\infty}\cos k_x x\sin k_y y\sin k_z^{(1)}z$$
$$\cdot\Bigg\{\frac{\kappa_{ab}\cos k_x x'\sin k_y y'\tan k_z^{(2)}(h-c)}{d_{1mn}\cos k_z^{(1)}h}\left(1-\frac{k_x^2}{k_1^2}\right)$$
$$-\frac{k_x k_z^{(1)}}{k_1^2}\left[\frac{\kappa_{ab}(1-\epsilon_r^*)k_x\cos k_x x'\sin k_y y'\tan k_z^{(1)}h\tan k_z^{(2)}(h-c)}{d_{1mn}d_{2mn}\cos k_z^{(1)}h}\right]\Bigg\} \tag{E.10}$$

which can be rearranged in the following form:

$$\Gamma_{xx}^{(1)} = j\omega\mu_0\sum_{m=1}^{\infty}\sum_{n=0}^{\infty}\Bigg\{\frac{1}{d_{1mn}d_{2mn}\cos k_z^{(1)}h}$$

$$\cdot\left[\kappa_{ab}\cos k_x x \sin k_y y \sin k_z^{(1)} z \cos k_x x' \sin k_y y' \tan k_z^{(2)}(h-c)\right]$$
$$\cdot\left[k_z^{(2)}\epsilon_r^*\left(1-\frac{k_x^2}{k_1^2}\right)\tan k_z^{(2)}(h-c) - k_z^{(1)}\left(1-\frac{\epsilon_r^* k_x^2}{k_1^2}\right)\tan k_z^{(1)}h\right]\Bigg\} \quad \text{(E.11)}$$

where the expression for d_{2mn} from (D.73) has been used in combining the terms inside the brackets of (E.10). Evaluation of (E.11) at $z = h$ gives

$$\begin{aligned}\Gamma_{xx}^{(1)}(z=h) &= j\omega\mu_0 \sum_{m=1}^{\infty}\sum_{n=0}^{\infty}\Bigg\{\left(\frac{1}{d_{1mn}d_{2mn}}\right)\\ &\cdot\left[\kappa_{ab}\cos k_x x \sin k_y y \cos k_x x' \sin k_y y' \tan k_z^{(1)}h \tan k_z^{(2)}(h-c)\right]\\ &\cdot\Bigg[k_z^{(2)}\epsilon_r^*\left(1-\frac{k_x^2}{k_1^2}\right)\tan k_z^{(2)}(h-c)\\ &-k_z^{(1)}\left(1-\frac{\epsilon_r^* k_x^2}{k_1^2}\right)\tan k_z^{(1)}h\Bigg]\Bigg\}\,. \end{aligned} \quad \text{(E.12)}$$

Proceeding in a similar fashion for region 2, we have from (2.33) and (2.34)

$$G_{xx}^{(2)} = \sum_{m=1}^{\infty}\sum_{n=0}^{\infty} A_{mn}^{(2)}\cos k_x x \sin k_y y \sin k_z^{(2)}(z-c) \quad \text{(E.13)}$$

$$\frac{\partial G_{xx}^{(2)}}{\partial x} = -\sum_{m=1}^{\infty}\sum_{n=0}^{\infty} k_x A_{mn}^{(2)}\sin k_x x \sin k_y y \sin k_z^{(2)}(z-c)$$

$$\frac{\partial^2 G_{xx}^{(2)}}{\partial x^2} = -\sum_{m=1}^{\infty}\sum_{n=0}^{\infty} A_{mn}^{(2)} k_x^2 \cos k_x x \sin k_y y \sin k_z^{(2)}(z-c) \quad \text{(E.14)}$$

$$G_{xz}^{(2)} = \sum_{m=1}^{\infty}\sum_{n=0}^{\infty} B_{mn}^{(2)}\sin k_x x \sin k_y y \cos k_z^{(2)}(z-c) \quad \text{(E.15)}$$

$$\frac{\partial G_{xz}^{(2)}}{\partial z} = -\sum_{m=1}^{\infty}\sum_{n=0}^{\infty} k_z^{(2)} B_{mn}^{(2)}\sin k_x x \sin k_y y \sin k_z^{(2)}(z-c)$$

$$\frac{\partial^2 G_{xz}^{(2)}}{\partial x \partial z} = -\sum_{m=1}^{\infty}\sum_{n=0}^{\infty} k_x k_z^{(2)} B_{mn}^{(2)}\cos k_x x \sin k_y y \sin k_z^{(2)}(z-c) \quad \text{(E.16)}$$

Substitution from (E.13)-(E.16) into (E.5) yields

$$\Gamma_{xx}^{(2)} = -j\omega\mu_0 \sum_{m=1}^{\infty}\sum_{n=0}^{\infty}\cos k_x x \sin k_y y \sin k_z^{(2)}(z-c)\left[A_{mn}^{(2)}\left(1-\frac{k_x^2}{k_0^2}\right) - \frac{k_x k_z^{(2)}}{k_0^2}B_{mn}^{(2)}\right]$$

We now replace $A_{mn}^{(2)}$ and $B_{mn}^{(2)}$ with the expressions from (2.42)and (2.44)

$$\begin{aligned}\Gamma_{xx}^{(2)} &= -j\omega\mu_0 \sum_{m=1}^{\infty}\sum_{n=0}^{\infty}\cos k_x x \sin k_y y \sin k_z^{(2)}(z-c)\\ &\cdot\left\{\left[\frac{-\kappa_{ab}\cos k_x x' \sin k_y y' \tan k_z^{(1)}h}{d_{1mn}\cos k_z^{(2)}(h-c)}\right]\left(1-\frac{k_x^2}{k_0^2}\right) - \frac{k_x k_z^{(2)}}{k_0^2}\right.\end{aligned}$$

$$\cdot \left[\frac{-\kappa_{ab}(1-\epsilon_r^*) k_x \cos k_x x' \sin k_y y' \tan k_z^{(1)} h \tan k_z^{(2)}(h-c)}{d_{1mn} d_{2mn} \cos k_z^{(2)}(h-c)} \right] \Bigg\}$$

which can be rearranged as follows

$$\begin{aligned} \Gamma_{xx}^{(2)} &= j\omega\mu_0 \sum_{m=1}^{\infty} \sum_{n=0}^{\infty} \Bigg\{ \frac{1}{d_{1mn} d_{2mn} \cos k_z^{(2)}(h-c)} \\ &\cdot \left[\kappa_{ab} \cos k_x x \sin k_y y \sin k_z^{(2)}(z-c) \cos k_x x' \sin k_y y' \tan k_z^{(1)} h \right] \\ &\cdot \left[k_z^{(2)} \epsilon_r^* \left(1 - \frac{k_x^2}{k_1^2} \right) \tan k_z^{(2)}(h-c) - k_z^{(1)} \left(1 - \frac{\epsilon_r^* k_x^2}{k_1^2} \right) \tan k_z^{(1)} h \right] \Bigg\} \quad . \text{(E.17)} \end{aligned}$$

Evaluation at z=h yields

$$\begin{aligned} \Gamma_{xx}^{(2)}(z=h) &= j\omega\mu_0 \sum_{m=1}^{\infty} \sum_{n=0}^{\infty} \Bigg\{ \left(\frac{1}{d_{1mn} d_{2mn}} \right) \\ &\cdot [\kappa_{ab} \cos k_x x \sin k_y y \cos k_x x' \sin k_y y' \tan k_z^{(1)} h \tan k_z^{(2)}(h-c)] \\ &\cdot \left[k_z^{(2)} \epsilon_r^* \left(1 - \frac{k_x^2}{k_1^2} \right) \tan k_z^{(2)}(h-c) \right. \\ &\left. - k_z^{(1)} \left(1 - \frac{\epsilon_r^* k_x^2}{k_1^2} \right) \tan k_z^{(1)} h \right] \Bigg\} \quad . \end{aligned} \tag{E.18}$$

Upon comparison of (E.18) with (E.12) we can readily see that

$$\Gamma_{xx}^{(1)}(z=h) = \Gamma_{xx}^{(2)}(z=h) = \Gamma_{xx}(z=h) \, . \tag{E.19}$$

APPENDIX F

EVALUATION OF CLOSED FORM INTEGRALS OVER SUBSECTIONAL SURFACES

Consider the surface integral given by (2.66)

$$\mathcal{I}_{qmn} = \int\int_{S_q} \cos k_x x' \sin k_y y' \, \psi(y') \alpha_q(x') \, dx' dy' \, . \tag{F.1}$$

where from (2.5)

$$\psi\left(y'\right) = \begin{cases} \dfrac{\frac{2}{\pi W}}{\sqrt{1-\left[\frac{2(y'-Y_0)}{W}\right]^2}} & Y_0 - \frac{W}{2} \leq y' \leq Y_0 + \frac{W}{2} \\ 0 & else \, . \end{cases} \tag{F.2}$$

From (2.6)

$$\alpha_q\left(x'\right) = \begin{cases} \frac{\sin[K(x_{q+1}-x')]}{\sin(Kl_x)} & x_q \leq x' \leq x_{q+1} \\ \frac{\sin[K(x'-x_{q-1})]}{\sin(Kl_x)} & x_{q-1} \leq x' \leq x_q \\ 0 & else \, , \end{cases} \tag{F.3}$$

for $q \neq 1$, and from (2.7)

$$\alpha_1\left(x'\right) = \begin{cases} \frac{\sin[K(l_x-x')]}{\sin(Kl_x)} & 0 \leq x' \leq l_x \\ 0 & else \end{cases} \tag{F.4}$$

for $q = 1$. In the above,

$$l_x = x_{q+1} - x_q = x_q - x_{q-1}$$

and, for our purposes here[1] , we let

$$x_q = (q-1)l_x \, .$$

Figure F.1 illustrates the strip geometry used to determine the integration limits in (F.1). The boundaries of the q^{th} subsection depend on q as follows:

$$S_q = \begin{cases} 0 \le x' \le l_x \\ Y_0 - \frac{W}{2} \le y' \le Y_0 + \frac{W}{2} \quad \text{for } q = 1 \\ \\ x_{q-1} \le x' \le x_{q+1} \\ Y_0 - \frac{W}{2} \le y' \le Y_0 + \frac{W}{2} \qquad else \, . \end{cases} \tag{F.5}$$

With these subsection boundaries, $\mathcal{I}_{qmn}$ may be expressed as

$$\mathcal{I}_{qmn} = \mathcal{I}^{y'} \mathcal{I}_q^{x'} \tag{F.6}$$

where

$$\mathcal{I}^{y'} = \int_{Y_0 - W/2}^{Y_0 + W/2} \psi(y') \sin k_y y' \, dy' \tag{F.7}$$

$$\mathcal{I}_q^{x'} = \begin{cases} \int_0^{l_x} \cos k_x x' \, \alpha_q(x') dx' & \text{for } q = 1 \\ \int_{x_{q-1}}^{x_{q+1}} \cos k_x x' \alpha_q(x') dx' & \text{for } q \neq 1 \, . \end{cases} \tag{F.8}$$

INTEGRATION OVER y'

From (F.7) and (F.2) we have

$$\mathcal{I}^{y'} = \frac{2}{\pi W} \int_{Y_0 - W/2}^{Y_0 + W/2} \frac{\sin k_y y'}{\sqrt{1 - \left[\frac{2(y' - Y_0)}{W}\right]^2}} dy' \, . \tag{F.9}$$

---

[1] Note that for strip geometries other than an open circuit and a straight thru section of transmission line, the position function x_q will be more complicated in general.

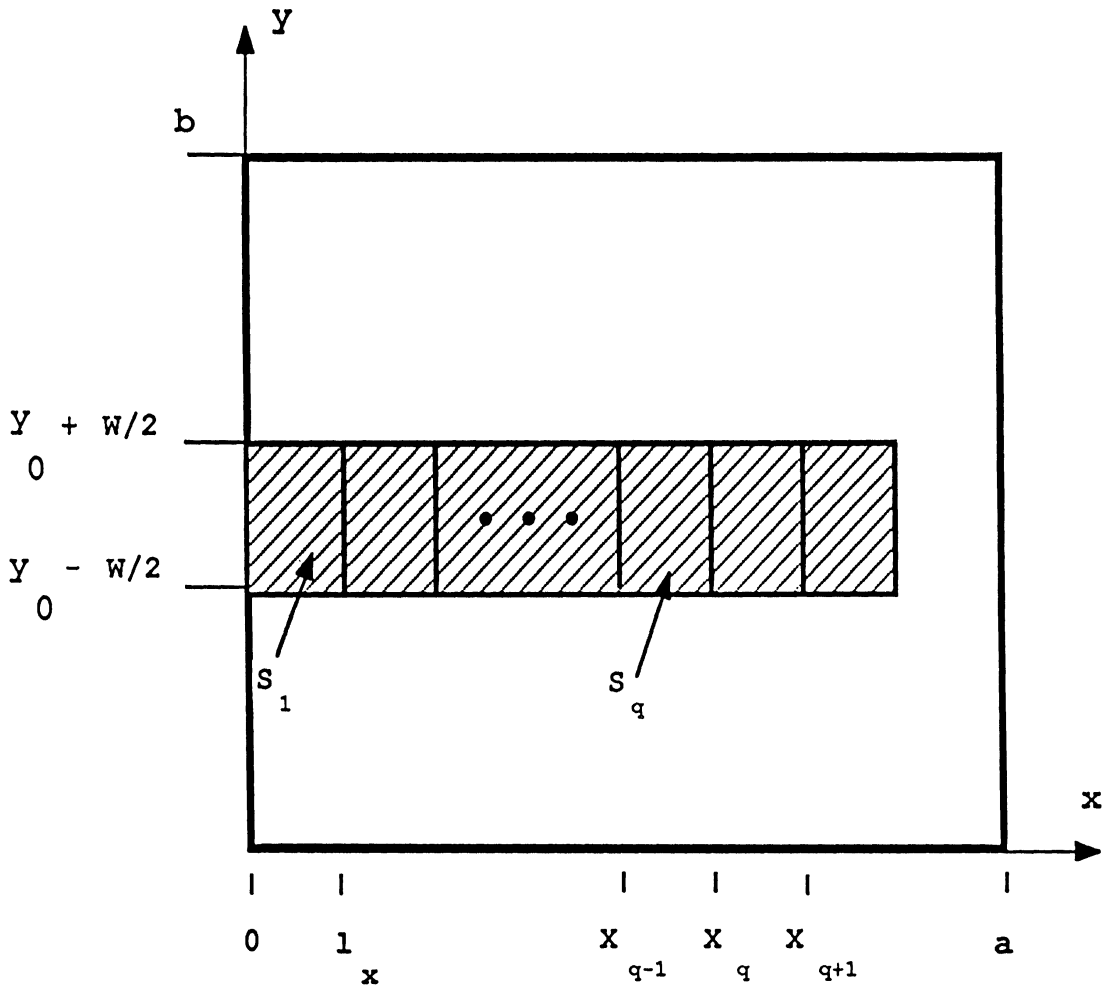

Figure F.1: Strip geometry used in evaluation of surface integrals

Now, let

$$\begin{aligned} \sin\phi &= \tfrac{2(y'-Y_0)}{W} \quad \Longrightarrow \quad \cos\phi\, d\phi = \tfrac{2}{W} dy' \\ y' &= \tfrac{W}{2}\sin\phi + Y_0 \quad \Longrightarrow \quad dy' = \tfrac{W}{2}\cos\phi\, d\phi \end{aligned} \tag{F.10}$$

with these substitutions

$$\mathcal{I}^{y'} = \frac{1}{\pi}\int_{-\frac{\pi}{2}}^{\frac{\pi}{2}} \sin\left[k_y(\frac{W}{2}\sin\phi + Y_0)\right] d\phi \tag{F.11}$$

which can be expanded, with the use of trigonometric identities, as follows:

$$\begin{aligned} \mathcal{I}^{y'} &= \frac{1}{\pi}\left[\int_{-\frac{\pi}{2}}^{\frac{\pi}{2}} \sin(k_y\frac{W}{2}\sin\phi)\cos k_y Y_0\, d\phi \right. \\ &\quad \left. + \int_{-\frac{\pi}{2}}^{\frac{\pi}{2}} \cos(k_y\frac{W}{2}\sin\phi)\sin k_y Y_0\, d\phi\right] \\ &= \int^{(1)y'} + \int^{(2)y'} . \end{aligned} \tag{F.12}$$

Consider the first term:

$$\begin{aligned} \int^{(1)y'} &= \frac{1}{\pi}\cos k_y Y_0 \int_{-\frac{\pi}{2}}^{\frac{\pi}{2}} \sin(k_y\frac{W}{2}\sin\phi)\, d\phi \\ &= \frac{1}{\pi}\cos k_y Y_0 \left[\int_{-\frac{\pi}{2}}^{0} \sin(k_y\frac{W}{2}\sin\phi)\, d\phi + \int_{0}^{\frac{\pi}{2}} \sin(k_y\frac{W}{2}\sin\phi)\, d\phi\right] . \end{aligned}$$

Now, if in the second integral above we let

$$\phi' = -\phi \;\; ; \;\; d\phi' = -d\phi$$

then

$$\begin{aligned} \int^{(1)y'} &= \frac{1}{\pi}\cos k_y Y_0 \left[\int_{-\frac{\pi}{2}}^{0} \sin(k_y\frac{W}{2}\sin\phi)\, d\phi + \int_{0}^{-\frac{\pi}{2}} \sin(-k_y\frac{W}{2}\sin\phi)(-d\phi)\right] \\ &= 0 . \end{aligned}$$

Hence, (F.12) becomes

$$\begin{aligned} \mathcal{I}^{y'} &= \int^{(2)y'} = \frac{1}{\pi}\sin k_y Y_0 \int_{-\frac{\pi}{2}}^{\frac{\pi}{2}} \cos(k_y\frac{W}{2}\sin\phi)\, d\phi \\ &= \frac{1}{\pi}\sin k_y Y_0 \left[\int_{-\frac{\pi}{2}}^{0} \cos(k_y\frac{W}{2}\sin\phi)\, d\phi + \int_{0}^{\frac{\pi}{2}} \cos(k_y\frac{W}{2}\sin\phi)\, d\phi\right] . \end{aligned}$$

If, in the first integral, we let

$$\phi' = -\phi \ \ and \ \ d\phi' = d\phi$$

we obtain

$$\mathcal{I}^{y'} = \frac{1}{\pi} \sin k_y Y_0 \int_0^{\frac{\pi}{2}} \cos(k_y \frac{W}{2} \sin\phi)\, d\phi \,. \tag{F.13}$$

By comparison of the Bessel function of the 2η order given by [27]

$$J_{2\eta}(z) = \frac{2}{\pi} \int_0^{\frac{\pi}{2}} \cos 2\eta\theta \cos(z \sin\theta)\, d\theta$$

with (F.13) we may readily see that

$$\mathcal{I}^{y'} = \sin k_y Y_0 \, J_0 \left(k_y \frac{W}{2} \right) \tag{F.14}$$

This completes the y'-portion of the integration.

INTEGRATION OVER x'

From (F.8), let us first consider the case for $q \neq 1$

$$\mathcal{I}_q^{x'} = \int_{x_{q-1}}^{x_{q+1}} \cos k_x x' \alpha_q(x') dx' \quad (q \neq 1) \tag{F.15}$$

Substitution from (F.3) yields

$$\begin{aligned} \mathcal{I}_q^{x'} &= \frac{1}{\sin K l_x} \left[\int_{x_{q-1}}^{x_q} \sin K(x' - x_{q-1}) \cos k_x x' \, dx' \right. \\ &\quad \left. + \int_{x_q}^{x_{q+1}} \sin K(x' + x_{q-1}) \cos k_x x' \, dx' \right] \\ &= \frac{1}{\sin K l_x} \left[\mathcal{I}_q^{(1)x'} + \mathcal{I}_q^{(2)x'} \right] \,. \end{aligned} \tag{F.16}$$

For the first integral we have

$$\begin{aligned} \mathcal{I}_q^{(1)x'} &= \int_{x_{q-1}}^{x_q} \sin K(x' - x_{q-1}) \cos k_x x' dx' \\ &= \frac{1}{2} \int_{x_{q-1}}^{x_q} \left\{ \sin\left[(K + k_x)x' - K x_{q-1}\right] + \sin\left[(K - k_x)x' - K x_{q-1}\right] \right\} dx' \\ &= -\frac{1}{2} \left\{ \frac{1}{K + k_x} \left[\cos(K l_x + k_x x_q) - \cos k_x x_{q-1} \right] \right. \\ &\quad \left. + \frac{1}{K - k_x} \left[\cos(K l_x - k_x x_q) - \cos k_x x_{q-1} \right] \right\} \,. \end{aligned} \tag{F.17}$$

We can solve for $\mathcal{I}_q^{(2)x'}$ in a similar fashion to yield

$$\begin{aligned}\mathcal{I}_q^{(2)x'} &= \int_{x_q}^{x_{q+1}} \sin\left[K(x_{q+1}-x')\right]\cos k_x x' dx' \\ &= \frac{1}{2}\left\{\frac{1}{K-k_x}\left[\cos k_x x_{q+1} - \cos(Kl_x + k_x x_q)\right]\right. \\ &\quad \left.+\frac{1}{K+k_x}\left[\cos k_x x_{q+1} - \cos(Kl_x - k_x x_q)\right]\right\} . \end{aligned} \tag{F.18}$$

Substitution from (F.17) and (F.18) back into (F.16) yields

$$\mathcal{I}_q^{x'} = \frac{1}{\sin Kl_x}\left(\frac{1}{K+k_x}+\frac{1}{K-k_x}\right)\left[\frac{1}{2}(\cos k_x x_{q+1} + \cos k_x x_{q-1}) - \cos Kl_x \cos k_x x_q\right] . \tag{F.19}$$

After some manipulation, this expression may be put in the following form

$$\begin{aligned}\mathcal{I}_q^{x'} &= \frac{-4K\cos k_x x_q \sin\left[\frac{1}{2}(k_x+K)l_x\right]\sin\left[\frac{1}{2}(k_x-K)l_x\right]}{\sin Kl_x\,(K+k_x)\,(K-k_x)} \\ &= -\frac{Kl_x^2\cos k_x x_q}{\sin Kl_x}\,\mathrm{Sinc}\left[\frac{1}{2}(k_x+K)l_x\right]\,\mathrm{Sinc}\left[\frac{1}{2}(k_x-K)l_x\right] \quad (q\neq 1) \end{aligned} \tag{F.20}$$

where

$$\mathrm{Sinc}(t) = \begin{cases} \frac{\sin t}{t} & t \neq 0 \\ 1 & t = 0 . \end{cases} \tag{F.21}$$

Recall now the integral for the case $q = 1$ from (F.8)

$$\mathcal{I}_1^{x'} = \int_0^{l_x} \cos k_x x' \alpha_1(x') dx' .$$

Substitution from (F.4) for $\alpha_1(x)$

$$\mathcal{I}_1^{x'} = \frac{1}{\sin Kl_x}\int_0^{l_x} \cos k_x x' \sin(l_x - x') dx' . \tag{F.22}$$

Comparison of this expression to the integral of (F.18) it becomes clear that if we let $x_q \to 0$ and $x_{q+1} \to l_x$ in (F.18) we can obtain the solution for the integral in (F.22). The result is

$$\begin{aligned}\mathcal{I}_1^{x'} &= \frac{1}{2\sin Kl_x}\left\{\frac{1}{K-k_x}\left[\cos k_x l_x - \cos Kl_x\right] + \frac{1}{K+k_x}\left[\cos k_x l_x - \cos Kl_x\right]\right\} \\ &= \frac{1}{2\sin Kl_x}\left(\frac{1}{K-k_x}+\frac{1}{K+k_x}\right)\left[\cos k_x l_x - \cos Kl_x\right] . \end{aligned}$$

The above can be rearranged to give

$$\mathcal{I}_1^{x'} = \frac{-Kl_x^2}{2\sin Kl_x} \operatorname{Sinc}\left[\frac{1}{2}(k_x + K)l_x\right] \operatorname{Sinc}\left[\frac{1}{2}(k_x - K)l_x\right] \quad (\text{for } q = 1)\,. \tag{F.23}$$

Combination of this with (F.20) yields

$$\mathcal{I}_q^{x'} = -\frac{\zeta_q Kl_x^2 \cos k_x x_q}{2\sin Kl_x} \operatorname{Sinc}\left[\frac{1}{2}(k_x + K)l_x\right] \operatorname{Sinc}\left[\frac{1}{2}(k_x - K)l_x\right] \quad (\text{for any } q) \tag{F.24}$$

where

$$\zeta_q = \begin{cases} 2 & \text{for } q = 1 \\ 4 & \text{for } q \neq 1\,. \end{cases} \tag{F.25}$$

Finally, substitution from (F.14) and (F.24) back into (F.6) yields

$$\begin{aligned} \mathcal{I}_{qmn} &= \int\int_{S_q} \cos k_x x' \sin k_y y' \psi(y') \alpha_q(x') dx' dy' \\ &= -\frac{\zeta_q Kl_x^2 \cos k_x x_q}{2\sin Kl_x} \operatorname{Sinc}\left[\frac{1}{2}(k_x + K)l_x\right] \operatorname{Sinc}\left[\frac{1}{2}(k_x - K)l_x\right] \\ &\quad \cdot \sin k_y Y_0 \; J_0(k_y \frac{W}{2})\,. \end{aligned} \tag{F.26}$$

APPENDIX G

EVALUATION OF THE MAGNETIC FIELD COMPONENTS

The magnetic field components anywhere inside the cavity are given by the surface integrals of (2.89) and (2.90)

$$H^i_{qy} = \int\int_{S_q} \left(\frac{\partial G^i_{xx}}{\partial z} - \frac{\partial G^i_{xz}}{\partial x} \right) \psi(y')\alpha_q(x')ds' \tag{G.1}$$

$$H^i_{qz} = -\int\int_{S_q} \frac{\partial G^i_{xx}}{\partial y} \psi(y')\alpha_q(x')ds' \,. \tag{G.2}$$

We will evaluate H^i_{qy} first.

EVALUATION OF THE $y-$ COMPONENT OF THE MAGNETIC FIELD

From (2.31) and (2.32)

$$\begin{aligned} \frac{\partial G^{(1)}_{xx}}{\partial z} - \frac{\partial G^{(1)}_{xz}}{\partial x} &= \sum_{m=1}^{\infty}\sum_{n=0}^{\infty} k_z^{(1)} A^{(1)}_{mn} \cos k_x x \sin k_y y \cos k_z^{(1)} z \\ &\quad - \sum_{m=1}^{\infty}\sum_{n=0}^{\infty} k_x B^{(1)}_{mn} \cos k_x x \sin k_y y \cos k_z^{(1)} z \,. \end{aligned}$$

Using the expressions for $A^{(1)}_{mn}$ and $B^{(1)}_{mn}$ from (D.68) and (D.72) yields

$$\begin{aligned} \frac{\partial G^{(1)}_{xx}}{\partial z} - \frac{\partial G^{(1)}_{xz}}{\partial x} &= -\sum_{m=1}^{\infty}\sum_{n=0}^{\infty} \frac{\varphi_n \cos k_x x \sin k_y y \cos k_z^{(1)} z \tan k_z^{(2)}(h-c)}{d_{1mn} d_{2mn} \cos k_z^{(1)} h} \\ &\quad \cdot \left[k_z^{(1)} d_{2mn} - k_x^2 (1-\epsilon_r^*) \tan k_z^{(1)} h \right] \cdot \cos k_x x' \sin k_y y' \,. \end{aligned} \tag{G.3}$$

Substitution from (2.47) for d_{2mn} in the bracketed term yields

$$\left[k_z^{(1)} d_{2mn} - k_x^2 (1-\epsilon_r^*) \tan k_z^{(1)} h \right] = k_z^{(1)} \left[k_z^{(2)} \epsilon_r^* \tan k_z^{(2)}(h-c) - k_z^{(1)} \tan k_z^{(1)} h \right]$$

$$
\begin{aligned}
& -k_x^2(1-\epsilon_r^*)\tan k_z^{(1)}h \\
= \; & k_z^{(1)}k_z^{(2)}\epsilon_r^*\tan k_z^{(2)}(h-c) \\
& -\left[(k_z^{(1)})^2+k_x^2(1-\epsilon_r^*)\right]\tan k_z^{(1)}h\,. \qquad \text{(G.4)}
\end{aligned}
$$

Use of (G.4) in (G.3) results in

$$
\begin{aligned}
\frac{\partial G_{xx}^{(1)}}{\partial z}-\frac{\partial G_{xz}^{(1)}}{\partial x} &= -\sum_{m=1}^{\infty}\sum_{n=0}^{\infty}\frac{\varphi_n\tan k_z^{(2)}(h-c)}{d_{1mn}d_{2mn}\cos k_z^{(1)}h} \\
&\cdot\left\{k_z^{(1)}k_z^{(2)}\epsilon_r^*\tan k_z^{(2)}(h-c)-\left[(k_z^{(1)})^2+k_x^2(1-\epsilon_r^*)\right]\tan k_z^{(1)}h\right\} \\
&\cdot\cos k_x x\sin k_y y\cos k_z^{(1)}z\cos k_x x'\sin k_y y'\,. \qquad \text{(G.5)}
\end{aligned}
$$

Similarly, substitution from (2.33) and (2.34) yields after similar algebraic manipulations

$$
\begin{aligned}
\frac{\partial G_{xx}^{(2)}}{\partial z}-\frac{\partial G_{xz}^{(2)}}{\partial x} &= \sum_{m=1}^{\infty}\sum_{n=0}^{\infty}k_z^{(2)}A_{mn}^{(2)}\cos k_x x\sin k_y y\cos k_z^{(2)}(z-c) \\
&\quad -\sum_{m=1}^{\infty}\sum_{n=0}^{\infty}k_x B_{mn}^{(2)}\cos k_x x\sin k_y y\cos k_z^{(2)}(z-c) \\
&= \sum_{m=1}^{\infty}\sum_{n=0}^{\infty}\frac{\varphi_n\tan k_z^{(1)}h}{d_{1mn}d_{2mn}\cos k_z^{(2)}(h-c)} \\
&\cdot\left\{k_z^{(1)}k_z^{(2)}\tan k_z^{(1)}h-\left[(k_z^{(2)})^2\epsilon_r^*-k_x^2(1-\epsilon_r^*)\right]\tan k_z^{(2)}(h-c)\right\} \\
&\cos k_x x\sin k_y y\cos k_z^{(2)}(z-c)\cos k_x x'\sin k_y y'\,. \qquad \text{(G.6)}
\end{aligned}
$$

We are now ready to evaluate the $y-$component of the magnetic field. Substitution from (G.5) into (G.1) yields

$$
\begin{aligned}
H_{qy}^{(1)} &= -\sum_{m=1}^{\infty}\sum_{n=0}^{\infty}\frac{\varphi_n\tan k_z^{(2)}(h-c)}{d_{1mn}d_{2mn}\cos k_z^{(1)}h} \\
&\cdot\left\{k_z^{(1)}k_z^{(2)}\epsilon_r^*\tan k_z^{(2)}(h-c)-\left[(k_z^{(1)})^2+k_x^2(1-\epsilon_r^*)\right]\tan k_z^{(1)}h\right\} \\
&\cdot\cos k_x x\sin k_y y\cos k_z^{(1)}z\;[\mathcal{I}_{qmn}] \qquad \text{(G.7)}
\end{aligned}
$$

where from Appendix F (F.26)

$$
\begin{aligned}
\mathcal{I}_{qmn} &= \int\!\!\int_{S_q}\cos k_x x'\sin k_y y'\psi(y')\alpha_q(x')dx'dy' \\
&= -\frac{\zeta_q K l_x^2\cos k_x x_q}{2\sin K l_x}\,\mathrm{Sinc}\left[\frac{1}{2}(k_x+K)l_x\right]\,\mathrm{Sinc}\left[\frac{1}{2}(k_x-K)l_x\right] \\
&\cdot\sin k_y Y_0\;J_0(k_y\frac{W}{2})\,. \qquad \text{(G.8)}
\end{aligned}
$$

So

$$
\begin{aligned}
H_{qy}^{(1)} &= \frac{\zeta_q K l_x^2}{2 \sin K l_x} \sum_{m=1}^{\infty} \sum_{n=0}^{\infty} \frac{\varphi_n \tan k_z^{(2)}(h-c)}{d_{1mn} d_{2mn} \cos k_z^{(1)} h} \\
&\cdot \left\{ k_z^{(1)} k_z^{(2)} \epsilon_r^* \tan k_z^{(2)}(h-c) - \left[(k_z^{(1)})^2 + k_x^2 (1-\epsilon_r^*) \right] \tan k_z^{(1)} h \right\} \\
&\cdot \cos k_x x_q \, \mathrm{Sinc} \left[\frac{1}{2}(k_x + K) l_x \right] \, \mathrm{Sinc} \left[\frac{1}{2}(k_x - K) l_x \right] \sin k_y Y_0 \, J_0(k_y \frac{W}{2}) \\
&\cdot \cos k_x x \sin k_y y \cos k_z^{(1)} z \, . \qquad \text{(G.9)}
\end{aligned}
$$

Substitution from (G.6) into (G.1) and again making use of (F.26) yields

$$
\begin{aligned}
H_{qy}^{(2)} &= \frac{-\zeta_q K l_x^2}{2 \sin K l_x} \sum_{m=1}^{\infty} \sum_{n=0}^{\infty} \frac{\varphi_n \tan k_z^{(1)} h}{d_{1mn} d_{2mn} \cos k_z^{(2)}(h-c)} \\
&\cdot \left\{ k_z^{(1)} k_z^{(2)} \tan k_z^{(1)} h - \left[(k_z^{(2)})^2 \epsilon_r^* - k_x^2 (1-\epsilon_r^*) \right] \tan k_z^{(2)}(h-c) \right\} \\
&\cdot \cos k_x x_q \, \mathrm{Sinc} \left[\frac{1}{2}(k_x + K) l_x \right] \, \mathrm{Sinc} \left[\frac{1}{2}(k_x - K) l_x \right] \sin k_y Y_0 \, J_0(k_y \frac{W}{2}) \\
&\cdot \cos k_x x \sin k_y y \cos k_z^{(2)}(z-c) \, . \qquad \text{(G.10)}
\end{aligned}
$$

We now proceed to the evaluation of H_{qz}^i.

EVALUATION OF THE $z-$ COMPONENT OF THE MAGNETIC FIELD

Substitution from (2.31)

$$
\begin{aligned}
\frac{\partial G_{xx}^{(1)}}{\partial y} &= \sum_{m=1}^{\infty} \sum_{n=0}^{\infty} k_y A_{mn}^{(1)} \cos k_x x \cos k_y y \sin k_z^{(1)} z \\
&= -\sum_{m=1}^{\infty} \sum_{n=0}^{\infty} \frac{\varphi_n k_y \tan k_z^{(2)}(h-c)}{d_{1mn} \cos k_z^{(1)} h} \\
&\cdot \cos k_x x \cos k_y y \sin k_z^{(1)} z \cos k_x x' \sin k_y y' \qquad \text{(G.11)}
\end{aligned}
$$

Similarly, from (2.33)

$$
\begin{aligned}
\frac{\partial G_{xx}^{(2)}}{\partial y} &= \sum_{m=1}^{\infty} \sum_{n=0}^{\infty} k_y A_{mn}^{(2)} \cos k_x x \cos k_y y \sin k_z^{(2)}(z-c) \\
&= -\sum_{m=1}^{\infty} \sum_{n=0}^{\infty} \frac{\varphi_n k_y \tan k_z^{(1)} h}{d_{1mn} \cos k_z^{(2)}(h-c)} \\
&\cdot \cos k_x x \cos k_y y \sin k_z^{(2)}(z-c) \cos k_x x' \sin k_y y' \qquad \text{(G.12)}
\end{aligned}
$$

Substitution from (G.11) into (G.2) and using (F.26) yields

$$\begin{aligned} H_{qz}^{(1)} &= \frac{\zeta_q K l_x^2}{2\sin Kl_x} \sum_{m=1}^{\infty}\sum_{n=0}^{\infty} \frac{\varphi_n k_y \tan k_z^{(2)}(h-c)}{d_{1mn}\cos k_z^{(1)}h} \\ &\quad \cdot \cos k_x x_q \,\mathrm{Sinc}\left[\frac{1}{2}(k_x+K)l_x\right] \mathrm{Sinc}\left[\frac{1}{2}(k_x-K)l_x\right] \\ &\quad \cdot \sin k_y Y_0 \; J_0(k_y\frac{W}{2}) \cos k_x x \cos k_y y \sin k_z^{(1)} z \end{aligned} \tag{G.13}$$

Likewise, substitution from (G.12) in (G.2) yields

$$\begin{aligned} H_{qz}^{(2)} &= \frac{\zeta_q K l_x^2}{2\sin Kl_x} \sum_{m=1}^{\infty}\sum_{n=0}^{\infty} \frac{\varphi_n k_y \tan k_z^{(1)}h}{d_{1mn}\cos k_z^{(2)}(h-c)} \\ &\quad \cdot \cos k_x x_q \,\mathrm{Sinc}\left[\frac{1}{2}(k_x+K)l_x\right] \mathrm{Sinc}\left[\frac{1}{2}(k_x-K)l_x\right] \\ &\quad \cdot \sin k_y Y_0 \; J_0(k_y\frac{W}{2}) \cos k_x x \cos k_y y \sin k_z^{(2)} (z-c) \end{aligned} \tag{G.14}$$

In summary, the $\hat{y}$ and $\hat{z}$ components of the magnetic field anywhere in the cavity may be expressed as follows:

$$H_{qy}^{(1)} = H_{q0} \sum_{m=1}^{\infty}\sum_{n=0}^{\infty} c_{nq} c_{ymn}^{(1)} \cos k_x x \sin k_y y \cos k_z^{(1)} z \tag{G.15}$$

$$H_{qz}^{(1)} = H_{q0} \sum_{m=1}^{\infty}\sum_{n=0}^{\infty} c_{nq} c_{zmn}^{(1)} \cos k_x x \cos k_y y \cos k_z^{(1)} z \tag{G.16}$$

$$H_{qy}^{(2)} = H_{q0} \sum_{m=1}^{\infty}\sum_{n=0}^{\infty} c_{nq} c_{ymn}^{(2)} \cos k_x x \sin k_y y \cos k_z^{(2)} (z-c) \tag{G.17}$$

$$H_{qz}^{(2)} = H_{q0} \sum_{m=1}^{\infty}\sum_{n=0}^{\infty} c_{nq} c_{zmn}^{(2)} \cos k_x x \cos k_y y \sin k_z^{(2)} (z-c) \tag{G.18}$$

where

$$\begin{aligned} H_{q0} &= \frac{\zeta_q K l_x^2}{2\sin Kl_x} \\ c_{nq} &= \cos k_x x_q \,\mathrm{Sinc}\left[\frac{1}{2}(k_x+K)l_x\right] \mathrm{Sinc}\left[\frac{1}{2}(k_x-K)l_x\right] \end{aligned}$$

and

$$\begin{aligned} c_{ymn}^{(1)} &= \frac{c_{zmn}^{(1)}}{k_y d_{2mn}} \Big\{ k_z^{(1)} k_z^{(2)} \epsilon_r^* \tan k_z^{(2)}(h-c) \\ &\quad - \left[(k_z^{(1)})^2 + k_x^2(1-\epsilon_r^*)\right] \tan k_z^{(1)} h \Big\} \end{aligned} \tag{G.19}$$

$$c_{zmn}^{(1)} = \frac{\varphi_n k_y \tan k_z^{(2)}(h-c)}{d_{1mn}\cos k_z^{(1)}h} \sin k_y Y_0 \; J_0(k_y\frac{W}{2}) \tag{G.20}$$

$$c^{(2)}_{ymn} = \frac{c^{(1)}_{zmn}}{k_y d_{2mn}} \Big\{ k_z^{(1)} k_z^{(2)} \tan k_z^{(1)} h - \Big[(k_z^{(2)})^2 \epsilon_r^* - k_x^2 (1 - \epsilon_r^*) \Big] \tan k_z^{(2)} (h - c) \Big\} \tag{G.21}$$

$$c^{(2)}_{zmn} = \frac{\varphi_n k_y \tan k_z^{(1)} h}{d_{1mn} \cos k_z^{(2)} (h - c)} \sin k_y Y_0 \; J_0(k_y \frac{W}{2}) \; . \tag{G.22}$$

BIBLIOGRAPHY

BIBLIOGRAPHY

[1] T.C. Edwards, *Foundations for Microstrip Circuit Design*, John Wiley and Sons, 1981.

[2] K. C. Gupta, R. Garg, and I. J. Bahl, *Microstrip Lines and Slotlines*, Artech House, 1979.

[3] K. C. Gupta, R. Garg, R. Chadha,*Computer-Aided Design of Microwave Circuits*, Artech House, 1981.

[4] Y. C. Shih, T. S. Chu, and T. Itoh, "Comparative Study for Microstrip Discontinuity Problems", *1985 IEEE MTT-S Digest*, pp. 435-438.

[5] P. Katehi and N. Alexopoulos, "Microstrip Discontinuity Modeling For Millimeter Integrated Circuits", *1985 IEEE MTT-S Digest*, pp. 571-573.

[6] P. Katehi and N. Alexopoulos,"Frequency-Dependent Characteristics of Microstrip Discontinuities in Millimeter-wave Integrated Circuits", *IEEE Trans. Microwave Theory Tech.*, Vol. MTT-33 No. 10, Oct. 1985, pp. 1029-1035.

[7] R. Jansen and N. Koster, "A Unified CAD Basis for the Frequency Dependent Characteristics of Strip, Slot, and Coplanar MIC Components", *11th European Microwave Conference*, pp. 682-687.

[8] R. Jansen, "Hybrid Mode Analysis of End Effects of Planar Microwave and Millimeter-Wave Transmission Lines", *IEEE Proc.*, Vol 128, April 1981, pp. 77-86.

[9] N. Koster and R. Jansen, "The Equivalent Circuit of the Asymmetrical Series Gap in Microstrip and Suspended Substrate Lines", *IEEE Trans. Microwave Theory Tech.*, August 1982, pp. 1273-1279.

[10] J. Boukamp and R. Jansen, "The High Frequency Behaviour of Microstrip Open Ends in Microwave Integrated Circuits Including Energy Leakage", *14th European Microwave Conference*, 1984, pp. 142-147.

[11] J. Rautio and R. Harrington, "Preliminary Results of a Time-Harmonic Electromagnetic Analysis of Shielded Microstrip Circuits",*Automatic RF Techniques Group (ARFTG) Conf. Dig.* June 1986.

[12] J. Rautio *A Time-Harmonic Electromagnetic Analysis of Shielded Microstrip Circuits*, Ph.D. dissertation, Syracuse University, August 1986.

[13] L. Dunleavy and P. Katehi "Repeatability Issues for De-embedding Microstrip Discontinuity S-parameter Measurements By the TSD Technique" *Automatic RF Techniques Group (ARFTG) Conf. Dig.* June 1986.

[14] R. Mittra ed., *Computer Techniques for Electromagnetics*, Pergamon Press 1973.

[15] R.Harrington,*Field Computation by Moment Methods* New York, 1968.

[16] J.C. Maxwell *A Treatise on Electricity and Magnetism* 3rd. ed., vol. 1,New York: Dover 1954 pp 296-297.

[17] E. Denlinger, "A Frequency Dependent Solution for Microstrip Transmission Lines", *IEEE Trans. Microwave Theory Tech.* vol. MTT-19, Jan. 1971, pp30-39.

[18] E. Yamashita, Variational Method for the Analysis of Microstrip-like Transmission Lines" *IEEE Trans. Microwave Theory Tech.*, Vol. MTT-16, Aug. 1968, pp529-535.

[19] A. Sommerfeld, *Partial Differential Equations in Physics* vol. VI, Academic Press, 1949, pp257-258.

[20] C. Chi and N. Alexopoulos "Radiation by a Probe Through a Substrate" *IEEE Trans. Antennas Propagat.* vol. AP-34, Sept. 1986, pp 1080-1091.

[21] A.H. Stroud *Approximate calculation of Multiple Integrals*, Prentice Hall, New Jersey 1971, p255.

[22] R. Jansen, and H. Koster, "Accurate Results on the End Effect of Single and Coupled Lines for Use in Microwave Circuit Design " *A.E.U.* Band 34 1980, pp 453-459.

[23] T. Itoh,"Analysis of Microstrip Resonators", *IEEE Trans. Microwave Theory Tech.*, Vol Mtt-24 1974, pp 946-951.

[24] *Super Compact* (a microwave computer aided design program), Compact Software Inc., 483 McLean Blvd., Patterson, NJ 07504

[25] *Touchstone* (a microwave computer aided design program) ,EESOF Inc., 31194 La Baya Drive, Westlake Village,CA 91362.

[26] C.T. Tai *Dyadic Green's Functions in Electromagnetic Theory* , Intext Educational Publishers 1971.

[27] G.N Watson,*A Treatise on the Theory of Bessel Functions* 2nd ed., Cambridge University Press 1980, p21.